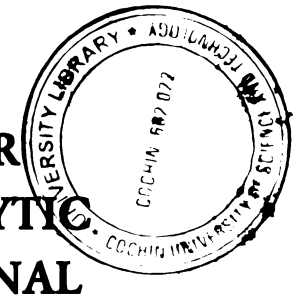

AQUEOUS SOL-GEL PROCESS FOR NANOCRYSTALLINE PHOTOCATALYTIC TITANIA, TRANSPARENT FUNCTIONAL COATINGS AND CERAMIC MEMBRANE

THESIS SUBMITTED TO

COCHIN UNIVERSITY OF SCIENCE AND TECHNOLOGY
IN PARTIAL FULFILMENT OF THE REQUIREMENTS
FOR THE DEGREE OF

DOCTOR OF PHILOSOPHY
IN CHEMISTRY

UNDER THE FACULTY OF SCIENCE

BY

BAIJU K.V.

Under the Supervision of
Dr. K.G.K. Warrier

Materials and Minerals Division
NATIONAL INSTITUTE FOR INTERDISCIPLINARY SCIENCE AND TECHNOLOGY
(formerly Regional Research Laboratory)
Council of Scientific and Industrial Research
Thiruvananthapuram, Kerala, India - 695019

November 2007

DECLARATION

I hereby declare that the work embodied in the thesis entitled **"Aqueous Sol-gel Process for Nanocrystalline Photocatalytic Titania, Transparent Functional Coatings and Ceramic Membrane"** is the result of the investigations carried out by me at Materials and Minerals Division, National Institute for Interdisciplinary Science and Technology (NIIST, formerly Regional Research Laboratory, RRL-T), CSIR, Thiruvananthapuram, under the supervision of **Dr. K. G. K. Warrier** and the same has not been submitted elsewhere for any other degree.

Baiju K. V.

Thiruvananthapuram

November 2007

राष्ट्रीय अंतर्विषयी विज्ञान तथा प्रौद्योगिकी संस्थान
National Institute for Interdisciplinary Science and Technology
(पहले क्षेत्रीय अनुसंधान प्रयोगशाला) **(formerly Regional Research Laboratory)**
An ISO 9001 Certified Organisation
वैज्ञानिक एंव प्रौद्योगिकी अनुसंधान प्रयोगशाला
Council of Scientific and Industrial Research

Dr. K. G. K. Warrier Ph.D., F.IICer
Deputy Director
Head, Materials & Minerals Division
Ceramic Technology

इन्डस्ट्रियल इस्टेट डाक घर, तिरुवनन्तपुरम ६९५०१९, भारत
Industrial Estate P.O., Thiruvananthapuram - 695 019, INDIA
Phone : +91- 471- 2490674, 2515280 (O)Fax : +91- 471- 2491712
E-mail:warrier@niist.res.in Website : www.nist.res.in, http//kgkwarrier.tripod.com

CERTIFICATE

This is to certify that the work embodied in the thesis entitled **"Aqueous Sol-gel Process for Nanocrystalline Photocatalytic Titania, Transparent Functional Coatings and Ceramic Membrane"** has been carried out by **Mr. Baiju K. V.** under my supervision at Materials and Minerals Division, National Institute for Interdisciplinary Science and Technology, (formerly Regional Research Laboratory), CSIR, Thiruvananthapuram, in partial fulfilment of the requirements for the award of the Degree of Doctor of Philosophy in Chemistry, under the faculty of science, Cochin University of Science and Technology, Kochi and the same has not been submitted elsewhere for any other degree.

K. G. K. Warrier

(Thesis Supervisor)

Thiruvananthapuram

November 2007

ACKNOWLEDGEMENTS

I have great pleasure to express my deep sense of gratitude to Dr. K. G. K. Warrier, my thesis supervisor, for suggesting the research problem and for his valuable guidance, leading to the successful completion of this work. I am greatly indebted to him for his keen interest in my work and guidance which served considerably to increase my level of confidence and freedom of thought. I also wish to remember him here as the one who has lead me to this fascinating world of Nano materials through Sol-Gel Science and as a never ending source of encouragement. He has been more than a guide, a friend and philosopher, to me.

I express my sincere thanks to Prof. T. K. Chandrashekar, Director, NIIST, Thiruvananthapuram for allowing me to use the facilities in the institute. I wish to acknowledge Senior Deputy Director Dr. B.C. Pai and former Directors of NIIST, Dr. Vijay Nair and Dr. Javed Iqbal at this juncture.

I extend my thanks to Dr. S. K. Ghosh, Dr. S. Anantha Kumar, Mr. P. Krishna Pillai, Dr. S. Shukla and Dr. S. K. Shukla for their help and support during the course of my work. I am immensely thankful to Mr. P. Mukundan for supporting my work with the instrumental facilities. Thanks are also due to Mr. P. Perumal for his kind co-operation. I wish to express my deep gratitude to Dr. C. Pavithran and Mr. K. Muraleedharan Nair for their help and support.

I am extremely pleased to express my indebtedness to Prof. G. Tomandl, Technical University - Freiberg, Germany for all the discussions we had and for showing genuine interest in the progress of my work. I wish to acknowledge Prof. W. Wunderlich, Tokai University, Japan and Dr. O. Seidel TU, Freiberg, Germany for supporting this work with TEM and AFM facility.
I extend my gratitude to Mr. Guruswamy, Mr. Chandran and Mr. Biju for instrumental support. I wish to acknowledge all scientists of MMD for their kind co-operation.

I am grateful to Mr. K. J. Jerly, my teacher for his constant encouragement and support throughout my life, with out which I would not have reached this level. I am deeply indebted to Dr. C. P. Sibu and Dr. B. Sivakumar for their support and encouragement. I value the sincere support rendered by my former colleagues P. Pradeepan, B. B. Anil Kumar, R. Rohith and Abhijit Sreekumar. I always cherish the warm friendship of Dr. Mahesh Hariharan, Dr. Reji Vargheese, Dr. Saji Alex, K. S. Santhosh, Prakash and Jithesh

I wish to thank my present colleagues Mr. K. Rajesh, Mrs. Smitha Ajith, Mr. P. R. Aravind, Mr. M. Jayasankar, Mr. Anas, Ms. N. Sumalatha, Mrs. Smitha, Mrs. Manju, Mrs. Divya Bose and Mr. Sabarinathan who helped me directly or indirectly during the tenure of my work. I

am thankful to all my friends especially, Mr. P. Shajesh and Mrs. P. N. Remya for their friendship and help during my days at NIST. I wish to thank friends in the other research divisions of NIST for their co-operation.

I would like to express my sincere thanks to former project students Mr. Deepak, Suresh, Vinod kumar, Jithesh for providing value inputs to my work.

At this juncture, I wish to remember all my teachers especially those from St. Albert's College, Ernakulam

Also I thank CSIR, New Delhi for the financial support and all the NIIST staff for their support.

Finally, I remember with gratitude my family members who were always a source of strength and support and all who are near and dear.

Baiju K. V.

Thiruvananthapuram
November 2007

CONTENTS

Preface

Nanostructured materials may be defined as those materials whose structural elements - clusters, crystallites or molecules - have dimensions in the 1 to 100 nm range. The explosion in both academic and industrial interest in these materials over the past decade arises from the remarkable variations in fundamental, electrical, optical and magnetic properties that occur as one progresses from an "infinitely extended" solid to a particle of material consisting of a countable number of atoms. The different forms in which these materials find applications include dry powders, liquid dispersions, films and bulk solids. The novel size-dependent physical and chemical behaviour of nanomaterials are the areas of great interest.

Titanium oxide is a well known wide band gap semiconductor with a wide range of applications. While the rutile form of titania is the common ingredient in paints and ceramic glazes, the anatse phase is mainly used for its photocatalytic and semiconductor applications. The interest in photocatalytic activity of titania has been fuelled by the demonstration of photolysis of water using titania, a promising method for the production of the future fuel hydrogen. Moreover titania is considered as the most ecofriendly environmental cleaning agent due to its photo degradation capacity of industrial effluents and its chemical inertness. Sol-gel method has been reported to be an effective route for the synthesis of nanocrystalline titanium oxide powders. Bulk of the sol-gel synthesis and property evaluation are reported using alkoxide precursors. Even though the method is well developed, certain difficulties are usually addressed including the use of various organic solvents in following commercialisation aspects. The much abundant industrial source of titania is still the metal salts. Hydrolysis condensation reactions are faster for the metal salts compared to the alkoxide and hence the control of the sol-gel reaction along with its application becomes difficult. So there is a need for the development of a sol-gel process using the cheaper salt precursors. The present thesis develops from this point of view of titania sol-gel chemistry and an

attempt is made to address the modification of the process for better photoactive titania by selective doping and also demonstration of utilization of the process for the preparation of supported membranes and self cleaning films.

The thesis is presented in four chapters, each consisting of an abstract, introduction, experimental section, results, discussion and conclusion.

A general introduction to nanomaterials, nanocrystalline titania and sol-gel chemistry are presented in the first chapter. A brief and updated literature review on sol-gel titania, with special emphasis on catalytic and photocatalytic properties and anatase to rutile transformation are covered. Based on critical assessment of the reported information the present research problem has been defined.

The second chapter describes a new aqueous sol-gel method for the preparation of nanocrystalline titania using titanyl sulphate as precursor. This approach is novel since no earlier work has been reported in the same lines proposed here. The sol-gel process has been followed at each step using particle size, zeta potential measurements on the sol and thermal analysis of the resultant gel. The prepared powders were then characterized using X-ray diffraction, FTIR, BET surface area analysis and transmission electron microscopy.

The third chapter presents a detailed discussion on the physico-chemical characterization of the aqueous sol-gel derived doped titania. The effect of dopants such as tantalum, gadolinium and ytterbium on the anatase to rutile phase transformation, surface area as well as their influence on photoactivity is also included.

The fourth chapter demonstrates application of the aqueous sol-gel method in developing titania coatings on porous alumina substrates for controlling the poresize for use as membrane elements in ultrafiltration. Thin coatings having ~50 nm thickness and transparency of ~90% developed on glass surface were tested successfully for self cleaning applications.

Abbreviations

A	Anatase
AFM	Atomic Force Microscopy
BET	Brunauer-Emmet-Teller
DTA	Differential Thermal Analysis
DMP	Dimethyl Pyridine
FTIR	Fourier Transform Infrared
R	Rutile
SEM	Scanning Electron Microscopy
TEM	Transmission Electron Microscopy
TGA	Thermo Gravimetric Analysis
XRD	X-ray Diffraction

Chapter 1: Introduction to Nanomaterials, Sol-gel Chemistry of Titanium oxide and Functional Applications

1.1. Overview on nanomaterials

Interest in the unique properties associated with materials having dimensions on nanometer scale has been increasing at an exponential rate.[1-4] In nanoparticulate materials, a large fraction of atoms is exposed on the surface of the particles. By restricting ordered atomic arrangements to increasingly smaller sizes, materials begin to be dominated by the atoms and molecules at the surfaces, often leading to properties that are strikingly different from the bulk material. For instance, a relatively inert metal or metal oxide may become a highly effective catalyst when manufactured as nanoparticles,[5] opaque particles may become transparent when composed of nanoparticles, or vice versa; conductors may become insulators, or vice versa; and moreover the nanophase materials may have many times the strength of the bulk material. Nanoparticles can comprise a range of different morphologies including nanotubes, nanowires, nanofibres, nanodots and a range of spherical or aggregated dendritic forms of different fractal dimensions. These materials have seen application in a wide range of industries including electronics, pharmaceuticals, chemical-mechanical polishing, materials for solid oxide fuel cells (SOFCs), catalysis, and it is likely that the next few years will see a dramatic increase in the industrial generation and use of nanoparticles. When the characteristic length scale of the microstructure is in the 1-100 nm range, it becomes comparable with the critical length scales of physical phenomena, resulting in the so-called "size and shape effects." This leads to unique properties and the opportunity to use such nanostructured materials in novel applications and devices. Phenomena occurring on this length scale are of

interest to physicists, chemists, biologists, electrical and mechanical engineers, and computer scientists, making research in nanotechnology a frontier activity in materials science. Besides, the extremely high surface to volume ratio characterized by the nanomaterials makes them highly reactive in terms of surface energy, which in turn let the surface to undergo suitable reactions to reduce its surface energy. This possibility can be exploited by using the nanomaterials in catalysis/photocatalysis.

1.2 Titanium Oxide

Titanium oxide has been known for many years as a constituent of naturally occurring mineral ilmenite ($FeO.TiO_2$) and belongs to the family of transition metal oxides. In the beginning of the 20^{th} century, industrial production started with titanium dioxide replacing toxic lead oxides as pigments for white paints. Extraction of titanium oxide from the mineral is a chemical process followed through a sulphate route or a chloride route.[6] Many other processes such as plasma decomposition and direct reduction have also been reported. Presently titanium oxide is well recognized as a valuable material with application as a white pigment in paints, as filler in paper, textile and in rubber/plastics.[7] Titania has received a great deal of attention due to its chemical stability, non-toxicity, low cost and other advantageous properties. While very high refractive index (~2.4) and low visible absorptivity favour in the field of anti-reflection coatings and in thin film optical devices, the wide band gap (~3.2 eV) combined with the high ultraviolet absorption could be exploited in the field of optical coatings. Further, it finds use in wastewater purification,[8] inorganic membranes,[9, 10] and as catalyst support. Titania is a potential ceramic sensor element.[11, 12] Titanium oxide is also being used in heterogeneous catalysis, as a photocatalyst, in solar cells for the production of hydrogen

and electric energy,[13-18] in ceramics, and in electric devices such as varistors. Titania has excellent biocompatibility with respect to bone implants, a candidate material for gate insulator in the new generation of MOSFETS, spacer material in magnetic spin-valve systems, and also finds applications in nanostructured form in Li-based batteries[19] and electrochromic devices.[20]

Titania exists in three forms, rutile, anatase and brookite. Anatase (tetragonal, D_{4h}^{19}-$I4_1/amd$, $a=b=3.733$ Å, $c=9.37$ Å), rutile (tetragonal, D_{4h}^{14}-$P4_2/mmm$, $a=b=4.584$ Å, $c=2.953$ Å and brookite (rhombohedral, D_{2h}^{15}-Pbca, $a=5.436$ Å, $b=9.166$ Å).[21,22] Anatase and rutile are in tetragonal structure and brookite is orthorhombic. In all three TiO_2 structures, the stacking of the octahedra results in threefold coordinated oxygen atoms.[23] Thermodynamically rutile structure is most stable. Brookite has an orthorhombic crystal structure and spontaneously transforms to rutile at ~750 °C.[24] Its mechanical properties are very similar to those of rutile, but it is the least common of the three phases and is rarely used commercially. In all the three crystalline forms each of the Ti^{4+} ions are surrounded by an irregular octahedron of oxide ions. Both in rutile and anatase the six oxide ions that surround the Ti^{4+} ions can be grouped into two. The two oxygen atoms are farthest from Ti^{4+} and the other four oxide ions are relatively closer to Ti^{4+}. In rutile these distances are 2.01A° and 1.92A° respectively and in the anatase they are 1.95A° and 1.91A° (Figure 1.1). The anatase to rutile transformation is a metastable to thermodynamically stable transformation and therefore there is no unique phase transformation temperature as in the case of equilibrium reversible transformation.[25] Anatase transforms irreversibly and exothermally to rutile in the temperature range 600-800 °C. The schematic diagram of unit cells for rutile and anatase is shown in Figure 1.1.

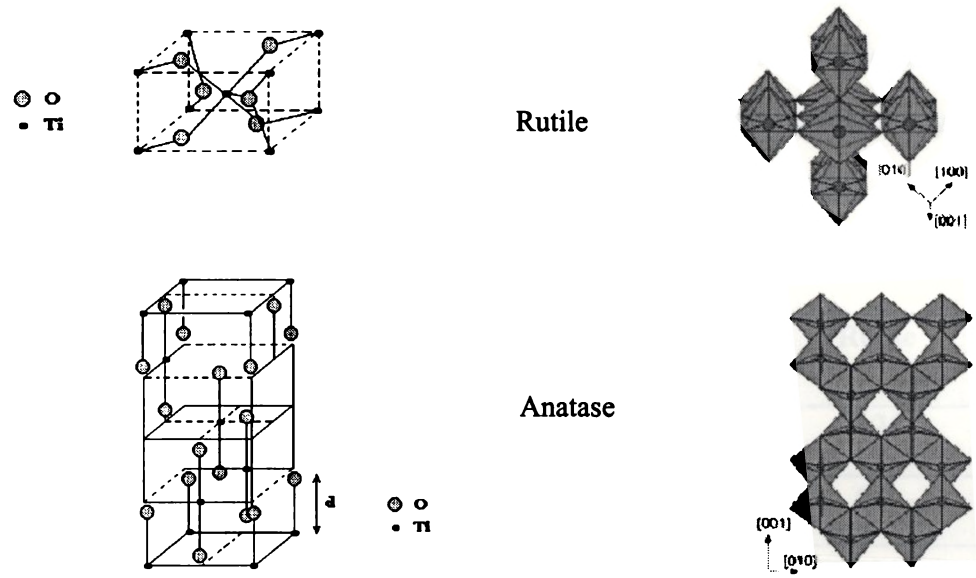

Figure 1.1. Anatase and rutile unit cells and crystals

Anatase has a tetragonal crystal structure in which the Ti-O octahedrals are connected by their vertices as shown in Figure 1.1. Rutile has a crystal structure similar to that of anatase, with the exception that the octahedrals are connected through the edges. This

leads to the formation of chains, which are subsequently arranged in a four-fold symmetry as shown in Figure 1.1. A comparison of layers in Figure 1.1 shows that the rutile structure is more densely packed than anatase. As a point of reference, the densities of the anatase and rutile phases are known to be 3.83 g/cm^3 and 4.24 g/cm^3 respectively.[26] Typical properties of the major two crystal forms of titania are provided in Table 1.1.

Table 1.1. Typical properties of TiO_2

Crystal form	**Anatase**	**Rutile**
Density (g/cm^3)	3.83	4.24
Hardness (moh)	5-6	6-7
Crystal structure	Tetragonal, Uniaxial, negative	Tetragonal, Uniaxial, positive
Compressibility coefficient (10^{-6} cm^2 Kg^{-1})	--	0.53 – 0.58
Melting point (°C) In Air At higher % O_2	 -- --	 1830 ± 15 1879 ± 15
Specific heat (Cal $°C^{-1}$ g^{-1})	0.17	0.17
Dielectric constant	48	114

1.2.1 TiO_2 Photo catalysis

Photocatalytic applications of titania gained considerable emphasis in the 1990s with the emerging demands on clean energy and protecting environment. Other oxides of similar behaviour are zinc oxide, iron oxide, cadmium sulphide and zinc sulphide. Zinc oxide is also a reasonable substitute for titania, except for its property of undergoing incongruent dissolution resulting in formation of zinc hydroxide coating on the ZnO

particles which in turn leads to slow catalyst inactivation. Ideally, a semiconductor photocatalyst should be chemically and biologically inert, photocatalytically stable, easy to produce and use, efficiently activated by sunlight, able to efficiently catalyze reactions, cheap and without risks to the environment or humans. Titanium dioxide (with sizes ranging from clusters to colloids to powders and large single crystals) is close to being an ideal photocatalyst, displaying almost all the above properties. The single exception is that it does not absorb visible light. Both crystal structures, anatase and rutile, are commonly used as photocatalyst, [27-31] with anatase showing a greater photocatalytic activity [32, 33] for most reactions. This increased photoreactivity is due to anatase's slightly higher Fermi level, lower capacity to adsorb oxygen and higher degree of hydroxylation (i.e., number of hydroxy groups on the surface).[34-36] Reactions in which both crystalline phases have the same photoreactivity[37] or rutile have a higher one[38] are also reported. Furthermore, there are also studies which claim that a mixture of anatase (70–75%) and rutile (30–25%) is more active than pure anatase.[39-41] The disagreement of the results may lie in the intervening effect of various coexisting factors, such as specific surface area, pore size distribution, crystal size, and preparation methods, or in the way the activity is expressed. The behaviour of Degussa P25 commercial TiO_2 photocatalyst, consisting of an amorphous state together with a mixture of anatase and rutile in an approximate proportion of 80/20, is for many reactions more active than both the pure crystalline phases.[42,43] The enhanced activity arises from the increased efficiency of the electron–hole separation due to the multiphase nature of the particles. Another commercial TiO_2 photocatalyst, Sachtlebem Hombikat UV 100, consisting only of anatase, has a high photoreactivity due to fast interfacial electron-transfer rate.[44] Main processes occurring

on a semiconductor particle are: (a) electron–hole generation, (b) oxidation of donor (c) reduction of acceptor and (d) electron–hole recombination at surface and in bulk, respectively.[15] There are numerous photocatalytic reactions reported for titania. Photocatalytic decomposition of trichloroethylene in water was investigated[45] in which anatase form was found to be better compared with rutile form. Titania prepared by sol-gel route was porous, having high specific surface area of ~ 600 m^2g^{-1} containing anatase microcrystallites of the size of ~50 Å and was highly photoactive.[46] Chloroform was subjected to photo degradation in a medium containing suspended particles of titania.[47] Similarly, phenol photo decomposition has been reported using fine titanium oxide.[48] Photocatalytic reactions involving NO were conducted in presence of titania.[49] Silica as support and titania as the active catalyst were tested for photo reactions and was compared with the precursor characteristics.[50] Titania supported on alumina and silica was used for photo catalytic decomposition of salicylic acid and found that the titania-alumina system showed improved performance.[51] On analysis, it has been found that titania-silica consisted of matrix isolated titania quantum particles while the TiO_2-Al_2O_3 did not have such particles. Pt/Pd metal particle carrying titania was also prepared and tested. Titania film containing well dispersed Au or Ag metal particles were prepared by sol-gel method, the effect of the dispersed metal particles on the photo-electrochemical properties of the titania electrodes has been reported.[52] The photo responsive formation of gold particles dispersed silica-titania composite gels were further investigated.[53] Photo reduction of such systems containing Au(III) ions yielded gold particles and this principle was used to produce micro patterns of gold particles on silica-titania films.

The titania sol-gel film coated on glass plate was exposed to water containing bacteria and the sterilization rate was found to be increasing with increasing amount of titania [54] and on the quantity of light absorbed by the titania thin film. Preparation and characterization of semiconductor devices based on porous titania films and the experimental result on photo conduction and trap states in titania have been reported.[55] Dye sensitized titania film electrodes containing gold nano particles were investigated and the results indicate that the UV photo response was lowered by the dispersion of gold particles.[56] The reason has been attributed to the shottky barriers at titania/gold interfaces and the band edge fluctuation induced by the gold particles. The possibility of a dissipative energy transfer from dyes to gold particles also has been indicated as a cause for any particle associated titania. Performance was improved at slightly elevated temperatures and a novel synergistic effect of photo and thermo catalytic behaviour has been identified.[57] Thin films of titanium dioxide (TiO_2) were deposited on variety of substrates by a simple sol-gel dip coating technique from the titanium peroxide precursor solution. The titanium oxide films were found to be very active for photocatalytic decomposition of salicylic acid and methylene blue.[58] Yoko et al. recently reported on the Photo electrochemical properties of TiO_2 coating films prepared using different solvents by the sol-gel method.[59] Chan et al. studied the effect of calcination on the microstructures and photocatalytic properties of nanosized titanium dioxide powders prepared by vapour hydrolysis.[60] A homogeneous-precipitation route was adopted by Lee et al.[61] for the preparation of nanosize photocatalytic titania powders. Also, Watanabe et al.[62] reported on the photocatalytic activity of TiO_2 thin film under room light. Recent

reports indicate the improvement in the performance of nanosized titania photocatalysts under sunlight excitation by using suitable dopants.[63, 64]

Table 1.2. TiO_2 compositions for photocatalysis

Titania System	Reaction system
TiO_2 films	Trichloroethylene [71]
TiO_2 aerogel	Aquatic decontamination [72]
TiO_2 suspension	Chloroform [73]
TiO_2 in zeolite structure	Phenol [74]
TiO_2 in zeolite	Reactions of NO [75]
TiO_2/SiO_2, TiO_2/ Al_2O_3	Salicylic acid & phenol[76]
TiO_2 thin film	Microbial sterilisation [54]
TiO_2 nanofibrils	Salicylic acid [77]

A few other reports on lanthanum oxide doped titania include the work of Gopalan et al.[65] and LeDuc et al.[66] There are reports on the effects of addition of metal ion dopants on quantum efficiency of heterogeneous photocatalysis of titanium dioxide.[67] The enhanced photo activity of titania doped by rare-earth oxides such as Europium, Praseodymium and Ytterbium oxides were reported by Ranjit et al.[68] The high activity of oxide /TiO_2 photo catalysts is attributed to the enhanced electron density imparted to titania surface by the dopant oxides. Also, Lin et al.[69] reported the effect of addition of Y_2O_3, La_2O_3 and CeO_2 on the photo catalytic activities of titania for the oxidation of acetone. The catalytic property of V_2O_5/ La_2O_3-TiO_2 mixed oxide systems prepared by co-precipitation route was reported by Reddy et al.[70] The anatase form of titania is believed to possess enhanced

catalytic activity, probably due to its open structure compared to rutile and its high specific surface area. Table 1.2 provides presence of various titania compositions and the major chemical conversions reported for photocatalytic reactions.

1.2.2 Sol-gel synthesis of TiO_2

The sol-gel process is a versatile solution process for making ceramic and glass materials. In general, the sol-gel process involves the transition of a system from a liquid sol into a solid gel phase. By applying the sol-gel process, it is possible to fabricate ceramic or glass materials in a wide variety of forms: ultra fine or spherical shaped powders, thin film coatings, ceramic fibres, microporous inorganic membranes, monolithic ceramics and glasses or extremely porous aerogel materials.[78-82] An overview of the sol-gel process is presented in Figure 2.2.

TiO_2 nanomaterials were synthesized by sol-gel method from hydrolysis of titanium precusor. These methods are used for the synthesis of thin films, powders, and membranes. Two types are known: the non-alkoxide and the alkoxide route. Depending on the synthetic approach used, oxides with different physical and chemical properties may be obtained. The sol–gel method has many advantages over other fabrication techniques such as purity, homogeneity, felicity, and flexibility in introducing dopants in large concentrations, stoichiometry control, ease of processing, control over the composition, and the ability to coat large and complex areas.

The non-alkoxide route uses inorganic salts [83-85] such as nitrates, chlorides, acetates, carbonates and acetylacetonates, which require removal of the inorganic anion, while the alkoxide route (the most employed) uses metal alkoxides as starting material.[86-88] This method involves the formation of a TiO_2 sol or gel or precipitate by hydrolysis and

condensation (with polymer formation) of titanium alkoxides. This process normally proceeds via an acid-catalyzed hydrolysis step of titanium (IV) alkoxide followed by condensation.[89, 90] The development of Ti-O-Ti chains is favoured with low content of water, low hydrolysis rates, and excess titanium alkoxide in the reaction mixture.

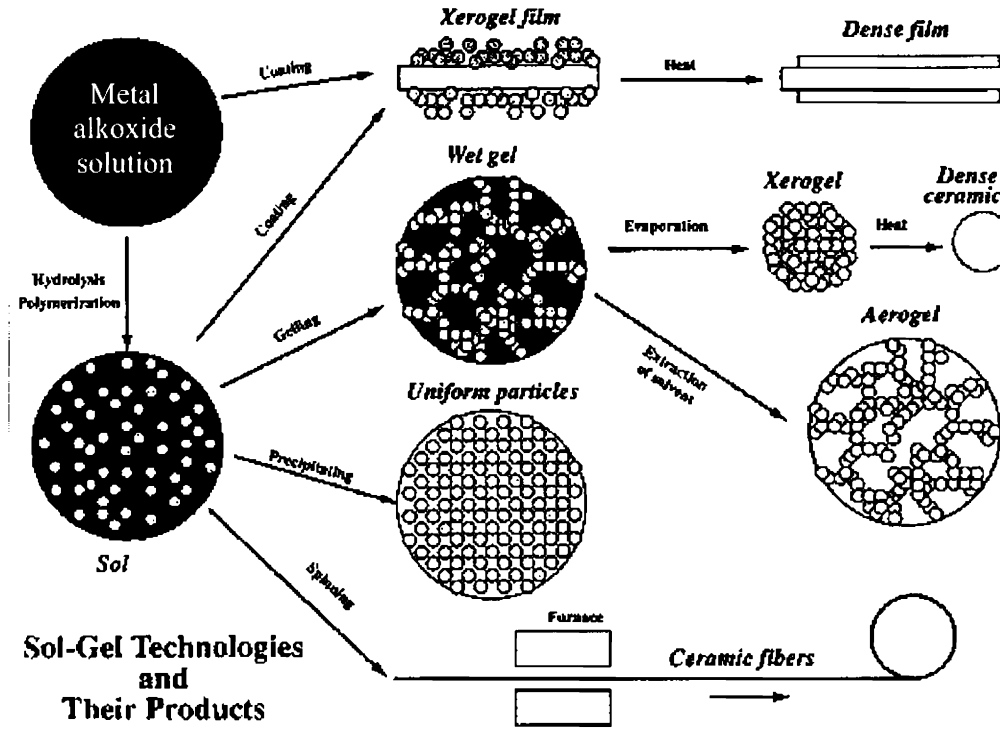

Figure 2.2. An overview of sol-gel process[79]

Three dimensional polymeric skeletons with close packing result from the development of Ti-O-Ti chains. The formation of $Ti(OH)_4$ is favoured with high hydrolysis rates in the presence of medium amount of water. The presence of a large quantity of Ti-OH and insufficient development of three-dimensional polymeric skeletons lead to loosely packed first-order particles. Polymeric Ti-O-Ti chains are developed in the presence of a large excess of water. Closely packed first order particles are yielded via a three-dimensionally

developed gel skeleton.[91-102] From the study on the growth kinetics of TiO_2 nanoparticles in aqueous solution using titanium tetraisopropoxide (TTIP) as precursor, it is found that the rate constant for coarsening increases with temperature due to the temperature dependence of the viscosity of the solution and the equilibrium solubility of TiO_2. Secondary particles are formed by epitaxial self-assembly of primary particles at longer times and higher temperatures, and the number of primary particles per secondary particle increases with time. The average TiO_2 nanoparticle radius increases linearly with time, in agreement with the Lifshitz-Slyozov- Wagner model for coarsening. In order to exhibit better control over the evolution of the microstructure, it is desirable to manipulate the steps of hydrolysis and condensation.[103] In order to achieve this goal, several approaches were adopted. One of them is alkoxide modification by complexation with coordination agents such as carboxylates[104-109] or diketonates that hydrolyze slower than alkoxide ligands. Additionally, the preferred coordination mode of these ligands can be exploited to control the evolution of the structure. In general, β-diketone[110] ligands predominately form metal chelates[111] which can cap the surface of the structure.[112] Carboxylate ligands have a strong tendency to bridge metal centers[113] which are likely to be trapped in the bulk of materials and on the surface of the particle.[114] Acid–base catalysis can also be used to enable separation of hydrolysis and condensation steps.[115] It has been demonstrated that acid catalysis increases hydrolysis rates and ultimately crystalline powders are formed from fully hydrolyzed precursors. Base catalysis is thought to promote condensation with the result that amorphous powders are obtained containing unhydrolyzed alkoxide ligands. On the other hand, acetic acid may be used in order to initiate hydrolysis via an esterification reaction, and alcoholic sols prepared from titanium

alkoxide using amino alcohols have been shown to stabilize the sol, reducing or preventing the condensation and the precipitation of titania.[116] These reactions are followed by a thermal treatment (450–600 °C) to remove the organic part and to crystallize either anatase or rutile TiO_2. Recent variants of the sol–gel method lowered the necessary temperature to less than 100 °C.[117] The calcination process will inevitably cause a decline in surface area (due to sintering and crystal growth), loss of surface hydroxyl groups, and even induce phase transformation. Washing steps have also been reported to cause surface modifications.[118, 119] Cleaning of particles is usually achieved by washing the surface with a solvent, followed by centrifugation. The solvent can affect the chemical composition and crystallization. It was also reported that particle washing could affect the surface charge of the particles by bonding onto the surface. An alternative washing technique is to dialyze particles against double-distilled water,[120] which could be an effective method of removing soluble impurities without introducing new species. As titanium sources, $Ti(O\text{-}Et)_4$,[121] $Ti(i\text{-}OP)_4$[122-124] and $Ti(O\text{-}nBu)_4$[125-127] are most commonly used. The sol–gel method has been widely studied particularly for multicomponent oxides where intimate mixing is required to form a homogeneous phase at the molecular level. Thus, metal ions such as Ca^{2+},[128] Sr^{2+} ,Ba^{2+} ,Cu^{2+},[129,130] Fe^{3+},[131-134] V^{5+},[135] Cr^{3+}, Mn^{2+}, Pt^{4+},[136] Co^{2+},[137] Ni^{2+}, Pb^{2+},[138] W^{6+}, Zn^{2+},[139] Ag^{+}, Au^{3+},[140,141] Zr^{2+},[142] La^{3+},[143] and Eu^{3+} were introduced into TiO_2 powders and films by this method and the photocatalytic activity was improved to varying extent. Most nanocrystalline-TiO_2 (nc-TiO_2) particles that are commercially obtainable are synthesized using sol–gel methods. Very recently, sol–gel and templating synthetic methods were applied to prepare very large surface area titania phases[144-146] which exhibit a mesoporous structure. Ionic and neutral surfactants

have been successfully employed as templates to prepare mesoporous TiO_2.[147-152] Block copolymers can also be used as templates to direct formation of mesoporous TiO_2.[153-155] In addition, many non-surfactant organic compounds have been used as pore formers such as diolates[156-157] and glycerine.[158, 159]

Sol–gel methods coupled with hydrothermal routes for mesoporous structures[160] lead to large surface area even after heating at temperatures up to 500 °C. This may be explained as follows: generally, mesopores collapse during calcination due to crystallization of the wall. When a hydrothermal treatment induces the crystallization of amorphous powders, the obtained powders can effectively sustain the local strain during calcination and prevent the mesopores from collapsing. For nanostructured thin films, the sols are often treated in an autoclave to allow controlled growth of the particles until they reach the desired size. Oswald ripening takes place during this process, leading to a homogeneous particle-size distribution. If a film is made using these particles, substances can be added to prevent cracking and agglomeration or increase the binding and viscosity after this ripening process. The resulting paste can be deposited on a substrate using doctor blading or screen printing. The solvent is evaporated and the particles are interconnected by a sintering process, normally at air temperatures around 450 °C. At this temperature, organic additives are also removed from the film. Slow heating and cooling is important to prevent cracking of the film. In most cases, the resulting film has a porosity of 50%. Thin films can also be made from the sol by dip coating.

1.2.3 Anatase - Rutile Phase Transformation

Anatase and rutile are the two polymorphs of titania at atmospheric pressure. The room temperature phase is anatase and the high temperature phase is rutile. Anatase transforms irreversibly and exothermically to rutile in the range 400 °C to 1200 °C[161, 162] depending on parameters such as the method of preparation, grain size, morphology, degree of agglomeration, nature of impurities and reaction atmosphere.[163-166] At atmospheric pressure the transformation is time and temperature dependent and is also a function of impurity concentration. The complexity of the transition is typically attributed to the reconstructing nature. The transition is a nucleation-growth process and follows the first order rate law with activation energy of ~90 kcal/mol.[167]

The anatase - rutile transformation involves an overall contraction of oxygen and movement of ions so that a cooperative rearrangement of Ti^{4+} and O^{2-} occur. The transformation implies that two of the six Ti-O bonds of anatase structure break to form a rutile structure. The removal of the oxygen ions, which generate lattice vacancies, accelerate the transformation and inhibit the formation of interstitial titanium. The impurities that have most pronounce inhibiting action are chloride, sulphate and fluoride ions whereas that accelerates the transformation includes alkaline and some of the transition metal ions. Those ions with valency greater than four reduce the oxygen vacancy concentration and will retard the reaction.[168]

The effect of reaction atmosphere shows that vacuum conditions and atmosphere of hydrogen, static air, flowing air, oxygen, argon, nitrogen and chlorine affect the phase transformation to different extents. Lida and Ozaka as well as Shannon found that the transformation rate in a hydrogen atmosphere is greater than in air and under vacuum the

rate of transformation decreases as oxygen partial pressure increases.[169] Oxygen vacancies are formed in hydrogen atmosphere whereas the interstitial Ti^{3+} ions are generated under vacuum. The rate constant of the transformation in hydrogen was 10 times larger than in air.[170] It has been reported that at 950 °C the phase transformation in Ar/Cl_2 atmosphere is about 300 times faster than in air.[171] The accelerating effect of chlorine atmosphere on the anatase-rutile phase transformation involves two mechanisms that probably occur simultaneously - vapour mass transport and oxygen vacancy formation in which the first generate nucleation and growth in the bulk. When the vapour transport is negligible, the primary mechanism is based on oxygen vacancies.

The effect of metal cations such as Li, Na, K, Mg, Ca, Sr, Ba, Al, Y, La, Er, Co, Ni, Cu and Zn on anatase - rutile transformation was studied earlier.[172] A linear relationship between phase transition temperature and ionic radius, for alkali and alkaline earth metals and group III elements are reported. Transition metals, which entered the matrix interstitially, gave a high transition temperature, whereas those dopants introduced substitutionally did not give a significant change in transition temperature. It was concluded that the oxidation state together with ionic radii of cations and type of sites occupied were the important parameters, which control phase transition temperature. Depending on the ionic radius of dopant compared with radius of titanium, it can be introduced substitutionally or interstitially or if the size of dopant is larger than oxygen, it could be intercalated into the matrix, producing a lattice deformation. From that study dopant appears to have no effect on the amorphous gel to anatase transformation temperature, but influenced the anatase - rutile transformation. If dopant ion size is less than that of titanium, anatase phase will be stabilized to a higher temperature. Dopants

bigger than oxygen ion produce large local deformation of lattice. Those dopant ions whose size fall in between titanium and oxygen stabilize the anatase phase. Those dopants near to oxygen size can stabilize the titania phase more. The enhancement or inhibiting effect of additives on anatase - rutile transformation depends on their ability to enter the TiO_2 lattice, thereby creating oxygen vacancies or interstitial Ti^{3+} ions. Oxides of Cu, Co, Ni, Mn and Fe mixed with anatase TiO_2 increases the transformation rate efficiently. Transition metals, which entered the matrix interstitially, gave a high transition temperature, whereas those dopants introduced substitutionally did not give a significant change in transition temperature. [172, 173]

Bacsa[174] reported an improvement of the anatase-to-rutile phase transformation by peptizing the hydrolyzed precipitates with nitric acid, however, the 100% rutile phase was not obtained. Bischoff [175] and Anderson found that acid peptization of TiO_2 particles favoured the formation of rutile, in comparison with the situation that occurred at higher temperatures. It is generally accepted that the adsorption of protons on the surface of hydrous TiO_2 particles creates a net positive charge, and thus yields an electrostatically stabilized sol during acid peptization. However, this adsorption model of peptization could not explain the rutile phase formation after peptization at low temperature. Zhang et al.[176] used hydrochloric acid as peptizing agent and the phase formation of nanoparticles during the antiaggregation process was attributed to its chloride ion. Ferreira reported the effect of inorganic acid and base concentration on the anatase to rutile phase transformation and proposed a reaction mechanism for rutile formation. It is interesting to note that an increased concentration of electrolyte enhanced the rutile formation and the effect was shown even at room temperature.[177]

1.2.4 High temperature catalysts

Most of the applications of titania ceramics at high temperature calls for the pure rutile phase which is usually formed by heating titanium salts above 600 °C. However, with the expanding applications in the area of catalysts, photo catalysts, membranes and active humidity sensors, the need for obtaining anatase phase stable at elevated temperatures become significant. Earlier work indicates that even as a surface modifier for anatase titania pigments, alumina was used as a coating in order to improve gloss property as well as to prevent degradation. Recent identification of 'self-cleaning' surfaces by transparent anatase coatings on glass, ceramic tiles and bricks,[178] the anatase phase has to be retained at the processing temperature above 1000 °C. The anatase-rutile transformation temperatures are fairly dependent on the history of the sample.[179, 173] Further, the low temperature densification in titania could be associated with the phase formation temperature. Early indicative reports on the incorporation of aluminium oxide, copper oxide, manganese oxide, iron oxide and zinc oxide postulated that the mechanism for modification of anatase-rutile transformation is related to oxygen vacancies on titania. This was also explained that the dispersion of alumina on titania stabilizes its surface and increases the apparent activation energy for the rutile nucleation at titania-alumina interfaces. By using copper chloride as a dopant solution, a modified titania having nanocrystalline brookite stable at 400 °C and having a narrow band gap than normal titania, could be produced through sol-gel route.[180] However, a detailed investigation using thermal analysis and XRD techniques on the role of alumina in increasing the anatase-rutile transformation indicate[181] that a metastable anatase solid solution containing alumina is formed at relatively low temperatures, and alumina is formed from

exsolution process of the as formed anatase solid solution, in which rutile is formed at higher temperature. This argument is further supported by the fact that ∝-alumina is formed at as early as 900 °C in presence of titania while the usual ∝-alumina formation is above 1100 °C. The influence of addition of zirconia in the raising of transformation temperature of anatase to rutile is also reported. Since zirconia is not expected to involve in any oxygen vacancy change in titania, the role of zirconia was identified to be due to incorporation of Zr ions into anatase lattice. The formation of a limited solid solution of zirconia in anatase at low temperature increased the strain energy and thus leads to a higher anatase to rutile transformation temperature.[182] An investigation on the effect of several cations of lanthanum, zinc, aluminum, potassium, sodium, calcium, barium and cobalt on the anatase-rutile transformation has been reported.[183] The dopants were introduced into the titania gel in the form of nitrates, heat treated in the range 350-1100 °C and was characterized by wide angle X-ray diffraction (WAXS) and thermogravimetry. Lanthanum oxide was doped in titania membrane precursors in order to study the thermal stability and it was seen that there was an increase of 150 °C in the anatase to rutile transformation in the doped composition.[184] SnO_2, Al_2O_3, and Fe_2O_3 were doped in nanocrystalline titania precursors and found that while SnO_2 and Fe_2O_3 decrease the transformation temperature, Al_2O_3 increased the same. However, the interesting fact is that these oxides were successful in controlling grain growth, which normally occurs in rutile as a result of the transformation. As is known in the case of nanocrystalline materials, the grain growth can be regarded as coalescence of smaller neighbouring grains, where grain boundary motion is mainly involved, and the role of these dopant oxides would be to restrict the movement of these grain boundaries thus lowering the

grain growth.[185] The transformation kinetics in presence of Fe_2O_3 has been reported,[186] where Fe_2O_3-TiO_2 mixture was heated in air and in argon atmosphere to different temperatures and the phases formed were analyzed by using XRD techniques. As found in the earlier study, the Fe_2O_3 primarily decreases the anatase to rutile transformation temperature.

Platinum was incorporated in titania prepared through titanium butoxide and platinum acetyl acetonate.[187] Platinum promoted the formation of rutile probably through metal catalyzed dehydroxylation of anatase precursor or through the presence of PtO_2 which has the rutile structure, as an intermediate phase. Platinum atoms, however, did not go into crystalline structure of rutile. In another study, chromium (III) was incorporated in anatase titania catalyst in different concentrations and analysis of the cell parameters indicated that there is a stability limit for the system at ~1.4 atomic percentage. Acceleration in the rate of anatase to rutile phase transition was also reported.[188] Further, nanosize silver was incorporated in titania precursor gel and its effect of A>R transformation was investigated using impedance spectral measurements. The transformation was delayed in presence of silver.[189]

1.2.5 Titania Functional Coatings

The concept of development of 'self-cleaning' surfaces was reported in the ninentees,[190] which was a step further on the application of photo responsive behaviour of titanium oxide. They prepared a thin TiO_2 polycrystalline film from anatase sol on a glass substrate which on UV irradiation, the contact angle of the surface decreased to $0 \pm 1°$ from that of $72 \pm 1°$. They found that irradiation created a surface that was highly hydrophilic and oleophilic. This was due to the creation of surface oxygen vacancies at

bridging sites on UV irradiation, which resulted in conversion of Ti^{4+} sites to Ti^{3+} sites that favoured the dissociative adsorption of water molecules and also influenced the affinity to chemisorbed water of its surrounding sites. This increase in surface wettability due to the formation of functional groups such as hydroxyl groups that is increased by the irradiation of light.[191-194] A drop of water falling on a surface spreads very uniformly and therefore provides an even surface and excellent transparency. Super hydrophilic surfaces also provide antifogging property.[195] However, organic additives, which usually are responsible for this function, have low stability with respect to mechanical, thermal and environmental considerations. Titania is a potential candidate in this line in view of their availability, stability and possibility to prepare in the form of nano coatings.[196] Thus, a successful self-cleaning property is associated with synergic effect of photo catalytic decomposition of compounds and also by hydrophilicity, by which drops of water spread out evenly and clean the surface by removing decomposition products. These combination surfaces will have wide applications on windows of high rise buildings, optical glass, automobile window shields and rear view mirrors, removal of oil smears from surfaces when immersed in water, self cleaning of kitchen exhaust fans and floors of public comfort stations and hospitals.[14,197, 198] Contaminants on exterior walls of buildings can be washed by rain water much more efficiently or can be cleaned easily by jets of water. Sol-gel derived mesoporous titania films are also reported for applications in catalytic nano and ultra filtration membranes required in technologies such as gas separation, catalysis, membrane reactors, sensors and adsorbents. Sol-gel technique is a very good means to control the porosities of both bulk and thin film materials.[199] Recently, the use of organic or microporous templates is catching up in the process of

porosity control, besides the more traditional particle packing approach to prepare controlled porosity materials. Titanium oxide having macropores to micro pores and nanopores have been investigated [200] for drawing conclusions on preparation parameters and correlation to end properties, with considerable success.

1.3 Definition of the present problem

Titanium oxide is used in heterogeneous catalysis and as a photocatalyst for the decomposition of organics, in the treatment of industrial waste water, for elimination of harmful bacteria and in the photocleavage of water, in solar cells for the production of hydrogen and electric energy and in antifogging and self cleaning coatings. Even though lots of studies are reported on the synthesis and on various properties of titania, sol-gel method is shown to be an effective route for the synthesis of nanocrystalline titanium oxide powders. Bulk of the sol-gel synthesis and property evaluation are reported on titania derived from alkoxide precursors. Even though the method is well investigated, the commercialization aspect of various technologies using titania is not addressed well when alkoxide precursors are used. The much abundant industrial source of titania is still the metal salts. Hydrolysis condensation reactions are faster for the metal salts compared to the alkoxide and hence the control of the sol-gel reaction along with its application becomes difficult. So there is a need for development of a sol-gel process using the cheaper salt precursors. The present thesis develops from this point of view of titania sol-gel chemistry and an attempt is made to address the modification of the process for better photoactive titania by selective doping and also demonstration of utilization of the process for the preparation of supported ceramic membranes. Therefore, in the present work an attempt is made to

1. Study the synthesis of nanocrystalline titania using an aqueous sol-gel method starting from titanyl sulphate and optimising process parameters.
2. Modify the textural properties of titania by selective doping (Ta^{5+}, Gd^{3+} and Yb^{3+}) using tantalum oxalate, gadolinium nitrate, ytterbium nitrate.

3. Characterize the powder for anatase to rutile phase transformation, crystallite size, specific surface area, catalytic and photocatalytic properties. Correlation of synthetic procedure and properties of photocatalytic titanium oxide.
4. Fabrication and detailed morphological investigation of titania membrane on porous alumina substrates and filtration studies.
5. Photoactive nanocrystalline titania coatings on glass surfaces for possible self cleaning applications.

1.4 References

1. H. Gleiter, *Prog. Mater. Sci.*, 33, **1989**, 223.
2. M. J. Mayo, *Int. Mater. Rev.*, 41, **1996**, 85.
3. K. Lu, *Mater. Sci. & Eng. R16, Reports: A Rev. J.*, **1996**, 161.
4. C. Suryanarayana, *Int. Mater. Rev.*, 40, **1995**, 41.
5. M. Valden, X. Lai, D. W. Goodman, *Science*, 281, **1998**, 1647.
6. R. Thompson, *Industrial inorganic chemicals, Production and uses*, The Royal Society of Chemistry, **1995**.
7. J. P. Jalava, *Part. Part. Syst. Charact.*, 23, **2006**,159.
8. X. Z. Li, F. B. Li, *Environ. Sci. Technol.*, 35, **2001**, 2381.
9. K. N. P. Kumar, K. Keizer, A. J. Burggraaf, *J. Mater. Chem.*, 3a, **1993**, 1141.
10. K. N. P. Kumar, K. Keizer, A. J. Burggraaf, T. Okubo, H. Nagamoto, *J. Mater. Chem. 3b.*, **1993**, 1151.
11. A. A. Azad, L. B. Younkman, S. A. Akbar, M. A. Alim, *J. Am. Ceram. Soc.*, 77, **1994**, 481.
12. P. I. Gouma, M. J. Mills, K. H. Sandhage, *J. Am. Ceram. Soc.*, 83, **2000**, 1007.

13. B. O'Regan, M. Gratzel, *Nature*, 353, **1991**,737.

14. A. Fujishima, X. T. Zhang, *C. R. Chim.*,9, **2006**, 750.

15. A. Fujishima, T. N. Rao, D. A. Tryk, *J. Photochem. Photobiol. Photochem. Rev.*, 1, **2000**, 1.

16. S. Nakade, Y. Saito, W. Kubo, T. Kitamura, Y. Wada, S. Yanagida, *J. Phys. Chem. B*, 107, **2003**, 8607.

17. K. Hashimoto, H. Irie, A. Fujishima, *Jpn. J. Appl. Phys. Part 1*, 44, **2005**, 8269.

18. O. Harizanov, P. Stefchev, R. Kirilov, *Proceedings of Solar World Congress, Budapest*, **1993**, 357.

19. Y-G. Guo, Y-S. Hu, J. Maier, *Chem. Comm.*, **2006**, 2783.

20. E. Da Costa, C. O. Avellaneda, A. Pawlicka, *J. Mater. Sci.*, 36, **2001**, 1407.

21. F. A. Grant, *Rev. Mod. Phys.*, 31, **1959**, 646.

22. G. V. Samsonov, *The Oxide Handbook, IFI/Plenum Press, New York, 1982./ W. B. Pearson, A handbook of lattice spacings and structures of metals and alloys, Pergamon Press: London*, Vol. 2, **1967.**

23. U. Diebold, *Surf. Sci. Rep.*, 48, **2003**, 53.

24. K. I. Hadjiivanov, D. G. Klissurski, *Chem. Soc. Rev.*, 25, **1996**, 61.

25. K. N. P. Kumar, K. Keizer, A. J. Burggraaf, T. Okubo, H. Nagamoto, S. Morooka, *Nature*, 358, **1992**, 48.

26. I. J. McColm, *Ceramic science for materisls technologists, Leonard Hill, Chapman and Hall, New York*, **1983**.

27. T. van der Meulen, A. Mattson, L. Österlund, *J. Catal.*, 251, **2007**,131.

28. W. Qin, J-J. Liu, S-L. Zuo, Y-C. Yu, Z-P, Hao, *J. Inorg. Mater.*, 22, **2007**, 931

29. Y. Xie, Q. Zhao, X. Jian Zhao, Y. Li, *Catal. Lett.*, 118, **2007**, 231.

30. S-Y. Kim, T-S. Chang, C-H, Shin, *Catal. Lett.*, 118, **2007**, 224.

31. O. Gimeno, F. J. Rivasa, F. J. Beltrána, M. Carbajoa, *Chemosphere,* 69, **2007,** 595.

32. A. L. Linsbigler, G. Q. Lu, J. T Yates Jr. *Chem. Rev.,* 95, **1995,** 735.

33. K. Tanaka, M. F.V. Capule, T. Hisanaga, *Chem. Phys. Lett.,* 187, **1991,** 73.

34. H. P. Maruska, A. K. Ghosh, *Sol. Energy*, 20, **1978,** 443.

35. H. Gerischer, A. Heller, *J. Electrochem. Soc.*,139, **1992,** 113.

36. R. I. Bickley, T. Gonzales-Carreno, J. L. Lees, L. Palmisano, R. J. D. Tilley. *J Solid State Chem.*, 92, **1991,** 178.

37. X. Deng, Y. Yue, Z. Gao, *Appl. Catal. B-Environ.,* 39, **2002,** 135.

38. A. Mills, S. K. Lee, A. Lepre. *J. Photoch. Photobiol. A. Chem.,* 155, **2003,** 199.

39. R. R. Basca, J. Kiwi, *Appl. Catal B- Environ.*,16, **1998,** 9.

40. D. S. Muggli, L. Ding, *Appl. Catal. B-Environ.,* 32, **2001**,181.

41. T. Ohno, K. Sarukawa, K. Tokieda, M. Matsumura, *J. Catal.,* 203, **2001**, 82.

42. M. Nargiello, T. In. Herz, D. F. Ollis, H. Al-Ekabi, *Editors. Photocatalytic Purification and Treatments of Water and Air. Amsterdam: Elsevier*; **1993**, p. 801.

43. Q. Zhang, L. Gao, J. Guo, *Appl. Catal. B. Environ.,* 26, **2000**, 207.

44. S. T. Martin, H. Hermann, W. Choi, M. R. Hoffmann. *J. Chem. Soc. Faraday Trans.* 90, **1994,** 3315.

45. K. Yoshida, K. Okamura, K. Hirano, K. Iguchi, K. Ito and M. Murabayashi, *J Water Environ. Tech.,* 17, **1994,** 38.

46. G. Dagan, M. Tomkiewiez, *J. Phys. Chem.,* 97, **1993**, 12651.

47. C. A. Martin, M. A. Baltanas, A. E. Cassano, *Catal. Today*, 27, **1996**, 221.

48. S. F. Cheng, S. J. Sai, Y. F. Lee, *Catal. Today*, 26, **1995**, 87.

49. R. Carrera, A. L. Vazquez, E. Arce, M. Moran-Pineda, S. Castillo, *J. Alloy. Compd.,* 434, **2007**, 788.

50. S. Yoshida, S. Takenaka, T. Tanaka, T. Funabiki, *J. De Physique, IV*, 7 (C2) **1997,** 859.

51. C. Anderson, A. J. Bard, *J. Phys. Chem. B.*,101, **1997**, 2611.

52. G. Zhao, H. Kozuka, T. Yoko, *Thin Solid Films*, 277, **1996**,147.

53. H. Yanagi, *Chem. Mater.*, 10, **1998**, 1258.

54. Y. Horie, M. Taya, S. Tone, *Kagaku Kogaku Ronbunshu*, 22, **1996,** 1241.

55. R. Koenenkamp, P. Hoyer, *Porous Semiconductor Films for Photovaoltaic and Related Device Applications,* Ed. D. S. Ginley, Material Research Society, Pittsburg, USA **1996** p 551.

56. G. Zhao, H. Kozuka, T. Yoko, *J. Ceram. Soc. Jpn.*, 104, **1996**, 164.

57. F.X. Zeltner, W. A. Anderson, *A Comparison of the Catalytic and Photocatalytic Properties of Microporous Titania Materials,* Proc. Am. Chem. Soc. Meetings, Washington DC USA, **1995**, p 403.

58. R. S. Sonawane, S. G. Hegde, M. K. Dongare, *Mater. Chem. Phys.*, 77, **2003**, 744.

59. T. Yoko,*Thin Solid Films,* 283, **1996**, 188.

60. C. K. Chan, J. F. Porter, Y. G. Li, W. Guo, C. M. Chan, *J. Am. Ceram. Soc.*, 82, **1999**, 566.

61. K. R. Lee, S. J. Kim, J. S. Song, J. H. Lee, Y. J. Chung, S. D. Park, *J. Am. Ceram. Soc.*, 85, **2002**, 341.

62. T. Watanabe, A. Kitamura, E. Kojima, C. Nakayama, K. Hashimoto, A. Fujishima, *Photocatalytic activity of TiO_2 thin film under room light, Photocatalytic Purification and Treatment of Water and Air,* Elsevier Science Publishers B., Ollis et al., Eds. **1993**, p 747.

63. R. Asahi, T. Morikawa, T. Ohwaki, K. Aoki,Y. Taga, *Science*, 293, **2001**, 269.

64. A. Fuerte, M. D. Hernandezalonso, A. J. Maira, A. Martinezarias, M. Fernandezgarcia, J. C. Conesa, J. Soria, *Chem. Comm.*, 24, **2001**, 2718.

65. R. Gopalan, Y. S. Lin, *Ind. Eng. Chem. Res.*, 34, **1995**, 1189.

66. C. A. LeDuc, J. M. Campbell, J. A. Rossin, *Ind. Eng. Chem. Res.*, 35, **1996**, 2473.

67. W. Choi, A. Termin, M. R. Hoffmann, *J. Phys. Chem.*, 98, **1994**, 13669.

68. K. T. Ranjit, I. Willner; S. H. Bossmann, A. M. Braun, *Environ. Sci. Technol.*, 35 **2001**, 1544.

69. J. Lin, J. C. Yu, *J. Photochem. Photobiol .A-Chem.*, 116, **1998**, 63.

70. B. M. Reddy, I. Ganesh, *J. Mol. Catal. A-Chem.*,169, **2001**, 207.

71. M. Keshmiri, T. Troczynski, M. Mohseni. *J. Hazard. Mater.*, 128, **2006**, 130.

72. C. A. Martin, M. A. Baltanas, A. E. Cassano, *Catal. Today*, 27, **1996**, 221.

73. E. A. Ustinovich, D. G. Shchukin , D. V. Sviridov. *J. Photoch. Photobiol.* A 175, **2005**, 249.

74. H. Yamashita, Y. Ichihashi, S. G. Zhang, Y. Matsumura, Y. Souma, T. Tatsumi, M. Anpo, *Appl. Surf. Sci.*, 121, **1997**, 305.

75. M. Takeuchi, T. Kimura, M. Hidaka, D. Rakhmawaty, M. Anpo, *J. Catal.*, 246, **2007**, 235.

76. G. An, G. Ma, Z. Sun, Z. Liu,B. Han, S. Miao, Z. Miao, K. Ding, *Carbon*, 45, **2007**, 1795.

77. J. Watthanaarun, P. Supaphol, V. Pavarajarn, *J. Nanosci. Nanotech.*, 7, **2007**, 2443.

78. H. Schroeder, *Opt. Acta.*, 9, **1962**, 249.

79. C. J. Brinker, G. W. Scherer, *Sol–Gel Science, The Physics and Chemistry of Sol-Gel Processing*, Academic Press, New York, **1990**.

80. J. D. Mackenzie, *Ultrasonic Processing of Ceramics, Glasses and Composites*; L. L. Hench, D. R. Ulrich, Eds.; Wiley: New York, **1984**, p 15.

81. J. Venzel, *Glass. Current Issues*; A. F. Wright, A. F. Dupuy; Eds.; Martinus Nijhojj: Dordrecht, Netherlands, **1985**, p 224.

82. J. A. Lewis, *J. Am. Ceram. Soc.*, 83, **2000**, 2341.

83. M. Iwasaki, M. Hara, S. Ito, *J. Mater. Sci. Lett.;* 17, **1988**, 1769.

84. U. Bach, D. Lupo, P. Comte, J. E. Moster, F. Weissortel, J. Salbeck, *Nature,* 395, **1998**, 583.

85. E. Matijevic, M. Budnik, L. Meites, *J. Colloid Interf. Sci.,* 61, **1997**, 302.

86. S. S. Watson, D. Beydoun, J. A. Scott, R. Amal, *Chem. Eng. J.*, 95, **2003**, 213.

87. Y. Haga, H. An, R.Yosomiya, *J. Mater. Sci.,* 32, **1997**, 3183.

88. K. J. Y. Yung, S. B. Park, *J. Photochem. Photobiol. A Chem* ., 127, **1999**, 177.

89. G. Oskam, A. Nellore, R. L. Penn, P. C. Searson, *J. Phys. Chem. B,* 107, 2003, 1734.

90. T. Sugimoto, *Adv. Colloid Interfac. Sci.,* 28, **1987**, 65.

91. M. A. Anderson, M. J. Gieselmann, Q. Xu, *J. Membrane Sci.,* 39, **1988**, 243.

92. C. J. Barbe, F. Arendse, P. Comte, M. Jirousek, F. Lenzmann, V. Shklover, M. Gratzel, *J. Am. Ceram. Soc.,* 80, **1997**, 3157.

93. E. A. Barringer, H. K. Bowen, *Langmuir* 1, **1985**, 414.

94. J. H. Jean, T. A. Ring, *Langmuir*, 2, **1986**, 251.

95. C. Kormann, D. W. Bahnemann, M. R. Hoffmann, *J. Phys. Chem.,* 92, **1988,** 5196.

96. J. Livage, M. Henry, C. Sanchez, *Prog. Solid State Chem.,* 18, **1988**, 259.

97. J. L. Look, C. F. Zukoski, *J. Am. Ceram. Soc.,* 78, **1995,** 21.

98. J. L. Look, C. F. Zukoski, *J. Am. Ceram. Soc.,* 75, **1992**, 1587.

99. Y. Bessekhouad, D. Robert, J. V. J. Weber, *Photochem. Photobiol. A Chem.,* 157, **2003**, 47.

100. R. L. Penn, J. F. Banfield, *Geochim. Cosmochim. Acta.,* 63, **1999**, 1549.

101. D. Vorkapic, T. Matsoukas, *J. Am. Ceram. Soc.,* 81, **1998**, 2815.

102. D. Vorkapic, T. Matsoukas, *J. Colloid Interfac. Sci.,* 214, **1999**, 283.

103. J. Livage, M. Henry, C. Sanchez, *Prog. Solid State Chem.*, 18, **1988,** 259.

104. S. Doeuff, Y. Dromzee, F. Taulelle, *Inorg. Chem.,* 28, **1989**, 4439.

105. S. Doeuff, M. Henry, C. Sanchez; *Mater Res. Bull.*, 25, **1990**, 1519.

106. C. Guillard, B. Beaugiraud, C. Dutriez, J. M. Herrmann, H. Jaffrezic, N. Jaffrezic-Renault, *Appl. Catal. B: Environ.*, 39, **2002**, 331.

107. R. Campostrini, M. Ischia, L. Palmisano., *J. Therm. Anal. Cal.;*71, **2003,** 997.

108. R. Campostrini, M. Ischia, L. Palmisano; *J. Therm. Anal. Cal.,*71, **2003**, 1011.

109. R. Campostrini, M. Ischia, L. Palmisano, *J. Therm. Anal. Cal.*, 75, **2004**,13.

110. O. Harizanov, A. Harizanov.; Solar Energy Mater. *Solar Cells,* 63, **2000**, 185.

111. K. Nakamoto, *Infrared Spectra of Inorganic Compound*, New York, London: John Wiley & Sons; **1963**.

112. S. Dick, C. Suhr, J. L. Rehspringer, M. Daire, *Mater. Sci. Eng., A,* 109, **1989**, 227.

113. S. Li, R. A. Condrate, S. D. Jang, R. M. Spriggs; *J. Mater. Sci.*, 24, **1989,** 3873.

114. C. Chandler, C. Roger, M. Hamden-Smith, *Chem. Rev.*, 93, **1993,** 1205.

115. E. A. Barringer, H. K. Bowen, *Langmuir,* 1, **1985,** 420.

116. Y. Takahashi, Y. Matsuoka, *J. Mater. Sci.*, 23, **1988**, 2259.

117. Y. Li, T. J. White, S. H. Lim, *J. Solid State Chem.*, 177, **2004,**1372.

118. D. C. Hague, M. J. Mayo, *J. Am. Ceram. Soc.*, 77, **1994,** 1957.

119. M. S. Kaliszewski, A. H. Heur, *J. Am. Ceram. Soc.,*73, **1990,** 504.

120. A. P. Philipse, M.P.B. Van Bruggen, C. Pathmamanoharan, *Langmuir,*10, **1994**, 92.

121. H. Okudera, Y. Yokogawa, *Thin Solid Films*, 423, **2003**, 119.

122. M. Tonejc, I. Djerdj, A. Tonejc, *Mater. Sci. Eng. B,* 85, **2001,** 55.

123. R. Phani, S. Santucci, *Mater. Lett.*, 50, **2001**, 240.

124. Y. F. Chen, C. Y. Lee, M. Y. Yeng, H. T. Chin, *J. Cryst. Growth,* 247, **2003**, 363.

125. P. Yang, C. Lu, N. Hua, Y. Du, *Mater. Lett.*, 57, **2002**, 794.

143. F. B. Li, X. Z. Li, M. F. Hou, *Appl. Catal. B: Environ.*, 48, **2004,** 185.

144. H. Zhang, A. Reller. *J. Mater. Chem.*, 11, **2001**, 2537.

145. V. F. Stone, R. J. Davis, *Chem. Mater.*, 10, **1998,** 1468.

146. D. M. Antonelli, J. Y. Ying, *Angew. Chem. Int. Ed. Engl.*, 34, **1995,** 2014.

147. S. Sato, S. Oimatsu, R. Takahashi, T. Sodesawa, F. Nozaki., *Chem. Comm.*, **1997**, 2219.

148. R. L. Putnam, N. Nakagawa, K. M. M. McGrath, N. Yao, I. A. Aksay, S. M. Gruner, *Chem. Mater.*, 9, **1997**, 2690.

149. M. Thieme, F. Schuth, *Micropor. Mesopor. Mater.*, 27, **1999,** 193.

150. S. Cabrera, J. E. Haskouri, A. Beltran-Porter, D. Beltran-Porter, M. D. Marcos, P. Amoros, *Solid State Sci.*, 2, **2000**, 513.

151. B. Singhal, A. Porwal, A. Sharma, R. Ameta, S. C. Ameta.; *J. Photochem. Photobiol. A Chem.*, 108, **1997,** 85.

152. K. Cassiers, T. Linssen, M. Mathieu, Y. Q. Bai, H. Y. Zhu, P. Cool, *J. Phys. Chem. B.*, 108, **2004,** 3713.

153. P. Yang, D. Zhao, D. I. Margolese, B. Chmelka, G. D. Stucky, *Nature,* 396, **1998,** 152.

154. D. L. Li, H. S. Zhou, M. Hibino, I. Honma, *J. Mater. Res.*, 18, **2003,** 2743.

155. I. Kartani, P. Meredith, J. C. D. da Costa, J. S. Riches, G. Q. M. Lu, *Curr. Appl. Phys.*, 4, **2004,**160.

156. H. Thoms, M. Epple, M. Froba, J. Wong, A. Reller, *J. Mater. Chem.*, 8, **1998**, 1447.

157. L. Saadoun, J. A. Ayllon, J. Jimenez-Becerril, J. Peral, X. Domenech, R. Rodriguez-Clemente, *Appl. Catal. B Environ.*, 21, **1999**, 269.

158. J. H. Zheng, K. Y.Qiu, Y. Wei, *Mol. Cryst. Liq. Cryst.*, 354, **2000**, 183.

159. C. Wang, Q. Li, R. Wang; *J. Mater. Chem.*, 39, **2004,** 1899.

160. C. Wang, H. Xi, R. D. Wang, *Chem. Lett.*, 33, **2004,** 20.

161. R. D. Shannon, J. A. Pask, *J. Am. Ceram. Soc.*, 48, **1965,** 391.

162. X-Z. Ding, X. K. Liu, *J .Mater. Res.*, 13, **1998,** 9.

163. S. Hishita, I. Mutoh, K. Koumoto, H. Yanagida, *Ceram. Int.*, 9, **1983,** 61.

164. A. A. Gribb, J. F. Banfield, *Am. Mineral,* 82, **1997,** 717.

165. K. N. P. Kumar, *Scr. Metall. Mater.*, 32, **1995,** 873.

166. C. Suresh, V. Biju, P. Mukundan, K. G. K. Warrier, *Polyhedron,* 17, **1998,** 3131.

167. R. L. Penn, J. F. Banfield, *Am. Mineral.*, 84, **1999,** 871.

168. J. A. Gamboa, D. M Pasquevich, *J. Am. Ceram. Soc.*, 75, **1992,** 2934.

169. K. D. Shannon, *Appl. Phys.*, 35, **1964,** 3414.

170. C. Fabiana, Gennari, D. M. Pasquevich, *J. Am. Ceram. Soc.*, 82, **1999,** 1915.

171. A. J. Gamboa, D. M. Pasquevich, *J. Am.Ceram. Soc.*, 87, **2004,** 1164.

172. S. Vargas, R. Arroyo, *J. Mater. Res.*, 14, **1999,** 3932.

173. R. R. Talavera, S. Vargas, R. A. Murillo, R. M. Compose, *J. Mater. Res., 1*2, **1994,** 860.

174. R. R. Bacsa, M. Gratzel, *J. Am. Ceram. Soc.*, 79, **1996,** 2185.

175. B. L. Bischoff, M. Anderson, *Chem. Mater.*, 7, **1995,** 1772.

176. R. Zhang, L. Gao, *Mater. Res. Bull.*, 36, 11, **2001,** 1957.

177. Y.Yang, S. Mei, J. M. F. Ferreirra, *J. Am. Ceram. Soc.*, 83, **2000**,1361.

178. R. Benedix, F. Dehn, J. Quaas, M. Orgass, *Lacer*, **2000,** 5.

179. S. Vargas, R. Arroyo, *J. Mat. Res.*, 14, **1999,** 3932.

180. X. Bokhimi, *Chem. Mater.*, 9, **1997,** 2616.

181. J. Yang, J. M. F. Ferreira, *J. Mater. Sci. Lett.*, 16, **1997,** 1933.

182. J. Yang, J. M. F. Ferreira, *Mater. Res. Bull.*, 33, **1998,** 124.

183. R. R. Talavera, S. Vargas, R. A. Murillo, R. M. Campos, E. H. Poniatowski, *J. Mater. Res.*,12, **1997,** 439.

184. J. Nair, P. Nair, F. Mizukami, Y. Oosawa, T. Okubo, *Mater. Res. Bull.*, 34, **1999,** 1275.

185. F. F. Lange, M. M. Hirlinger, *J. Am. Ceram. Soc.*, 67, **1984**,127.

186. F. C. Gennari, D. M. Pasquevich, *J. Mater. Sci.*, 33, **1998**, 1571.

187. E. Sanchez, T. Lopez, R. Gomez, *J. Solid State Chem.*, 122, **1996,** 309.

188. A. M. Venezia, L. Palmisano, M. Schiavello, *J. Solid State Chem.*, 114, **1995,** 364.

189. A. Vasudevan, P. P. Rao, S. K. Ghosh, G. M. Anilkumar, A. D. Damodaran, K. G. K.Warrier, *J. Mater. Sci. Lett.*, 16, **1997,** 8.

190. R. Wang, K. Hashimoto, A. Fujishima, M. Chikuni, E. Kojima A. Kitamura, M. Shimohigoshi, T. Watanabe, *Nature*, 388, **1997**, 31.

191. R. Wang, K. Hashimoto, A. Fujishima, M. Chikuni, E. Kojima, A. Kitamura, M. Shimohigoshi, T. Watanabe, *Adv. Mater.*, 10, **1998,** 135.

192. R. Wang, N. Sakai, A. Fujishima, T. Watanabe, K. Hashimoto, *J. Phys. Chem. B,* 103, **1999,** 2188.

193. N. Stevens, C. L. Priest, R. Sedev, J. Ralston, *Langmuir,* 19, **2003,** 3272.

194. X. S. Peng, A. C. Chen, *J. Mater. Chem.*, 14, **2004,** 2542.

195. S. Hata, Y. Kai, I.Yamanaka, H.Oosaki, K. Hirota, S. Yamazaki, *JSAE Review,* 21, **2000,** 97.

196. S. S. X. Chiaro, *Studies in Surf. Sci. Catal.*, 153, **1995,**165.

197. M. Machinda, W. K. Norimoto, T. Kimura, *J. Am. Ceram. Soc.*, 88, **2005,** 95.

198. K. P. Yu, W. M. Lee, W. M. Huang, C. C. Wu, C. L. Lou, S. H. Yang, *J. Air Waste Manage.*, 56, **2006,** 666.

199. C. J. Brinker, R. Sehgal, S. L. Hietala, R. Deshpande, D. M. Smith, D. Loy , C. S. Ashley, *J. Membrane Sci.*, 94, **1994,** 85.

200. A. Imhof, D. J. Pine, *Nature,* 389, **1997,** 948.

Chapter 2: Aqueous Sol-gel Synthesis of Nanocrystalline Titania from Titanyl Sulphate

2.1 Abstract

An aqueous sol-gel method based on hydrolysis-peptisation has been developed for the preparation of nanocrystalline titania using titanyl sulphate as precursor. The stability of the sol has been monitored using the zeta potential measurement. The sol has been stabilized in acidic and basic pH range. A stable titania sol with extremely narrow range of distribution of particles having an average size of 27 nm has been obtained at a pH range 1.8 to 2.2. Thermo gravimetric and differential thermal analyses were used for the characterisation of the sol-gel derived titania powder. X-ray diffraction analysis has been used for the phase identification of the titania sample heated at different temperatures. The crystalline anatase particles have average particle size of 12–32 nm and specific surface area of 48.7– 6.5 m^2g^{-1} between the calcination temperature 500–700 °C. The type IV isotherm indicates the mesoporous nature of the powder obtained through the present method. Transmission electron microscope image indicates that titania obtained through the present method after calcining at 600 °C have a crystallite size of 23 nm.

2.2 Introduction

Nanocrystalline anatase titania becomes increasingly important because of its potential application in catalysis/photocatalysis, coating for self-cleaning surfaces, ceramic membranes and sensors.[1-4] Crystalline structure, particle size, surface area, porosity, thermal stability and morphology of the titania determine their efficiency in

vivid applications. In developing novel catalytic/ photocatalytic systems, it is essential to develop a titania with possible higher surface area or equivalently, the smallest particle size.[5] Sol–gel method has become one of the successful and simple technique for preparing nanosized titania.[6] Most of the earlier attempts used titanium alkoxides as precursors in the sol–gel route. The novel approach to start from titanyl sulphate ($TiOSO_4$) or chloride ($TiCl_4$) followed by peptisation through aqueous medium to the pure anatase phase appears to be very interesting. In 1998, Tsevis et al.[7] investigated the preparation and characterisation of anatase powder starting from $TiOSO_4$ by hydrolysis with KOH and they obtained relatively high surface area ranging from 135 to 250 m^2g^{-1} but the method leads to preparation of bulk powders. Titania particles where prepared by controlling the hydrolysis conditions of the precursor and by using different catalysts. They were then characterized by X-ray diffraction and hence the structural parameters, concentration of anatase-rutile phases and average crystal size of titania were obtained.[8] Titania particles of submicron size have been prepared by aging a highly acidic solution of $TiCl_4$ at 95 °C by using sulphate ion as control agent.[9] Controlled hydrolysis of $TiCl_4$ below 0 °C resulted in nanosized anatase, but failed to hold the reproducibility of the anatase particle size.[10] Li et al.[11] reported a novel method for the preparation of nanocrystalline rutile titania powders by liquid hydrolysis of $TiCl_4$. The nanocrystalline nature of titania obtained by sol-gel method was examined using HRTEM, BET surface area analysis and XRD techniques[12] and found that the specific surface area from its intial value of 169 m^2g^{-1} at low temperature calcination of the gel got reduced to 2.7 m^2g^{-1} at 983K. The size of anatase crystallite changed from 4.5 to 6.5 nm. Studies based on electron microscopy and atomic force microscopy indicate that the size of titania also

depends on temperature of processing.[13] In the range 290K to 820K, the titania grains consisted of anatase and brookite phase. High resolution electron microscopy showed that sample gel heated to 573 K had grain sizes in the range of 4.5-7 nm which increased to 7-12 nm with an average of 9 nm when heated to 820 K and had pore sizes between 6-10 nm.[14] Possibility of obtaining rutile form of titania was also reported starting from titanyl salts.[15] Park et al.[16] reported thermal hydrolysis of $Ti(SO_4)_2$ at 80 °C in a mixed solvent of n-propyl alcohol and water. The as precipitated powder was amorphous hydrates of titania and were crystallised by calcination into anatase (>600 °C) and rutile (>800 °C). Wei et al.[17] prepared nanodispersed spherical TiO_2 powder, of average particle size of 80 nm, by forced hydrolysis of $Ti(SO_4)_2$ aqueous solution containing sulfuric acid under boiling reflux condition. Iwasaki et al.[18] synthesized nanocrystalline anatase by thermal hydrolysis of titanylsulphate in a mixed solution of alcohol and water. The size of the anatase crystallites was controlled between 2 and 7 nm, by adjusting the preparation conditions such as water/alcohol ratio and reflux time. The powder after calcinations at 400 °C had a specific surface area of 68 m^2g^{-1}, which reduced to 30 m^2g^{-1}on further calcination at 600 °C. Earlier, Kato et al.[19] reported the formation of spherical TiO_2 powders from an aqueous solution of titanyl sulfate by homogeneous precipitation using urea as the precipitating agent and claimed the essential presence of urea for obtaining spherical particles. Recently, the photoactivity of titania derived from titanylsulphate by thermal hydrolysis and precipitation has been reported, but these methods lead to bulk titania powders.[20-23] In this chapter we presented a new aqueous sol-gel method for the synthesis of nanosized anatase titania by homogeneous precipitation of titanyl sulphate

solution at room temperature. This method is useful for preparation of photoactive nanopowder, dense and porous coatings as well as photoactive nanodispersions.

2.3 Experimental

Titanyl sulphate (Aldrich Chemicals, 99.99 % purity) was dissolved in 500 ml of doubly distilled water (0.2 M) and was subjected to precipitation by the slow addition of ammonium hydroxide (sd Fine chemicals, 25%, India Ltd) solution under constant stirring at room temperature (32 °C). The hydrolysis was controlled with the addition of NH_4OH (sd Fine chemicals, 25%, India Ltd), until the reaction mixture attains a pH 8.5. The precipitate obtained was separated by filtration, and washed repeatedly with distilled water until the precipitate becomes free of sulfate ion (confirmed by $BaCl_2$ test). The peptisation of the precipitate was done by dispersing the precipitate in 1000 ml of hot distilled water by adjusting the pH in the acidic and basic range using HNO_3 (GR Merck, 69%, India Ltd) and Ammonia (sd Fine chemicals, 25%, India Ltd) solution respectively . Stability of the sol was followed by zeta potential measurement at different pH values using Malvern Zetasizer 3000HS (U.K). Sol particle size distribution was analysed by Malvern 3000 HS (U.K) particle size analyser. The sol to gel conversion was achieved by drying the sol in a water bath. The gel was again dried at 70 °C in an oven over a period of 24h. Thermal analysis of the gel was carried out in flowing nitrogen gas at a heating rate of 10 °C min^{-1} in Shimadzu TG /DT 50H thermal analyzer. The dried gel was then calcined at 500, 600, 700, 800 and 850 °C in separate batches for 1h with a heating rate of 10 °C min^{-1}. The flow chart for the preparation for stable titania sol is provided in Figure 2.1.

The gel and the calcined powders were characterised by powder X-ray diffraction, thermal analysis and N_2 adsorption surface area analysis. XRD patterns were obtained with a Philips PW 1710 diffractometer, using Ni-filtered Cu Kα radiation, and the crystallite size was calculated using Scherrer formula as given in equation 2.1.[24]

$$\Phi = K\lambda / \beta \cos\theta \qquad (2.1)$$

where K is the shape factor taken as 0.9 for the calculations presented, λ the wavelength of the X-ray, β the full width at half maxima, and θ the diffracting angle.

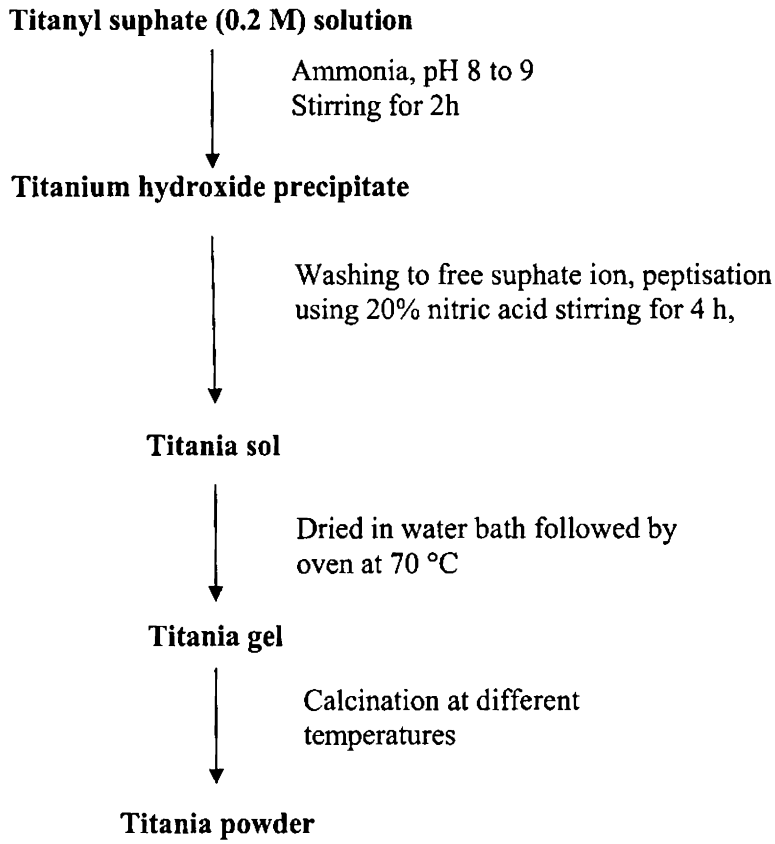

Figure 2.1. Flow chart for the preparation of titania sol

The rutile fraction in the sample was determined by measuring the XRD intensities of anatase (101) and rutile (110) from the equation 2.2.[25]

$$W_R = 1/1 + 0.8(I_A/I_R) \qquad (2.2)$$

where W_R is the weight fraction of the rutile present, I_A and I_R are the X-ray integrated intensities of anatase 101 plane and rutile 110 plane respectively. IR spectra were recorded in a Nicolet Magna 560, FTIR spectrometer in the range 400-4000 cm^{-1} on powders dispersed in KBr pellets. Surface area and pore analysis of the samples were carried out by N_2 adsorption in a Micromeritics Gemini 2375 surface area analyzer after degassing the samples at 200 °C for 2h. The TEM observation of the calcined titania powder was performed on a Hitachi HF 2200 TU field emission microscope operating at an accelerating voltage of 200 kV.

2.4 Results and Discussion

2.4.1 Zeta Potential, particle size Vs pH of the sol

Most particles dispersed in an aqueous system will acquire a surface charge, principally either by ionization of surface groups, or adsorption of charged species. These surface charges modify the distribution of the surrounding ions, resulting in a layer around the particle that is different from the bulk solution. If the particle moves, under Brownian motion, this layer also moves as part of the particle. The zeta potential is the potential at point in this layer where it moves past the bulk solution.[26] This is usually called the slipping plane. The charge at this plane will be very sensitive to the concentration and type of ions in solution. A schematic representation of the origin of zeta potential is given in Figure 2.2. Zeta potential is one of the main forces that mediate interparticle interactions. Particles with a high zeta potential of the same charge sign,

either positive or negative, will repel each other. Conventionally a high zeta potential can be high in a positive or negative sense, i.e., <-30mV and >+30mV would both be considered as high zeta potentials. For molecules and particles that are small enough, and of low enough density to remain in suspension, a high zeta potential will confer stability, i.e. the solution or dispersion will resist aggregation. So zeta potential is the measure of stability of colloidal particle in the suspension.

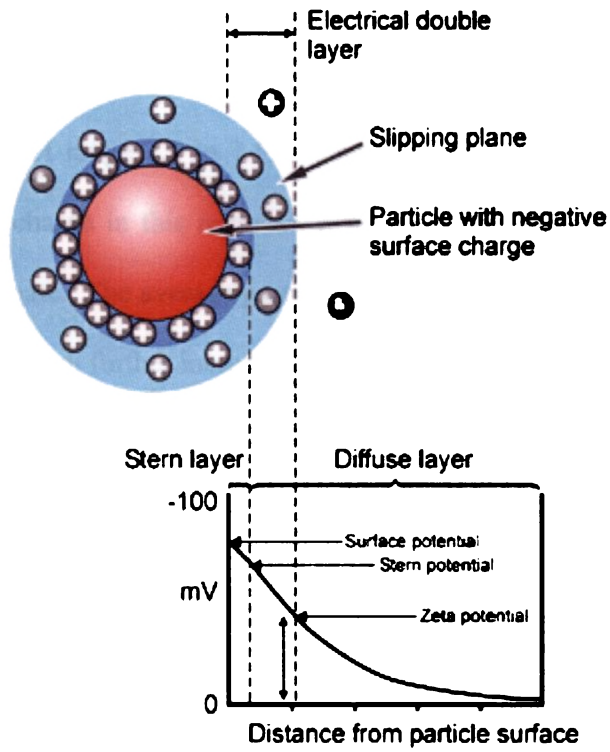

Figure 2.2. Schematic representation of the origin of zeta potential[26, 27]

Zeta potential and particle size against pH of titania particle was given in the Figure 2.3. It shows that at lower pH below 2.5 and higher pH above 7.5 the particle shows a zeta potential value above ± 30mV which indicates that the peptisation of the particle below pH 2.5 and above pH 7.5 may leads to stable colloid. From these observations we can conclude that at lower pH, the preferential absorption of H^+ ion on to

the surface of the titania particle from HNO_3 (used for peptisation) increases the surface charges and makes the particles repel each other and stay apart, i.e., the electrostatic stabilization occur. The zeta potential value indicates that the preferential adsorption of ions on the surface of the particles increases the zeta potential value above +30 mV. The same phenomena happened in the higher pH range also, where the preferential absorption of hydroxyl species from ammonium hydroxide (used for peptisation) on the surface increases the zeta potential value in the negative region. Zeta potential value between pH 2.5 to 7.5 also shows a value between +30 mV and -30 mV. The particle size number also indicates that in the pH range 2.5 to 7.5, the particles are aggregated, which is due to lowering of surface charge in this region which makes the particles to come closer to each other and aggregate. The average particle size increases from 27 nm obtained at pH 2 to 490 nm at pH 3 which further increases to 1250 nm at pH 6.5. However at pH 8.5 the average particle size has a value of 130 nm. The particle size distribution is given in Figure 2.4. It indicates that in the pH range 2.5 to 7.5, the surface charge is not enough to keep the particle apart.

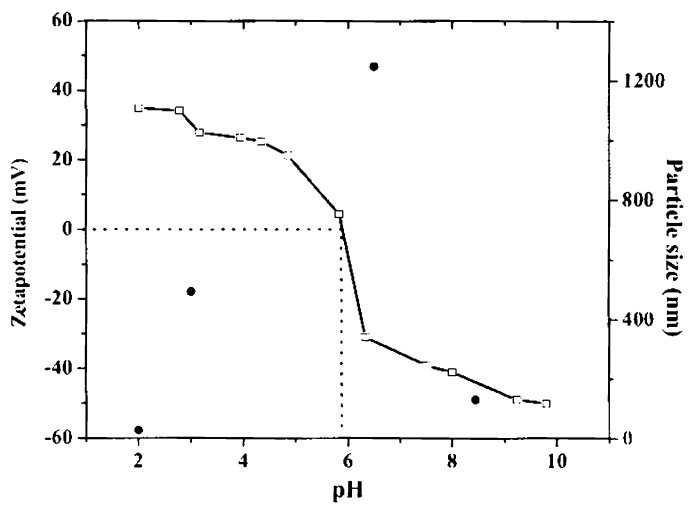

Figure 2.3. Zeta potential and particle size of titania colloids as a function of pH.

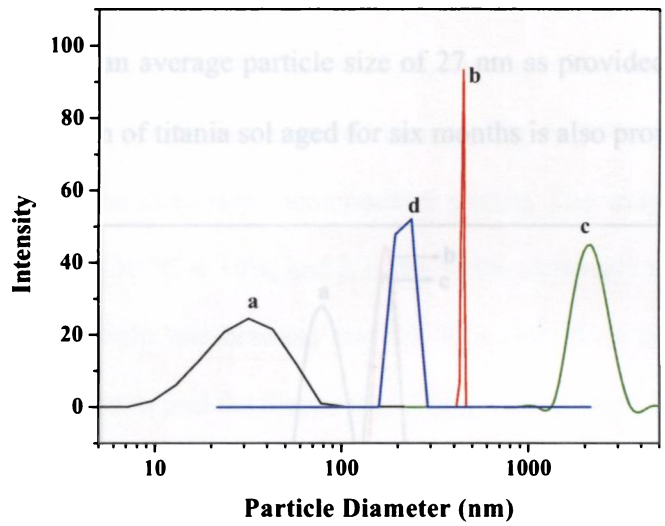

Figure 2.4. Particle size distribution curve of titania at (a) pH 2 (b) pH 3 (c) pH 6.5 and (d) pH 8.5.

The photograph of the titania nanoparticles peptised at different pH is given in Figure 2.5. From this photograph we can see that in between pH 2.5 and 7.5 the titania particles gets aggregated and settle down.

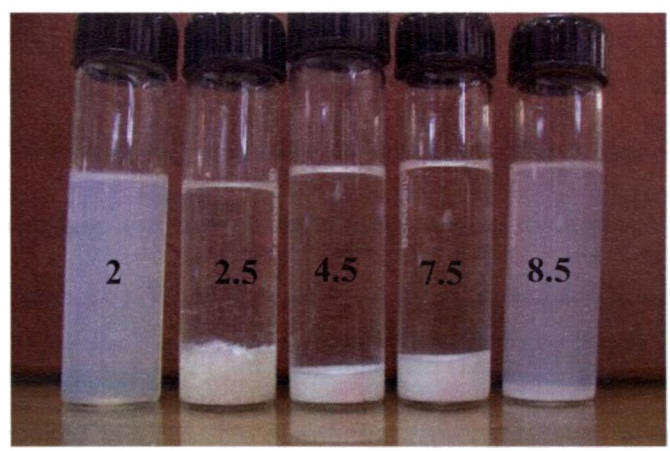

Figure 2.5. Photograph of the titania nanoparticles peptised at different pH (i) 2 (ii) 2.5 (iii) 4.5 (iv) 7.5 (v) 8.5

For further studies, the region related to lowest particle size which is at pH 2, was selected for the peptisation of particle. A monomodal distribution of particles was obtained at pH 2 with an average particle size of 27 nm as provided in Figure 2.6a. The particle size distribution of titania sol aged for six months is also provided in Figure 2.6.

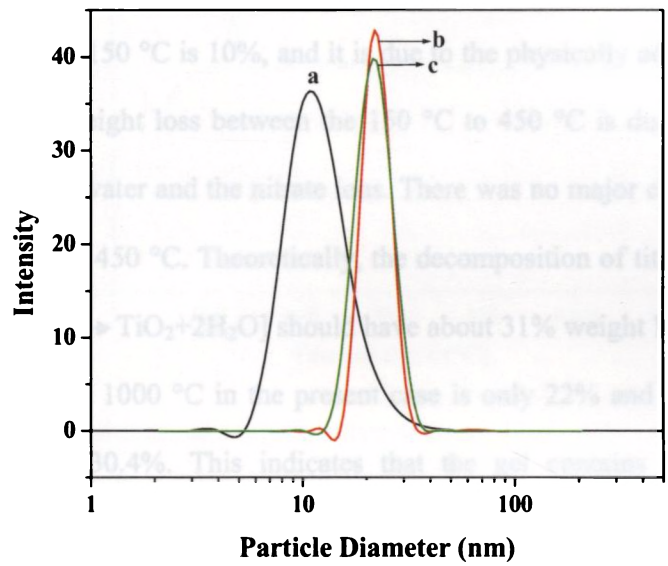

Figure 2.6. Particle size distribution curve of titania sol (a) at pH 2 (b) aged for six months and (c) aged for six months after ultrasonication for 10 min.

We could not observe any visible sedimentation or flocculation even after keeping the sol for six months. There was, however, a very slow tendency for the sol particles to undergo particle growth resulting in a slightly higher monomodal distribution of average size of about 32.7 nm (Figure 2.6). When this sol was ultrasonicated for 10 min, titania particles with an average particle size of 29 nm were obtained (Figure 2.6) This increase in particle size could be attributed to a possible dissolution-reprecipitation process occurring in the sol, on the larger particles at the expense of smaller particles.[28]

This is supported by the observations from the X-ray diffraction pattern of gel (Fig. 2.9) which gave well-defined anatase peaks.

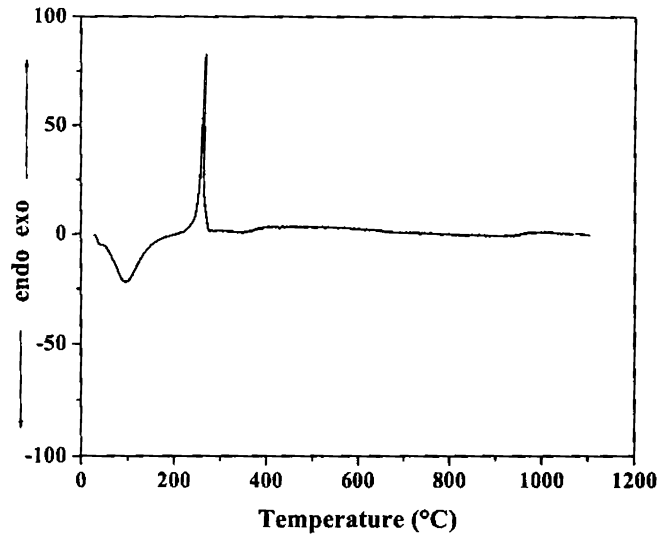

Figure 2.8. Differential thermal analysis curve of dried titania sol

The DTA analysis shows (Figure 2.8) an endothermic peak below 150 °C is due to the removal of physically adsorbed water in the titania gel matrix. An exothermic peak in the region 270 °C is due to the evoluation of nitrate used for peptisation of the sol.

2.4.3 X-ray Diffraction analysis

The X-ray diffraction pattern of anatase phase of titania has a main peak at 2θ = 25.2° corresponding to the 101 planes (JCPDS 21-1272) and the main peak of rutile phase is due to its 110 planes (JCPDS 21-1276) present at 2θ = 27.4°. X-ray diffraction patterns of the gel and the calcined powders are presented in Figure 2.9. A broad peak corresponding to the 101 plane peak of anatase phase is found in the X-ray diffraction pattern of 70 °C dried gel. This clearly indicates that the crystalline anatase is formed in the dried gel even at this low temperature. After calcination at 500 °C the crystalline

nature of titania increases, which resulted in distinct anatase peak in the X-ray diffraction pattern.

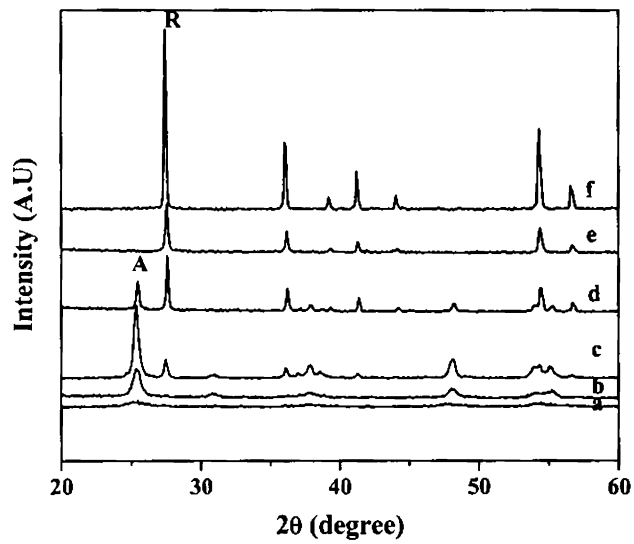

Figure 2.9. X-ray diffraction pattern of titania calcined at different temperatures (a) 70 (b) 500 (c) 600 (d) 700 (e) 800 (f) 850 °C. A stands for Anatase (101) plane and R is for Rutile (110) plane

At 600 °C the anatase to rutile conversion starts and about 28% rutile was present in the system after calcination at 600 °C for 1h. While 71 % of titania is present in the rutile phase after calcination at 700 °C, the titania completely transformed to rutile phase at 800 °C. The anatase to rutile ratio and crystallite size calculated using Scherrer equation are given in Table 2.1. The crystallite size also increases with temperature and it is 12.8 nm at 500 °C and it further increased to 20 nm after 600 °C calcination. One of the important observations is that the phase transformation also occurs from anatase to rutile in this temperature range. On heating, anatase irreversibly transforms into rutile with a moderate exothermic contribution. As reported in the literature, anatase to rutile phase transformation occurs at a temperature between 500 and 800 °C.[31]

Table 2.1. Anatase to rutile percentages and crystallite size of titania calcined at various temperatures

Calcination Temp. (°C)	Anatase: Rutile ratio	Crystallite Size of anatase (nm)
70	100:0	6
500	100:0	12.8
600	72:28	20
700	29:71	31.1
800	0:100	Rutile

However, it was recently demonstrated that a very low particle size (below 14 nm) causes the anatase phase to be thermodynamically stable.[32] This may be the reason for the phase transformation occuring between 500 to 600 °C.

2.4.4 FTIR spectroscopy

The IR spectra of gels calcined at various temperatures presented in Figure 2.10a indicate a broad band between 3500 and 3000 cm^{-1}, which is due to the presence of –OH groups on the surface of titania.[33-35] The δH_2O band around 1620 cm^{-1} demonstrates the presence of molecularly adsorbed water in the dried gel.[35] The shift of the νOH bands from 3750–3600 to around 3200 cm^{-1} is due to the presence of hydrogen bonding.[36] On calcination at high temperature (Figure 2.10b & c), the peaks get sharpened with less intensity, indicating the removal of –OH groups from the surface. Calcination to high temperatures decreased the intensity of the 1624 cm^{-1} band (Fig. 2.10). The presence of small absorbance in the high temperature calcined samples around 1600 cm^{-1} may be due to the water adsorption on dehydroxylated anatase.[37]

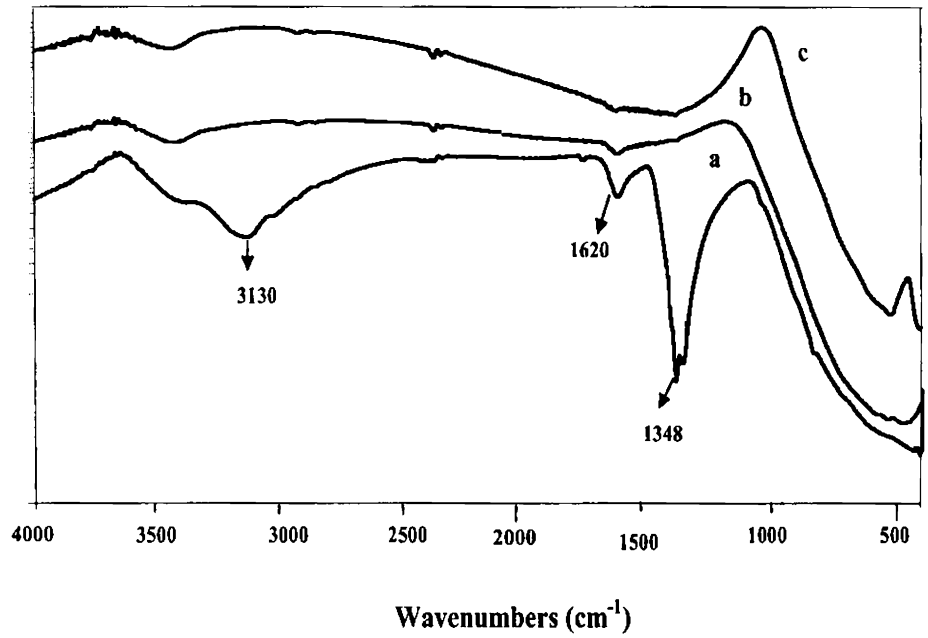

Figure 2.10. FTIR spectrum of the gel calcined at (a) 70 °C (b) 500 °C (c) 800 °C

The sharp absorbance at 1348 cm^{-1} in the gel (Fig. 2.10a) is due to the presence of nitrate species and is completely absent in the calcined samples. Ti–O–Ti bonds appear in the range 400–600 cm^{-1} and the sharpness of the peak increases with increase of calcination temperature. No characteristic peaks corresponding to chemisorbed SO_4^{2-} ions (1230, 1135, 1050 cm^{-1}) were observed in the prepared gel, [38] indicating that the surface of anatase is SO_4^{2-} free.

2.4.5 BET surface area analysis

Textural characteristics of the samples calcined at 500, 600,700 and 800 °C derived from N_2. adsorption analysis is presented in Table 2.2. Specific surface area (S_{BET}), total pore volume calculated at $p/p_0 = 0.99$, BJH mesopore volume and micro pore

volume which were calculated by t-plot method and average pore diameter values are presented in Table 2.2.

Table 2.2. N_2 adsorption characteristics of titania with calcination temperature

Temp. °C	BET surface area (m^2g^{-1})	Total pore volume (cm^3g^{-1})	Micro pore volume (cm^3g^{-1})	Meso pore volume (cm^3g^{-1})	Average Pore size (nm)
500	48.7	0.1084	0.00392	0.1045	7.9
600	19.1	0.0478	0.00015	0.0477	10
700	6.51	0.0267	0.0005	0.0262	16.3
800	Very low				

On increasing the temperature, the surface area, total pore volume and mesopore volume also decrease. This may be due to an increase in crystallite size and densification or collapse in pore structure of titania. The adsorption isotherms (Figure 2.11) of the samples show type IV behaviour with typical hysteresis loop. This hysteresis loop is characteristic of mesoporous materials.[39]

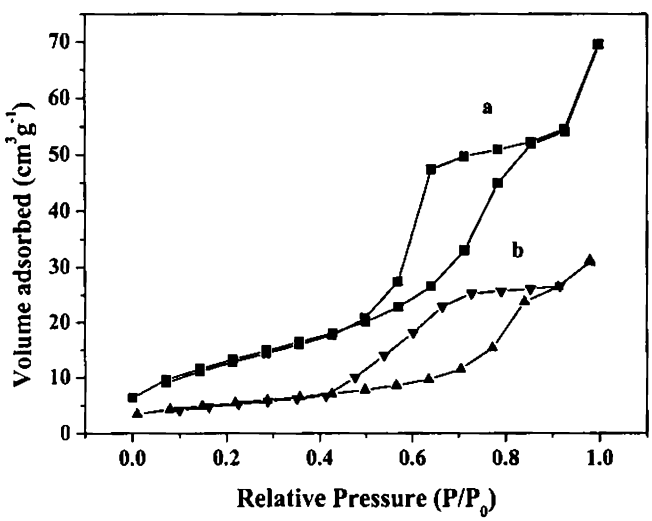

Figure 2.11. Adsorption isotherm of titania calcined at (a) 500 (b) 600 °C

The mesopore contributions towards the surface area of these samples are greater than that of the micropores. This is corroborated from mesopore volume and the micropore volume calculated by t-plot method. The micropore analysis indicated that the micropore volume decreases with increase of calcinations temperature, and is an evidence of the gradual collapse of the gel network when subjected to high temperature treatment. Titania powder calcined at 800 °C becomes almost nonporous as evidenced from the very low surface area which is less than 1 m^2g^{-1}, and it is not possible to measure through our BET surface area analyser.

2.4.6 Transmission Electron Micrographs

The Transmission electron microscope images of titania sample calcined at 600 °C are presented in Figure 2.12. The bright field image indicate the mesoporous nature of the titania (Figure 2.12.A). The titania has a crystallite size of 23 nm.

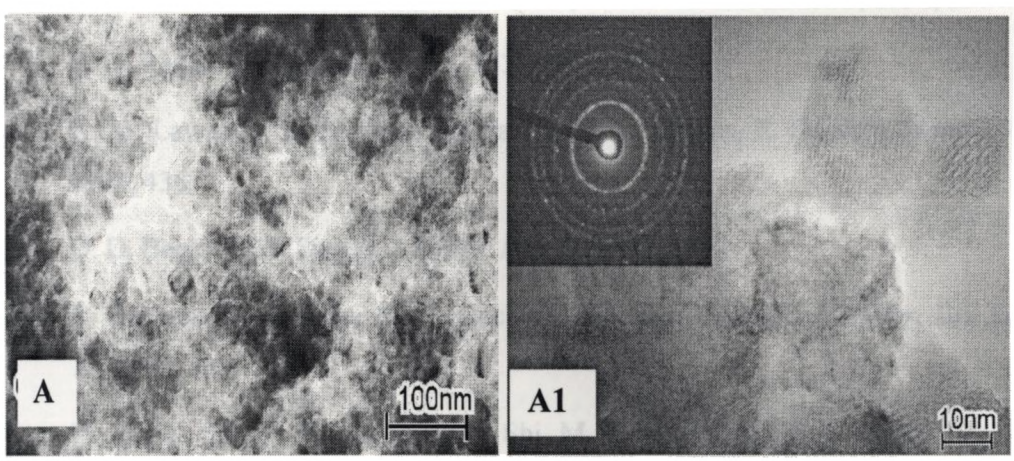

Figure 2.12. TEM images of the titania sample calcined at 600 °C

The electron diffraction image (Figure 2.12.A1) indicates that the titania sample is crystallized and sharp diffraction pattern indicates the crystallinity.

2.5 Conclusion

An aqueous sol-gel method for the preparation of titania sol using titanyl sulphate precursor was successfully developed. The stability of the sol was monitored using zeta potential measurement. The sol is stabilized both in acidic (below pH 2.5) and basic (above pH 7.5) region and the smallest particle size was obtained in the acidic range. An average particle size of 27 nm was obtained for the sol peptised at pH 2. The sol was aged for about 6 months and it was found that the sol was very stable. The X-ray diffraction image indicates that the anatase to rutile phase transformation starts above 500 °C and completes at 800 °C. The Transmission electron micrograph image indicates that the average crystallite size of titania prepared through aqueous sol-gel method is 23 nm at 600 °C.

2.6 References

1. L. D. Brikefield, A. M. Azad, S. A. Akbar, *J. Am. Ceram. Soc.,* 75, **1992,** 2964.
2. B. O. Regan, M. Gratzel, *Nature,* 353, **1991,** 737.
3. N. M. Lawandy, R. M. Balachandran, A. S. L. Gomes, E. Sauvaln, *Nature* 368, **1994**, 436.
4. D. D. Beck, R. W. Siegel, *J. Mater. Res.*, 7, **1992,** 2840.
5. S. Gablenz, D. Vollzke, H. P. Abicht, J. Neumann-Zdralek, *J. Mater. Sci. Lett.,* 17, **1998,** 537.
6. N. Xu, Z. Shi, Y. Fan, J. Dong, J. Shi, M. Z. C. Hu, *Ind. Eng. Chem. Res.,* 38, **1999,** 373.
7. A. Tsevis, N. Spanos, P.G. Koutsoukos, Ab J. van der Linde, J. Lyklema, *J. Chem. Soc. Faraday Trans.,* 94, **1998,** 295.
8. B. A. Morales, O. Novano, T. lopez, E. Sanchez, R. Gomez., *J. Mater. Res.,*10, **1995,** 2788.

9. E. Matijevic, M. Budnik, L. Meites, *J. Colloid Interfac. Sci.*, 61, **1977**, 302.

10. N. Serpone, D. Lawless, R. Khairutdinov, *J. Phys. Chem.*, 99, **1995**, 16646.

11. Y. Li, Y. Fan, Y. Chen, *J. Mater. Chem.*, 12, **2002**, 1387.

12. A. M. Tonejc, A. Tonejc, A. Turkovic, M. Gotic, S. Music, M. Vukovic, R. Trojko, *Mater. Lett.*, 31, **1997**, 127.

13. C. Li, M. Li, *Chinese Ceram. Soc.*, 24, **1996**, 338.

14. A. M. Tonejc, M. Goti, B. Grzeta, S. Music, S. Popovi, R. Trojko, A. Turkovic, I. Musevic., *Mater. Sci. Engg. B*, 40C, **1996**, 177.

15. S. J. Kim, S. D. Park, Y. H. Jeong, *J. Am. Ceram. Soc.*, 82, **1999**, 927.

16. H. K. Park, V. T. Moon, C. H. Kin, *J. Am. Ceram. Soc.*, 79, **1996**, 2727.

17. Y. Wei, R. Wu, Y. Zang, *Mater. Lett.*, 41, **1999**, 101.

18. M. Iwasaki, M. Hara, S. Ito, *J. Mater. Sci. Lett.*, 17, **1998**, 1769.

19. A. Kato, Y. Takshita, Y. Katatae, *Mater. Res. Soc. Symp. Proc.*,155, **1989**, 13.

20. J. Krysa, M. Keppert, J. Jirkovsky, V. Stengl, J. Subrt, *Mater. Chem. Phys.*, 86, **2004**, 333.

21. G. N. Kryukova, G. A. Zenkovets, A. A. Shutilov, M. Wilde, K. Gunther, D. Fassler, K. Richter, *Appl. Catal. B Environ.*, 71, **2007**, 169.

22. S. Sakthivel, M. C. Hidalgo, D. W. Bahnemann, S.-U. Geissen, V. Murugesan, A. Vogelpohl, *Appl. Catal. B: Environ.*, 63, **2006**, 31.

23. Q. Zhang, L. Gao, *J. Eur. Ceram. Soc.*, 26, **2006**, 1535.

24. W. Bai, K. L. Choy, N. H. J. Sytelzer, J. Schoonman, *Solid State Ionics*, 116, **1999**, 225.

25. R. A. Spurr, H. Myers, *Anal. Chem.*, 29, **1957**, 760.

26. E. J. W. Verway, J. Th. G. Overbeek, *Theory of the Stability of Lyophobic Colloids*, Elsevier, Amsterdam, **1948**.

27. J. Lyklema, *Fundamentals of Interface and Colloid Science: Volume1 (Fundamentals),* Academic Press, UK, **2000.**

28. S. M. Klein, J. H. Choi, D. J. Pine, F. F. J. Lange, *Mater. Res.,* 18, **2003,** 1457.

29. X. Liu, X. Wang, J. Zhang, X. Hu, L. Lu, *Thermochim. Acta,* 342, **1999**, 67.

30. X. Liu, J. Yang, L. Wang, X. Yang, L. Lu, X. Wang, *Mater. Sci. Eng. A,* 289, **2000,** 241.

31. P. I. Gouma, P. K. Dutta, M. J. Mills, *Nanostruct. Mater.*,11, **1999,** 1231.

32. H. Zhang, J. Banfield, *J. Mater. Chem.*, 8, **1998,** 2073.

33. M. Primet, P. Pichat, M. V. Mathieu, *J. Phys. Chem.,* 75, **1971,** 1216.

34. D. J. C. Yates, *J. Phys. Chem.,* 65, **1967,** 746.

35. C. Morterra, *J. Chem. Soc. Faraday Trans.,* 84, **1988,** 1617.

36. A. G. Alejandre, M. Trombetta, G. Busca, J. Ramirez, *Micropor. Mater.,* 12, **1997**, 79.

37. K. I. Hadjiivanov, D. G. Klissurski, *Chem. Soc. Rev.,* **1996,** 61.

38. T. Yamaguchi, T. Jin, T. Ishida, K. Tanabe, *Mater. Chem. Phys.,* 17, **1987**, 3.

39. S. J. Gregg, K. S. W. Sing, *Adsorption, Surface area and Porosity*, IInd Ed., Academic Press, **1982**.

Chapter 3: Incorporation of Selective Ions in Aqueous Sol-gel Titania

3.1 Abstract

In the present chapter the effect of doping of tantalum (Ta^{5+}, oxidation state of 5^{+}, ionic radius, 0.061nm) and two lanthanide ions gadolinium and ytterbium (Gd^{3+}, Yb^{3+} oxidation state 3^{+}, ionic radius, 0.094 and 0.081nm respectively) on the crystallite size, anatase to rutile phase transformation, surface area and photocatalytic property of aqueous sol-gel derived titania were investigated. Tantalum doping increases the anatase phase stability above 1000 °C, while gadolinium and ytterbium effectively hinder the anatase to rutile phase transformation upto 900 °C. Titania has a lower crystallite size in presence of these dopants and the anatase to rutile phase transformation initiates when the anatase grain reaches a critical size of ~12-20 nm in all compositions. The tantalum, gadolinium and ytterbium doped titania also has higher surface area than pure titania. The adsorption isotherms obtained are all typical of mesoporous materials. The total acidity, measured using pyridine adsorption followed by FTIR analysis indicate that doping with tantalum, gadolinium and ytterbium increases the number of acidic sites in titania. Brønsted acidity has been determined using 2,6-dimethyl pyridine as a probe molecule, followed by thermo gravimetric analysis. The photocatalytic property of titania was studied using methylene blue degradation and was compared with undoped and the commercially available Hombikat UV 100 titania.

3.2 Introduction

Titania is well known for its catalytic[1] and photocatalytic applications [2-4] like remediation of contaminants such as phenols, aromatic carboxylic acids, dyes, surfactants

and pesticides.[5-7] For an efficient photocatalytic titania, features such as predominant anatase phase, high surface area, mesoporous structure and particle size in the nanosize range are desirable along with a high anatase to rutile transformation temperature when uses are envisaged at high temperatures.[8,9] Many experimental results are reported for increasing photoactivity by selective doping with metal ions and oxides like Cr^{3+}, Fe^{3+}, Sb^{5+}, Pt, Si^{4+}, Mo^{5+}, WO_3, La^{3+}, Eu^{3+}, Nd^{3+}, Pr^{3+} , Er^{3+}, Dy^{3+}, ZrO_2.[10-18] The change in electrical property of titania with the addition of tantalum seems to be the more prominent interest in the tantalum doped titania system according to literature.[19,20] Bonini et al.[21] used a laser induced pyrolysis method for the preparation of tantalum doped titania and investigated the electrical conduction property as well as extent of inhibition of anatase to rutile phase transformation for use in CO and NO_2 sensing. XAS investigation on tantalum and niobium doped titania prepared by alkoxide sol-gel process indicates that the dopants substitute the Ti cations in the +5 valence state.[22] Further, anatase to rutile phase transformation and grain growth were found to be hindered by tantalum doping.[23] Thus from the earlier reports on tantalum doped titania, it can be seen that no significant investigations have been carried out with respect to photoactivity of these systems. Recently, Visinescu et al.[24] studied the photoactivity of dc sputtered tantalum doped titania films and Wang et al.[25] reported the photoactivity of polymer templated titania/ tantalum mixed oxide. Wang explained the high photoactivity of the mixed oxide system by considering the change in optical property and surface area. The photo catalytic property of the tantalum doped titania prepared through an aqueous sol-gel method i.e. all salt precursors, is yet to be reported. Effect of lanthanides on the anatase to rutile phase transformation and the photoactivity of titania has been subjected to investigation by

different researchers.[26-33] Effect of rare earth oxides in the anatase to rutile phase transformation was studied by Hishita et al.[34] Recently, Zhang et al.[35] reported the anatase phase stability and photoactivity of alkoxide derived Gd^{3+} and Yb^{3+}doped titania, but effects of textural properties were overlooked. In this chapter an alkoxide free sol-gel method for the preparation of tantalum, gadolinium and ytterbium doped titania in aqueous medium is presented along with its effect on anatase to rutile phase transformation, specific surface area, acidity and finally, photocatalytic activity.

3.3 Experimental

Titanyl oxysulphate ($TiOSO_4$, Aldrich Chemicals, 99.9% purity) was used as precursor for the synthesis of titania sol. In a typical experiment, titanyl oxysulphate was dissolved in 500 ml of distilled water (0.2 M) and hydrolysed by slow addition of ammonium hydroxide (25%, sd Fine Chemicals, India Ltd) solution under constant stirring at room temperature (32 °C), until the reaction mixture attained pH 8.5. The precipitate obtained was separated by filtration and was washed free of sulphate ions (confirmed by the $BaCl_2$ test) with distilled water. The precipitate was further peptised in 1000 ml of hot distilled water by the addition of 10% HNO_3 (Merck, India Ltd) solution. A stable sol was obtained in the pH range 1.7 to 2.2. Tantalum oxalate (M/s CMET, Hyderabad, AR grade) in oxalic acid was used as precursor for tantalum ions and the corresponding nitrate solutions were used as precursors for gadolinium (Aldrich Chemicals, 99.99% purity) and ytterbium (Aldrich Chemicals, 99.99% purity). The precursor solution of the respective dopant was added drop wise to the titania sol and kept under stirring for a period of 1h to obtain the doped compositions. Compositions containing 1, 2, 5 and 10 mol% of the dopant was prepared for all dopants. The sols were

concentrated over steam bath and subsequently dried in an electric hot air oven at 70 °C to obtain the xerogel. Thermal analyses of the gels were done at a rate of 10 °Cmin^{-1}. A Shimadzu, TGA 50H, Japan was used for the thermogravimetric analysis, while a Shimadzu, DTA 50H, Japan was used for the differential thermal analysis. To study the effect of calcination temperature these gels were calcined at different temperatures from 500 °C to 1100 °C and a heating rate of 10 °C min^{-1} was used with soaking for 1h at the peak temperature. The surface area measurements and pore analysis were carried out by nitrogen adsorption method using Micromeritics Gemini 2375 surface area analyser after degassing at 200 °C for 2 h. XRD patterns of the calcined gels were recorded on a Philips X' pert X-ray diffractometer in the 2θ range 20-60° using Cu Kα radiation. The amount of rutile in the sample was estimated using the Spurr equation (3.1).[36]

$$F_R = 1/ [1+ \{0.8\, I_A(101)/ I_R(110)\}] \qquad (3.1)$$

where, F_R is the mass fraction of rutile in the sample and I_A (101) and I_R (110) are the integrated main peak intensities of anatase and rutile respectively. The crystallite size was calculated using the Scherrer equation (3.2).[37]

$$\Phi = K\lambda / \beta \cos \theta \qquad (3.2)$$

where K is the shape factor taken as 0.9 for the calculations presented, λ the wavelength of the X-ray, β the full width at half maxima, and θ the diffracting angle.

The Transmission Electron Micrographs of the calcined titania powder was taken using a Hitachi HF 2200 TU field emission microscope operating at an accelerating voltage of 200 kV. The diffuse reflectance spectrum was recorded on a UV-visible spectrometer (Shimadzu, Japan, UV-2401 PC) using $BaSO_4$ as standard. Surface acidity of the system was determined using pyridine adsorption method. Samples were placed in a chamber

with saturated pyridine atmosphere at 50 °C for a period of 48h. The chamber was then evacuated using a vaccum pump for 2h. The titania samples were then mixed with KBr and pressed into the shape of pellets of diameter 10 mm and analysed in an FTIR spectrophotometer (Nicolet Magna 560, USA). The Brϕnsted acidity was determined by 2,6-dimethyl pyridine adsorption followed by TG analysis. Samples calcined at 600 °C were used for the Brϕnsted acidity measurements. The samples were kept in a desicator saturated with 2,6-dimethyl pyridine at 50 °C for 48h and then subjected to thermo gravimetric analysis in N_2 atmosphere at a heating rate of 10 °Cmin^{-1} (Shimadzu, TGA 50H, Japan) .

The photocatalytic activity of doped and undoped titania was studied by measuring the amount of methylene blue degraded under UV radiation. For the methylene blue degradation studies aliquots were prepared by dispersing 0.1 g of titania powder in 250 ml of 6.4×10^{-9} mol l^{-1} methylene blue solution (AR grade, Qualigens Fine Chemicals, India Ltd). The peak between 640 nm and 680 nm in the UV spectrum of methylene blue was used for determining the concentration. The suspension was equilibrated by stirring in the dark for 1h prior to measurements. To eliminate the error due to the adsorption of methylene blue by titania from the measurements the initial concentration of methylene blue was measured only after equilibration. The suspension was then irradiated with UV using a Rayonet Photoreactor (Netherlands) with constant stirring. The UV source was fifteen 15 W tubes (Philips G15 T8) arranged in circular fashion emitting radiation in the region 200–400 nm. The degradation of the dye was monitored after 60 min UV irradiation using a UV-visible spectrometer (Shimadzu,

Japan, UV-2401 PC). A blank dye solution was also irradiated, for about 1 h to confirm that the dye was not photobleached by the radiation in the UV chamber.

3.4 Results and Discussions

3.4.1 TGA and DTA analysis

The thermo gravimetric and differential thermal analyses were carried out on dried gels of undoped and 10 mol% doped compositions. The TGA curves (Figure 3.1) show that in pure titania the percentage of weight loss in the region 30 °C to 150 °C is 10%, and is due to the physically adsorbed water in the gel matrix. The weight loss of 20% between 150 °C and 450 °C is due to the removal of chemically adsorbed water and nitrate ion. There was no major weight loss beyond 450 °C. In the case of 10 mol% tantalum doped sample, the weight loss between 30 °C and 150 °C is 30%. The increased weight loss in this region is due to the change in gel structure as a result of tantalum doping. There is a weight loss of around 60% up to 450 °C, which is due to the decomposition of tantalum oxalate and oxalic acid used for tantalum doping. In the case of 10 mol% gadolinium doped sample there is a weight loss of 21% upto 150 °C and 19% weight loss between 150 and 450 °C. A similar pattern is observed for the 10 mol% ytterbium doped sample. Upto 150 °C a weight loss of 19% was observed corresponding to the loss of physically adsorbed water. The weight loss between 150 and 450 °C is 20% and is due to the chemically adsorbed water and nitrate species. The source of nitrates is the nitric acid used for peptisation and the nitrate solution used for doping gadolinium and ytterbium. DTA pattern shows (Figure 3.2) an endothermic peak below 150 °C corresponding to the removal of physically adsorbed water in the gel matrix.

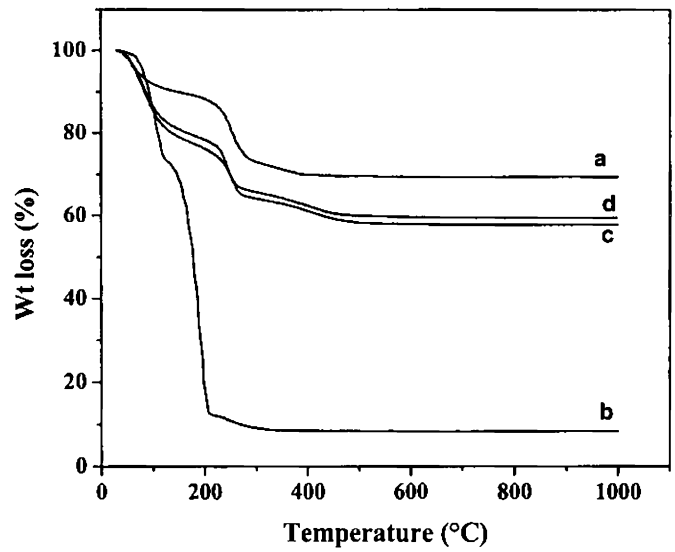

Figure 3.1. TGA pattern of dried gel (a) undoped titania (b) 10 mol% tantala doped titania (c) 10 mol% gadolinium doped titania (d) 10 mol% ytterbium doped titania

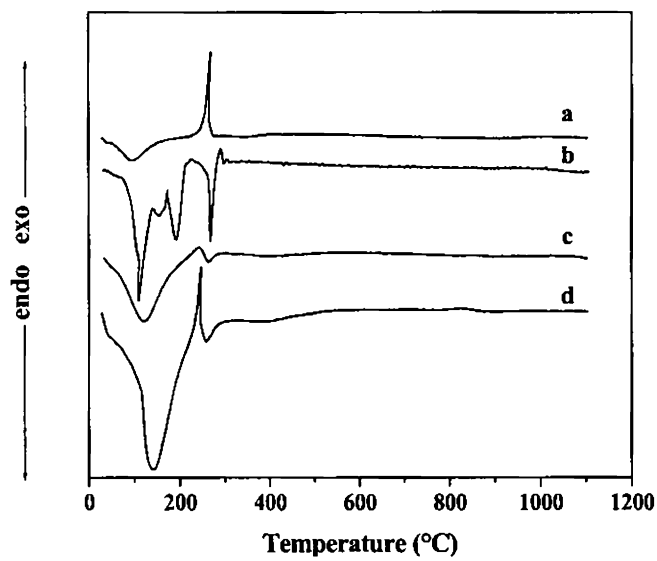

Figure 3.2. DTA patterns of dried gel (a) undoped titania (b) 10 mol% tantala doped titania (c) 10 mol% gadolinium doped titania (d) 10 mol% ytterbium doped titania

All compositions show an exothermic peak in the region 270 °C due to the evolution of nitrate. In the case of tantalum doped titania, the endotherm around 300 °C is due to the decomposition of tantalum oxalate.

3.4.2 X-ray Diffraction Analysis

X-ray diffraction was used for the determination of phase assemblage of undoped and doped titania at different temperatures. The X-ray diffraction pattern of anatase has a main peak at $2\theta = 25.2°$ corresponding to the 101 planes (JCPDS 21-1272) and the main peak of rutile phase is due to its 110 planes (JCPDS 21-1276) present at $2\theta = 27.4°$. The X-ray diffraction patterns of titania and tantalum doped titania calcined at different temperatures are given in Figures 3.3, 3.4 & 3.5.

Considerable stability of the anatase phase is observed for the tantalum doped samples and stability increases with increasing concentration of tantalum. While after calcination at 700 °C 71% of rutile titania was present in the case of undoped titania, only 12% was present in 5 mol% tantalum doped titania. The most significant observation is that, in the case of 10 mol% tantalum, there was no phase transformation from anatase to rutile (Figure 3.3). Pure titania completely transforms to rutile at 800 °C (Figure 3.4), while complete transformation occurs only above 1000 °C for the 10 mol% tantalum doped titania (Figure 3.5), indicating the high order of thermal stability of the anatase phase. The fraction of rutile present at different temperatures in the pure and tantalum doped titania compositions is given in Figure 3.6. X-ray diffraction patterns indicate the presence of small peaks corresponding to orthorhombic Ta_2O_5 (JCPDS 79-1375) in composition containing 5 and 10 mol% tantalum. From the X-ray diffraction studies it is clear that anatase to rutile phase transformation is supressed by tantalum doping.

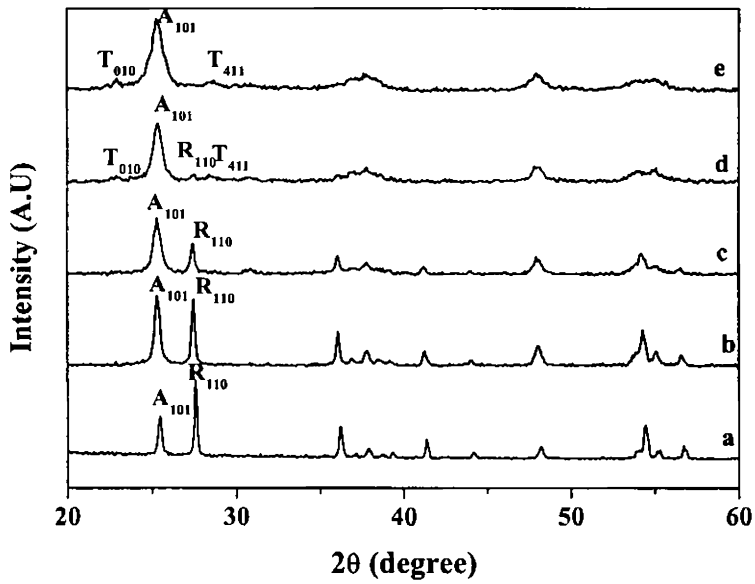

Figure 3.3. XRD patterns of different TiO_2 samples calcined at 700 °C for 1 h: (A) Anatase, (R) Rutile (T) Ta_2O_5 (a) Pure TiO_2, (b) 1 mol% Ta_2O_5 doped TiO_2, (c) 2 mol% Ta_2O_5 doped TiO_2, (d) 5 mol% Ta_2O_5 doped TiO_2, (e) 10 mol% Ta_2O_5 doped TiO_2

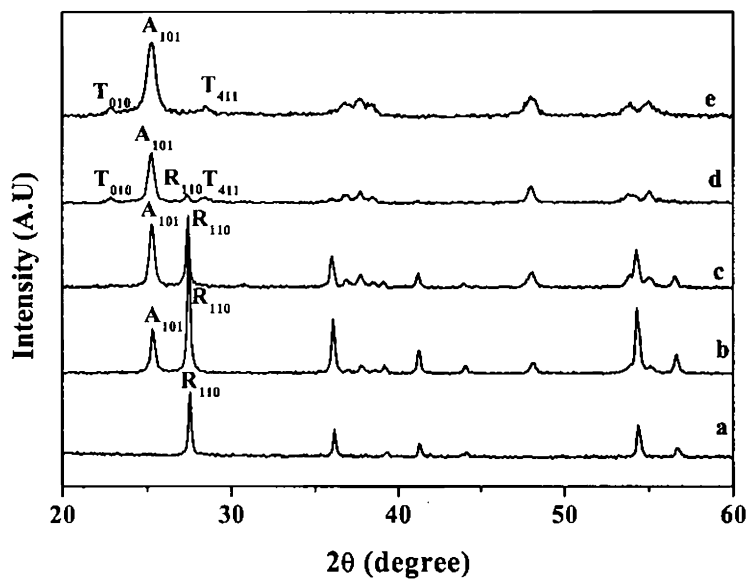

Figure 3.4. XRD patterns of different TiO_2 samples calcined at 800 °C for 1 h: (A) Anatase, (R) Rutile (T) Ta_2O_5 (a) Pure TiO_2, (b) 1 mol% Ta_2O_5 doped TiO_2, (c) 2 mol% Ta_2O_5 doped TiO_2, (d) 5 mol% Ta_2O_5 doped TiO_2, (e) 10 mol% Ta_2O_5 doped TiO_2.

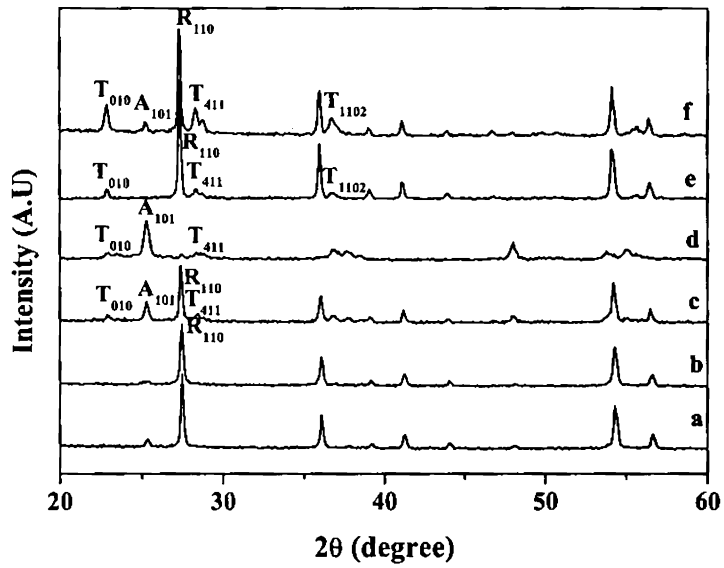

Figure 3.5. XRD patterns of different TiO_2 samples calcined at different temperatures for 1h: (A) Anatase, (R) Rutile (T) Ta_2O_5 (a) 1 mol% Ta_2O_5 doped TiO_2, (b) 2 mol% Ta_2O_5 doped TiO_2, (c) 5 mol% Ta_2O_5 doped TiO_2, (d) 10 mol% Ta_2O_5 doped TiO_2 calcined at 900 °C, (e) 5 mol% Ta_2O_5 doped TiO_2, (f) 10 mol% Ta_2O_5 doped TiO_2, calcined at 1000 °C

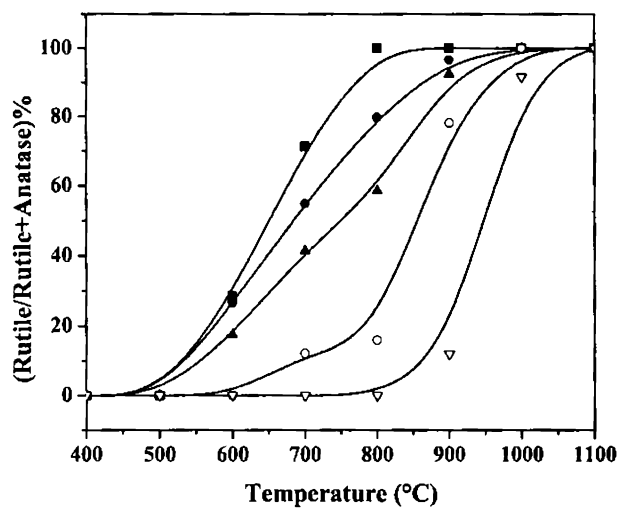

Figure 3.6. Phase transformation from anatase to rutile of pure and Ta_2O_5 doped TiO_2 calcined at different temperatures for 1h (■) Pure titania (●) 1 mol% Ta_2O_5 doped TiO_2 (▲) 2 mol% Ta_2O_5 doped TiO_2 (○) 5 mol% Ta_2O_5 doped TiO_2 (▽) 10 mol% Ta_2O_5 doped TiO_2

The crystallite size of anatase titania versus the temperature of calcination is plotted in Figure 3.7 for all tantalum doped titania compositions. It can be seen that tantalum doped compositions has lower anatase crystallite size compared to the undoped composition at all calcined temperatures. Hence by increasing the concentration of tantalum in the titania matrix, the crystallite size decreases and anatase to rutile phase transformation temperature increases.

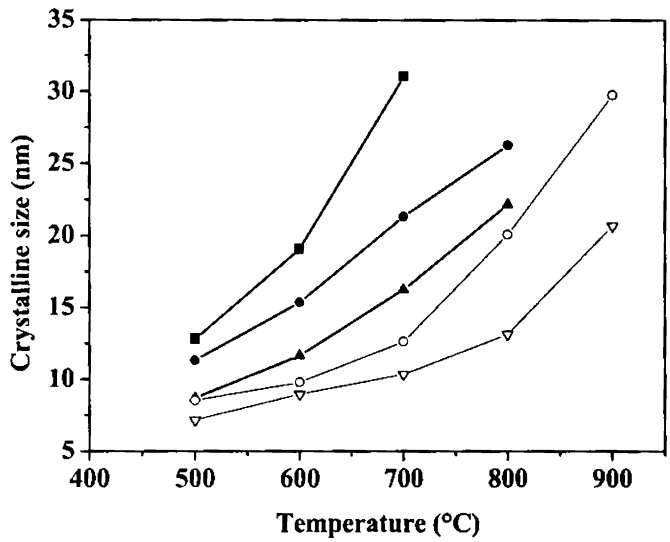

Figure 3.7. Crystallite size of the anatase phase in pure and Ta_2O_5-doped TiO_2 calcined at different temperatures for 1h (■) Pure titania (●) 1 mol% Ta_2O_5 doped TiO_2 (▲) 2 mol% Ta_2O_5 doped TiO_2 (○) 5 mol% Ta_2O_5 doped TiO_2 (▽) 10 mol% Ta_2O_5 doped TiO_2

Comparing the X-ray diffraction patterns of undoped and gadolinium doped titania, heated at 700 °C (Figure 3.8), it can be seen that more than 71% of anatase is converted to rutile in the undoped titania while all gadolinium doped titania compositions retains complete anatase phase. The undoped titania completely transforms to rutile at 800 °C, but 2, 5 and 10 mol% gadolinium doped titania retains the anatase phase indicating the excellent thermal phase stability (Figure 3.9 & 3.10). In all the compositions containing gadolinium, the complete rutilation occurs only above 900 °C.

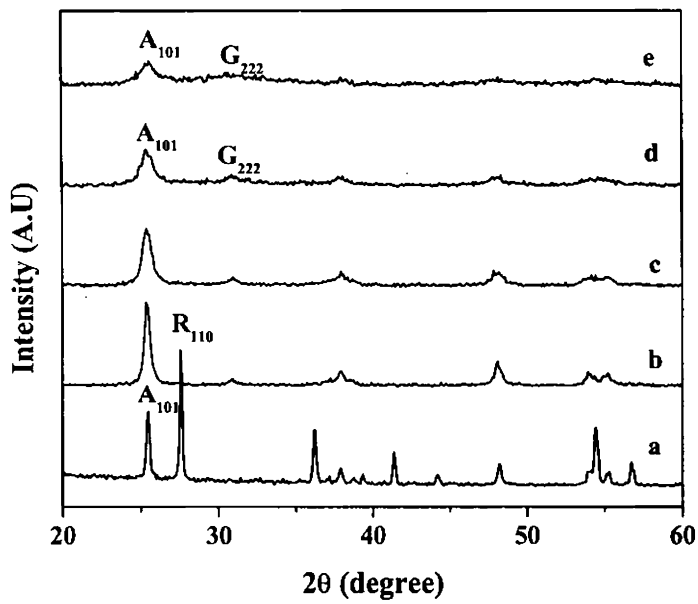

Figure 3.8. XRD patterns of different TiO_2 samples calcined at 700 °C for 1 h: (A) Anatase, (R) Rutile (G) Gd_2TiO_7 (a) Pure TiO_2, (b) 1 mol% Gd_2O_3 doped TiO_2, (c) 2 mol% Gd_2O_3 doped TiO_2, (d) 5 mol% Gd_2O_3 doped TiO_2, (e) 10 mol% Gd_2O_3 doped TiO_2

Thus, the anatase phase stability is achieved through gadolinium doping. In 2, 5 and 10 mol% gadolinium doped titania an additional phase of $Gd_2Ti_2O_7$ (JCPDS 23-0259) is formed at 700 °C (Figure 3.8). The main peak of $Gd_2Ti_2O_7$ corresponds to the 222 plane at a 2θ value 30.38°, and it is observed that $Gd_2Ti_2O_7$ peaks are amorphous at 700 °C. But increasing the temperature from 700 to 800 and 850 °C (Figure 3.9 & 3.10), crystallised peaks of $Gd_2Ti_2O_7$ are formed. Between 800 and 900 °C a sharp anatase to rutile phase transformation was observed. The fraction of rutile present at different temperatures in the pure and gadolinium doped titania is given in Figure 3.11. The crystallite size of anatase titania versus the temperature of undoped and gadolinium doped titania is given in Figure 3.12.

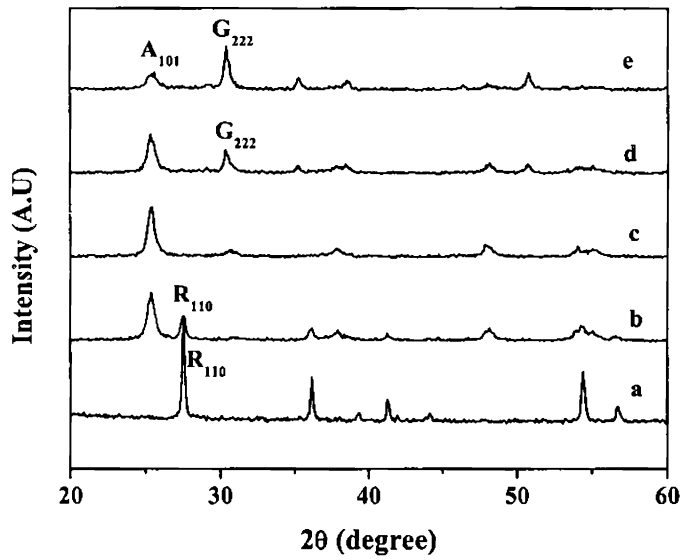

Figure 3.9. XRD patterns of different TiO_2 samples calcined at 800 °C for 1 h: (A) Anatase, (R) Rutile (G) Gd_2TiO_7 (a) Pure TiO_2, (b) 1 mol% Gd_2O_3 doped TiO_2, (c) 2 mol% Gd_2O_3 doped TiO_2, (d) 5 mol% Gd_2O_3 doped TiO_2, (e) 10 mol% Gd_2O_3 doped TiO_2

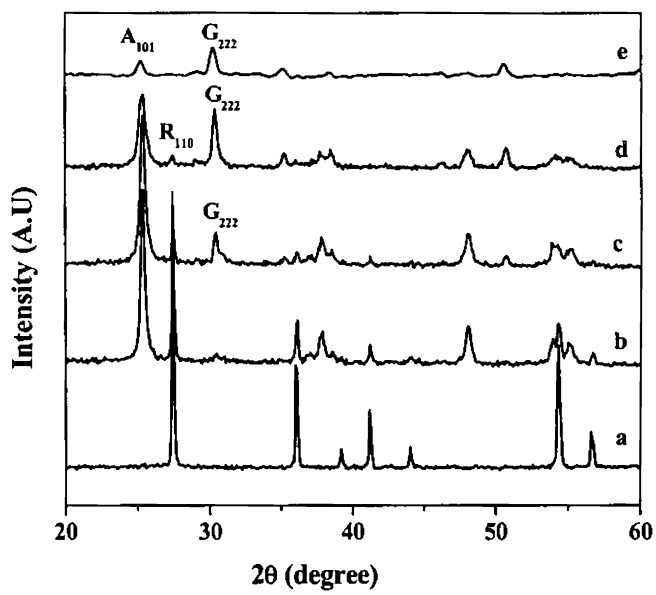

Figure 3.10. XRD patterns of different TiO_2 samples calcined at 850 °C for 1 h: (A) Anatase, (R) Rutile (G) Gd_2TiO_7 (a) Pure TiO_2, (b) 1 mol% Gd_2O_3 doped TiO_2, (c) 2 mol% Gd_2O_3 doped TiO_2, (d) 5 mol% Gd_2O_3 doped TiO_2, (e) 10 mol% Gd_2O_3 doped TiO_2

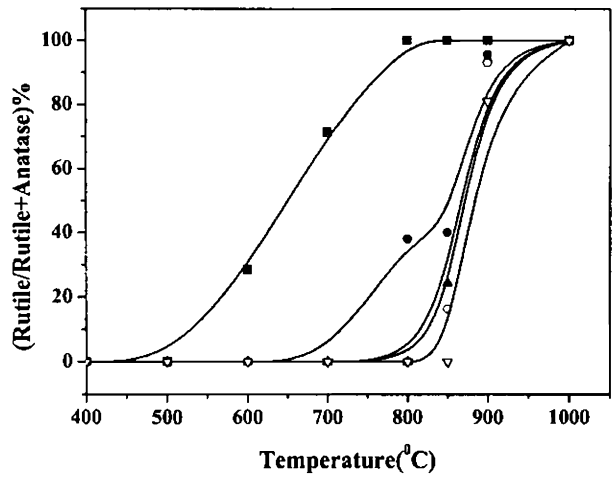

Figure 3.11. Phase transformation from anatase to rutile of pure and Gd_2O_3 doped TiO_2 calcined at different temperatures for 1h (■) Pure titania (●) 1 mol% Gd_2O_3 doped TiO_2 (▲) 2 mol% Gd_2O_3 doped TiO_2 (○) 5 mol% Gd_2O_3 doped TiO_2 (▽) 10 mol% Gd_2O_3 doped TiO_2

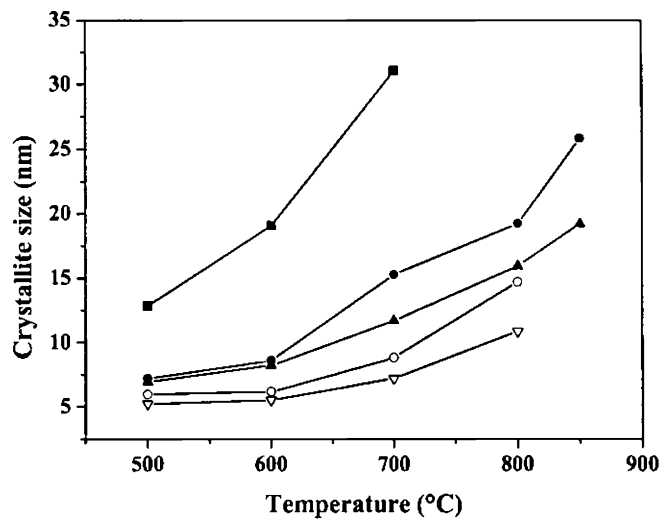

Figure 3.12. Crystallite size of the anatase phase in pure and Gd_2O_3-doped TiO_2 calcined at different temperatures for 1h (■) Pure titania (●) 1 mol% Gd_2O_3 doped TiO_2 (▲) 2 mol% Gd_2O_3 doped TiO_2 (○) 5 mol% Gd_2O_3 doped TiO_2 (▽) 10 mol% Gd_2O_3 doped TiO_2

Ytterbium doped titania also shows anatase phase stability. Upto 700 °C only anatase phase was present in all ytterbium doped titania samples (Figure 3.13). 1 mol% ytterbium doped titania contained 35% rutile after calcination at 800 °C (Figure 3.14), all the other ytterbium doped titania compositions remains in the anatase phase. At 850 °C (Figure 3.15) 1, 2, 5 mol% ytterbium doped titania samples had 39, 27 and 37% rutile phase respectievely. But the 10 mol% ytterbium doped titania exists completely as anatase phase at 850 °C. In addition to anatase and rutile phase an additional phase of crystalline Yb_2TiO_5 (JCPDS 33-1457) was formed at 850 °C in 2, 5 and 10 mol% ytterbium doped titania. The main peak of Yb_2TiO_5 corresponds to the reflections from its 111 planes and occurs at the 2θ value of 30.02°. The fraction of rutile present after calcination at different temperatures in the pure and ytterbium doped titania is given in Figure 3.16. A sharp anatase to rutile phase transformation was observed, as in the case of gadolinium and ytterbium doped samples between 800 and 900 °C. The additional phases, $Gd_2Ti_2O_7$ and Yb_2TiO_5 formed during calcination, may be aiding the anatase to rutile phase transformation in both cases. In both ytterbium and gadolinium doped titania the relative intensity of the peak corresponding to $Gd_2Ti_2O_7$ and Yb_2TiO_5 is increased by calcinations at 800 and 850 °C.

The crystallite size of anatase titania versus temperature of heat treatment in undoped and ytterbium doped titania is presented in Figure 3.17. The rutile phase in tantalum, gadolinium, ytterbium doped and pure titania is formed when the crystallite size reaches a critical value of ~12-20 nm (Figure 3.7, 3.12, 3.17), which is accordance with the critical sizes reported..[38, 39]

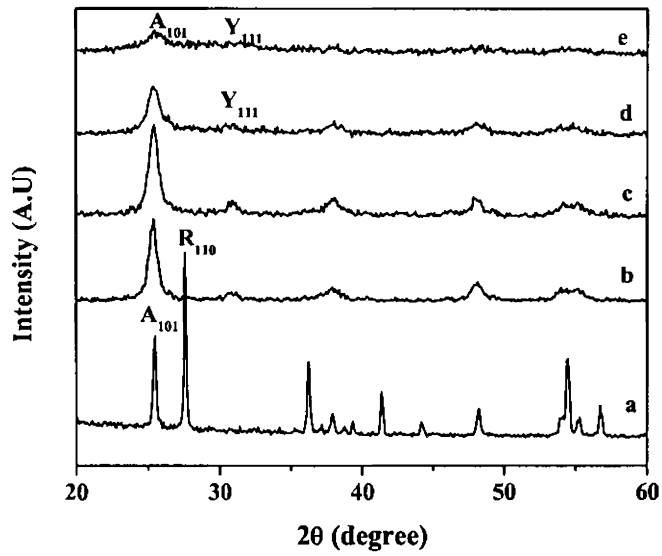

Figure 3.13. XRD patterns of different TiO_2 samples calcined at 700 °C for 1 h: (A) Anatase, (R) Rutile (Y) Yb_2TiO_5 (a) Pure TiO_2, (b) 1 mol% Yb_2O_3 doped TiO_2, (c) 2 mol% Yb_2O_3 doped TiO_2, (d) 5 mol% Yb_2O_3 doped TiO_2, (e) 10 mol% Yb_2O_3 doped TiO_2

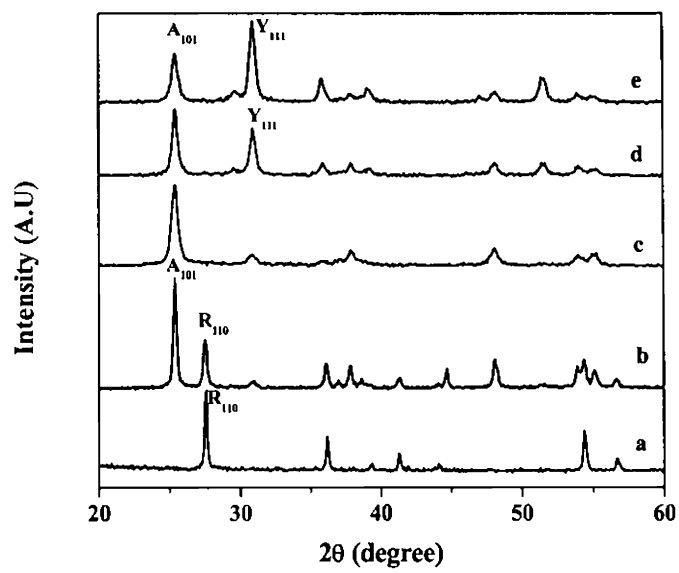

Figure 3.14. XRD patterns of different TiO_2 samples calcined at 800 °C for 1 h: (A) Anatase, (R) Rutile (Y) Yb_2TiO_5 (a) Pure TiO_2, (b) 1 mol% Yb_2O_3 doped TiO_2, (c) 2 mol% Yb_2O_3 doped TiO_2, (d) 5 mol% Yb_2O_3 doped TiO_2, (e) 10 mol% Yb_2O_3 doped TiO_2

The anatase phase is reported to be thermodynamically stable at low particle sizes (below 14 nm); when the temperature increases, the crystallite size will also increase leading to the formation of rutile phase. On increasing the dopant amount in the titania matrix, the anatase to rutile phase transformation temperature increases and crystallite size decreases. The reduction in crystallite size may be due to the segregation of dopant in the grain boundary which will restrict the contact of grains and inhibit the grain growth. Further, it is also reported [40-42] that the oxygen vacancies act as the nucleation centre for crystallite growth, which further leads to the phase transformation. Dopants can either go into the interstitial positions or to the lattice points by replacing Ti atoms. Cations with an oxidation state above +4, irrespective of their position in the lattice, will invariably reduce the oxygen vacancy concentration in the titania lattice.

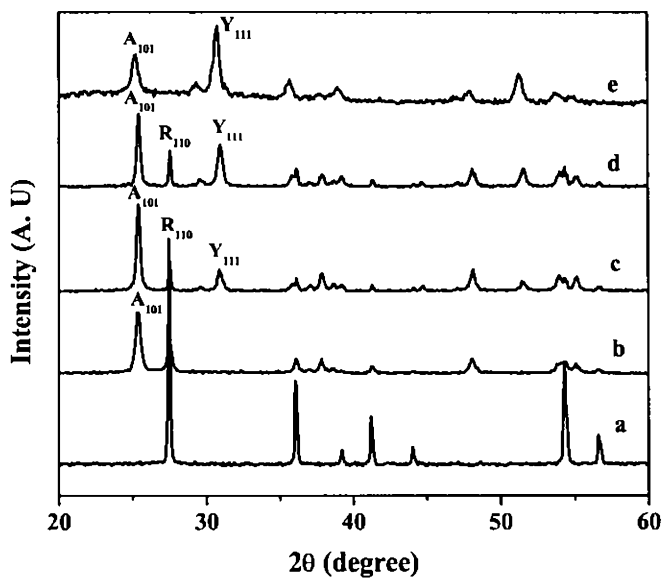

Figure.3.15. XRD patterns of different TiO_2 samples calcined at 850 °C for 1 h: (A) Anatase, (R) Rutile (Y) Yb_2TiO_5 (a) Pure TiO_2, (b) 1 mol% Yb_2O_3 doped TiO_2, (c) 2 mol% Yb_2O_3 doped TiO_2, (d) 5 mol% Yb_2O_3 doped TiO_2, (e) 10 mol% Yb_2O_3 doped TiO_2

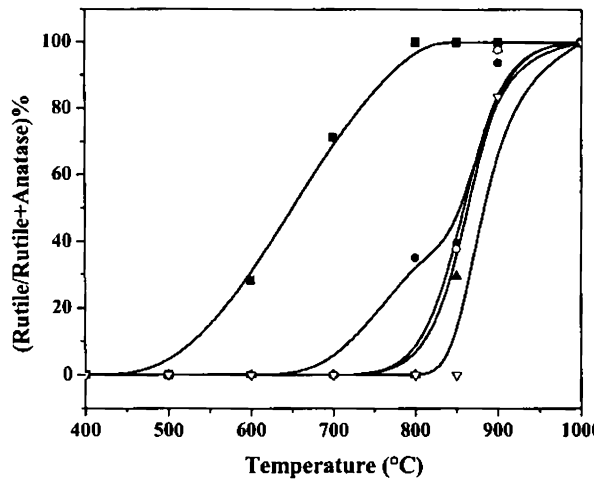

Figure 3.16. Phase transformation from anatase to rutile of pure and Yb_2O_3 doped TiO_2 calcined at different temperatures for 1h (■) Pure titania (●) 1 mol% Yb_2O_3 doped TiO_2 (▲) 2 mol% Yb_2O_3 doped TiO_2 (○) 5 mol% Yb_2O_3 doped TiO_2 (▽) 10 mol% Yb_2O_3 doped TiO_2

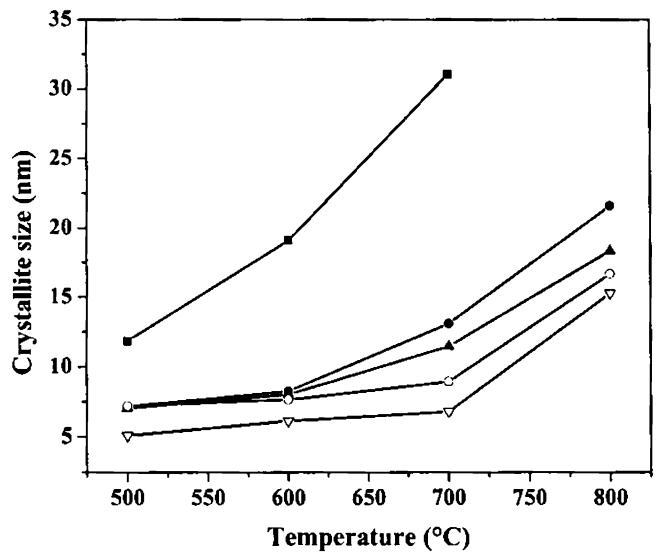

Figure 3.17. Crystallite size of the anatase phase in pure and Yb_2O_3- doped TiO_2 calcined at different temperatures for 1h (■) Pure titania (●) 1 mol% Yb_2O_3 doped TiO2 (▲) 2 mol% Yb_2O_3 doped TiO_2 (○) 5 mol% Yb_2O_3 doped TiO_2 (▽) 10 mol% Yb_2O_3 doped TiO_2

The influence of cations with an oxidation state of +4 or lower on the oxygen vacancy concentration will depend on their position in the titania lattice. If the cations with an oxidation state of +4 or lower are present in the lattice points, they increase the oxygen vacancies in the titania lattice and if placed in the interstitial position, they decrease the oxygen vacancy concentration.[40] In our study, tantalum, gadolinium and ytterbium are used as dopants. The stable oxidation state of tantalum is +5 and for gadolinium and ytterbium it is, +3 and the corresponding ionic radii are 0.064, 0.094 and 0.081 nm respectively. The ionic radius of Ti^{4+}, Ta^{5+}, Gd^{3+} and Yb^{3+} follow the order Ti^{4+} (0.061nm) ≈ Ta^{5+} (0.064 nm) < Yb^{3+} (0.081 nm) < Gd^{3+} (0.094 nm). Due to the similarity in ionic size Ta^{5+} can easily substitute Ti^{4+}in the titania lattice but due to the larger size $Gd^{3+}$and Yb^{3+} needs to occupy the interstitial position. The +5 tantalum irrespective of its position in the matrix decrease the oxygen vacancy concentration and hence will delay anatase to rutile phase transformation. On the other hand Gd^{3+} and Yb^{3+} decreases the oxygen vacancy concentration by their occupancy in the interstitial position. Increasing doping concentration of tantalum seems to result in the segregation of tantalum oxide as evident in the XRD pattern [JCPDS 79-1375]. This is in disagreement with the observation of Saeerdoti et al.[22] where they could not find any peak corresponding to tantalum oxide in the XRD patterns. But there is a significant difference in the preparation procedures adopted. While we have used salt precursors for both tantalum and titania, they had chosen alkoxide precursors.

In the case of Gadolinium and Ytterbium doping the formation of the corresponding lanthanide titaniumoxide is observed. Many researchers have observed the expulsion of dopants into the matrix with calcination temperature. Due to the mismatch

of the ionic sizes Gd^{3+} and Yb^{3+} has a higher probability of getting expelled than tantalum. According to Zhang et al.[35], lanthanides substituting for Ti^{4+} expelled into the matrix probably exist as amorphous lanthanide oxide, and can further react with titania to form lanthanide titanium oxide. Presence of lanthanide titaniumoxide has been found to favour anatase to rutile phase transformation by Lin et al. [33] while studying mixtures of TiO_2 and oxides of lanthanides. But in this study XRD results show the presence of amorphous peaks corresponding to $Gd_2Ti_2O_7$, Yb_2TiO_5 at low temperatures in the gadolinium and ytterbium doped titania and there is no evidence to the presence of rutile phase. But at higher temperatures, the peaks of $Gd_2Ti_2O_7$, Yb_2TiO_5 becomes more crystalline and an enhanced rate of anatase to rutile phase transformation is observed. This would mean that the degree of crystallinity of the lanthanide titaniumoxide phase is important in its role as an anatase to rutile phase transformation aid.

3.4.3 BET surface area analysis

Textural characteristics of all samples calcined at 500, 600 and 800 °C derived from N_2 adsorption analyses are presented in Table 3.1, 3.2 & 3.3. Specific surface area (S_{BET}), total pore volume calculated at $p/p_0 = 0.9$, BJH mesopore volume and micro pore volume calculated by t-plot method and average pore diameter are presented. The surface area of tantalum doped titania is considerably high and could be explained on the basis of the hindered crystallite growth.

All the tantalum doped compositions show higher surface area than pure titania at all calcined temperatures (Table 3.1). Pure titania after calcining at 500 °C have a surface area and total pore volume of 48.7 m^2g^{-1} and 0.1084cm^3g^{-1} respectively, while the 1, 2, 5 & 10 mol% tantalum doped titania have surface area of 78.8, 92.2, 87.9, 63.2 m^2g^{-1} and

total pore volume of 0.1431, 0.1425, 0.1133, 0.0885 cm^3g^{-1} respectively. In the case of 600 °C calcined samples the surface area values of pure and 1, 2, 5, 10 mol% tantalum doped titania samples are 19.1, 45.1, 67.1, 61.9, 49 m^2g^{-1} and total pore volume are 0.0478, 0.0935, 0.1708, 0.13, 0.0899 cm^3g^{-1} respectively. So there is a drastic reduction in the surface area and pore volume of pure titania when calcined at high temperature.

Table 3.1. N_2 adsorption characteristics of undoped and tantalum doped titania with calcination temperature

mol.% doping	BET surface area (m^2g^{-1})	Total pore volume (cm^3g^{-1})	Micro pore volume (cm^3g^{-1})	Meso pore volume (cm^3g^{-1})	Pore diameter (nm)
Calcined at 500 °C					
Undoped	48.7	0.1084	0.00392	0.1045	7.9
1 mol.% Ta_2O_5	78.8	0.1431	0.00158	0.1415	7.3
2 mol.% Ta_2O_5	92.2	0.1425	0.00246	0.1401	6.2
5 mol.% Ta_2O_5	87.9	0.1133	0.00144	0.1118	5.2
10 mol.% Ta_2O_5	63.2	0.0885	0.00264	0.0858	5.5
Calcined at 600 °C					
Undoped	19.1	0.0478	0.00015	0.0477	10.0
1 mol.% Ta_2O_5	45.1	0.0935	0.00073	0.0927	8.3
2 mol.% Ta_2O_5	67.1	0.1708	0.00155	0.1693	10.2
5 mol.% Ta_2O_5	61.9	0.13	0.00041	0.1296	8.5
10 mol.% Ta_2O_5	49	0.0899	0.0009	0.089	7.3
Calcined at 800 °C					
Undoped	Very low				
1 mol.% Ta_2O_5	8	0.0188	0.000611	0.0182	10.2
2 mol.% Ta_2O_5	17.5	0.0485	0.002046	0.0464	10.8
5 mol.% Ta_2O_5	17.1	0.0665	0.000934	0.0655	13.3
10 mol.% Ta_2O_5	13.4	0.1038	0.000928	0.1028	19.6

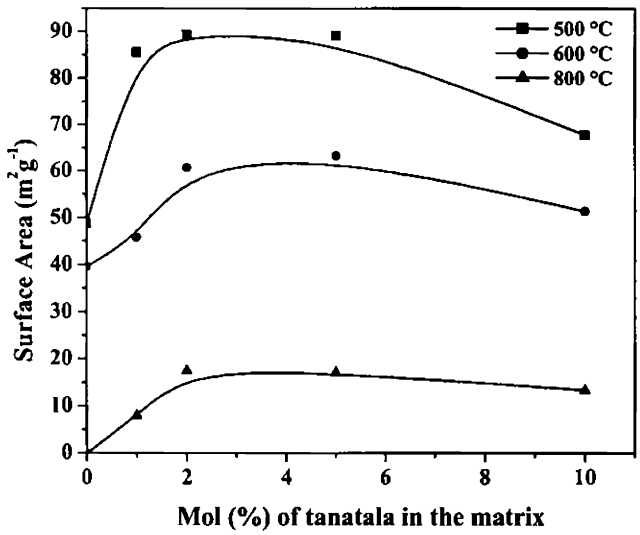

Figure 3.18. Surface area of titania and tantala doped titania calcined at different temperature for 1h

After 800 °C calcination 1, 2, 5, 10 mol% tantalum doped titania samples show surface area values of 7.9, 17, 17, 13 m^2g^{-1} and 0.0188, 0.0485, 0.0665, 0.1038 cm^3g^{-1} but at the same time pure titania has a very low surface area, below $1m^2g^{-1}$. From this observation it is confirmed that the tantalum doping in titania matrix hinders the nucleation of titania particle and there by prevents the decrease in surface area of the system. It is also observed that upto 2 mol% doping of tantalum an increase in surface area was observed and on further doping, the surface area decreases marginally (Figure 3.18). This may be due to the high amount of tantalum doping which leads to formation of a separate tantala phase having less surface area in the titania matrix. The adsorption isotherms (Figure 3.19 & 3.20) of all samples show type IV behaviour with the typical hysteresis loop. This hysteresis loop is characteristic of mesoporous materials.[43] The pore size distribution curve (Figure 3.19 & 3.20 inset) also indicates that the pores are in mesoporous region.

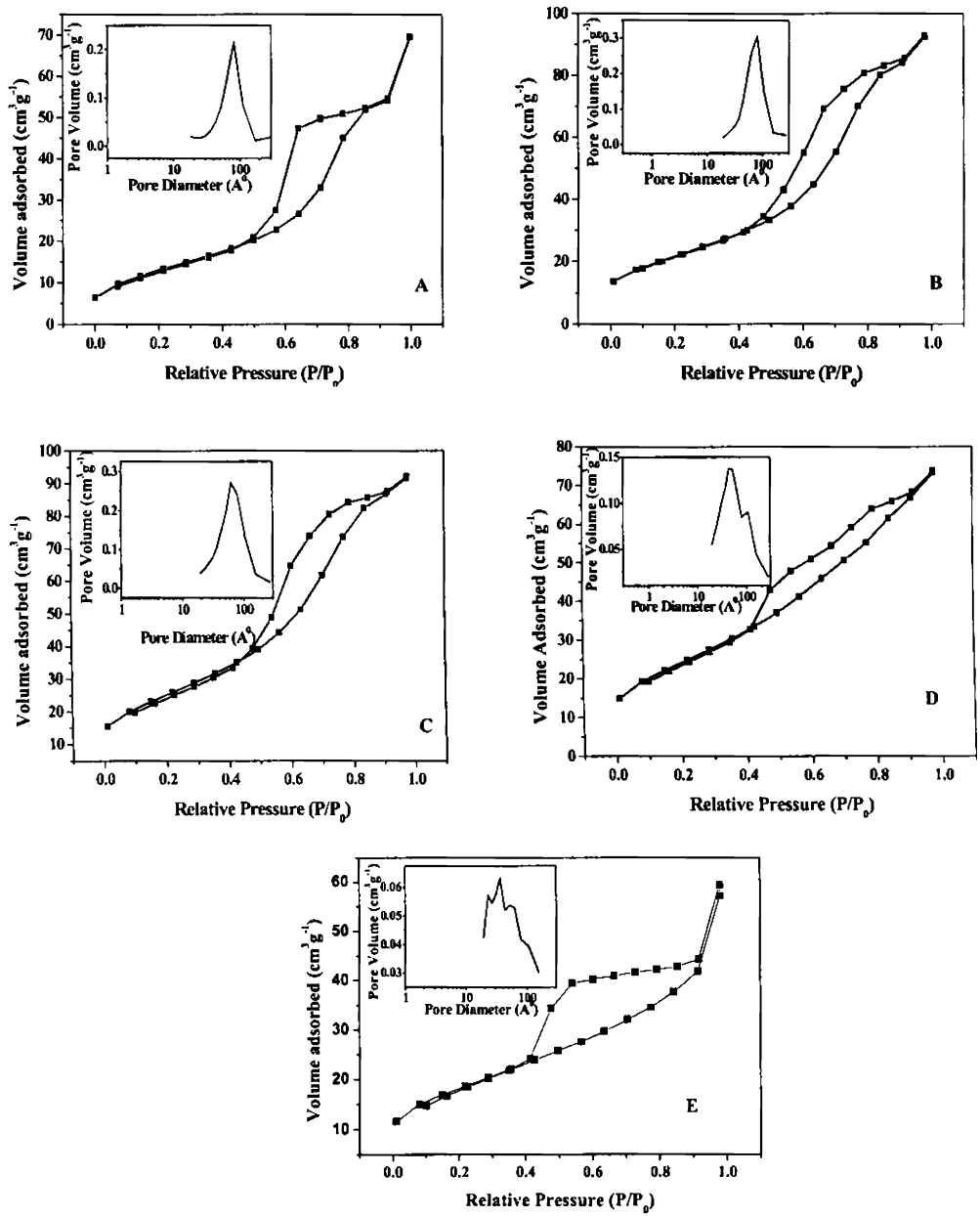

Figure 3.19. Adsorption isotherm and pore size distribution curve (inset) of (A) Pure titania (B) 1 mol% Ta_2O_5 doped TiO_2 (C) 2 mol% Ta_2O_5 doped TiO_2 (D) 5 mol% Ta_2O_5 doped TiO_2 (E) 10 mol% Ta_2O_5 doped TiO_2 , calcined at 500 °C

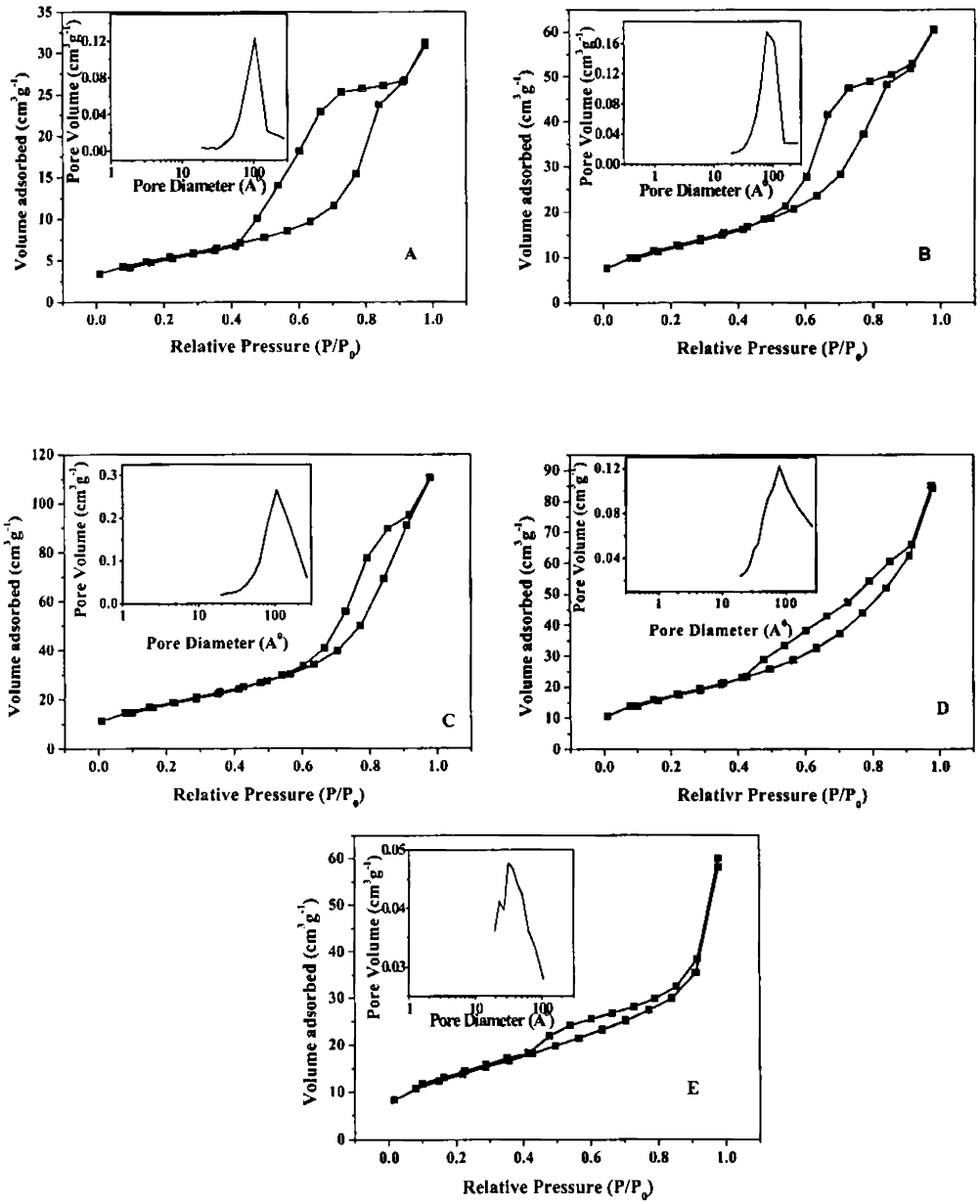

Figure 3.20. Adsorption isotherm and pore size distribution curve (inset) of (A) Pure titania (B) 1 mol% Ta_2O_5 doped TiO_2 (C) 2 mol% Ta_2O_5 doped TiO_2 (D) 5 mol% Ta_2O_5 doped TiO_2 (E) 10 mol% Ta_2O_5 doped TiO_2 , calcined at 600 °C

In gadolinium doped titania, it is clear that even the presence of 1mol% gadolinium increases the surface area of titania considerably. The increase is more than two times the value of undoped titania at all temperatures (Figure 3.21). The undoped sample has the highest average pore diameter. With increasing calcination temperature the average pore size increases for all compositions possibly due to the increasing crystallite size. Interparticle pores will be larger for larger particles. This is reflected in the surface area values and all compositions shows decrease in surface area with increasing temperature of calcination (Table 3.2).

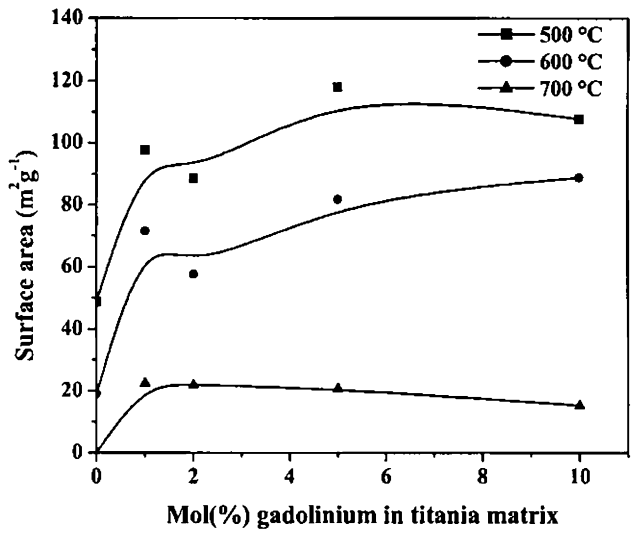

Figure 3.21. Surface area of pure and gadolinium doped titania calcined at different temperature for 1h

The decrease in pore volume for undoped and gadolinium doped titania is considerable when the calcination temperature is 800 °C. From the graph of rutile percentage versus calcination temperature, it is evident that all gadolinium doped compositions start converting to rutile phase around this temperature. This would mean that the anatase phase has its maximum particle size at this temperature. The mesoporous nature of the

gadolinium doped titania is evident from the adsorption desorption isotherm and pore size distribution curves (Figure 3.22 & 3.23).

Table 3.2. N_2 adsorption characteristics of undoped and gadolinium doped titania with different calcination temperature.

mol.% doping	BET surface area (m^2g^{-1})	Total pore volume (cm^3g^{-1})	Micro pore volume (cm^3g^{-1})	Meso pore volume (cm^3g^{-1})	Pore diameter (nm)
Calcined at 500 °C					
Undoped	48.7	0.1084	0.0039	0.104445	7.9
1 mol.% Gd_2O_3	97.7	0.1515	0.0022	0.14933	6.2
2 mol.% Gd_2O_3	88.5	0.1405	0.00265	0.137809	6.4
5 mol.% Gd_2O_3	117.9	0.1511	0.0041	0.146973	5.1
10 mol.% Gd_2O_3	107.7	0.1517	0.0030	0.14868	5.6
Calcined at 600 °C					
Undoped	19.1	0.0479	0.00015	0.047647	10.0
1 mol.% Gd_2O_3	71.5	0.1511	0.000386	0.150745	8.5
2 mol.% Gd_2O_3	57.6	0.1366	0.00096	0.135645	9.5
5 mol.% Gd_2O_3	81.8	0.1488	0.00114	0.14763	7.3
10 mol.% Gd_2O_3	88.9	0.1449	0.00285	0.142046	6.5
Calcined at 800 °C					
Undoped	Very low				
1 mol.% Gd_2O_3	22.5	0.0351	0.00107	0.034058	6.3
2 mol.% Gd_2O_3	21.9	0.0428	0.00036	0.042405	7.8
5 mol.% Gd_2O_3	20.8	0.0353	0.00022	0.035034	6.8
10 mol.% Gd_2O_3	15.3	0.0258	0.00041	0.025343	6.7

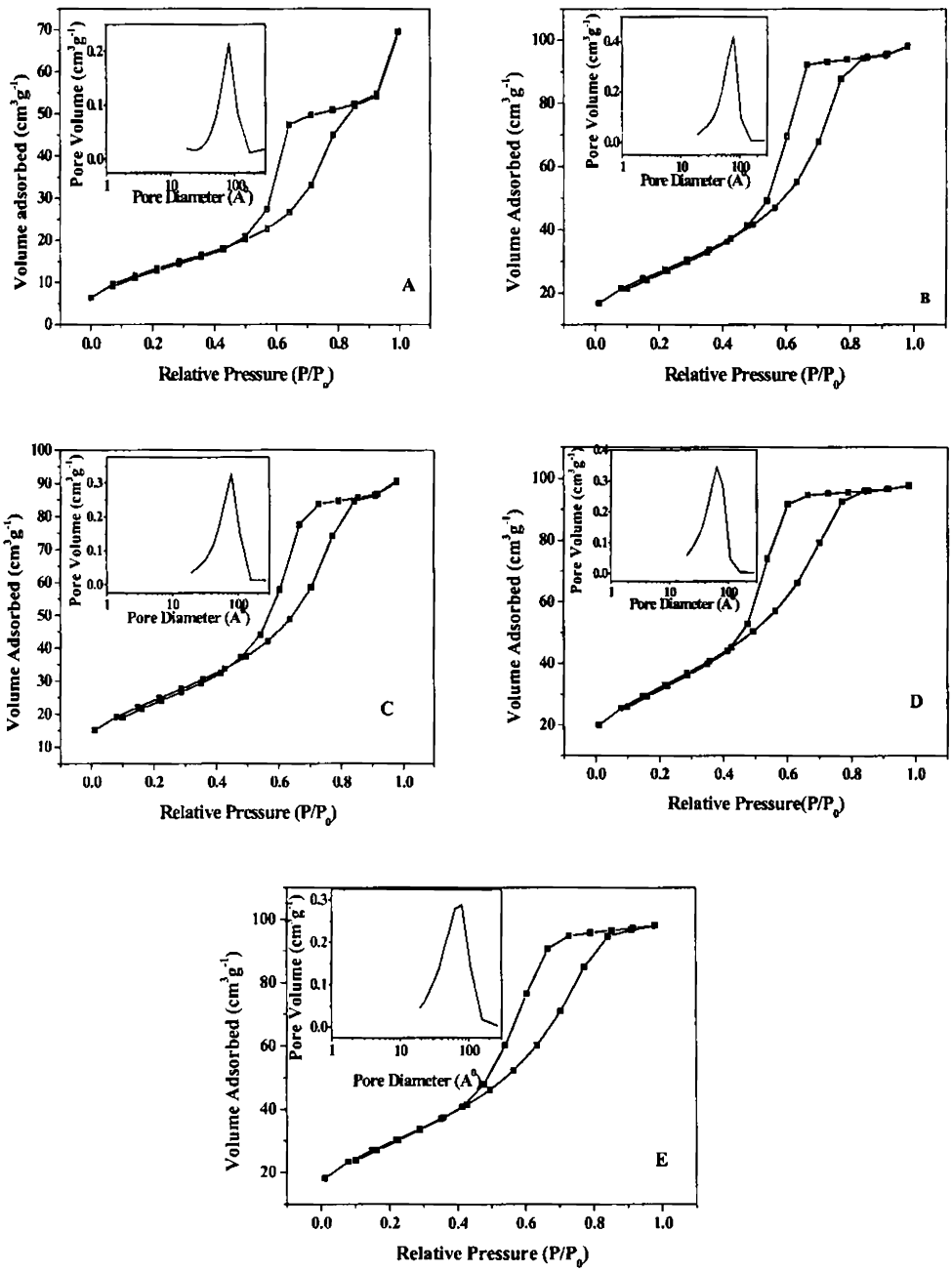

Figure 3.22. Adsorption isotherm and pore size distribution curve (inset) of (A) Pure titania (B) 1 mol% Gd_2O_3 doped TiO_2 (C) 2 mol% Gd_2O_3 doped TiO_2 (D) 5 mol% Gd_2O_3 doped TiO_2 (E) 10 mol% Gd_2O_3 doped TiO_2 , calcined at 500 °C

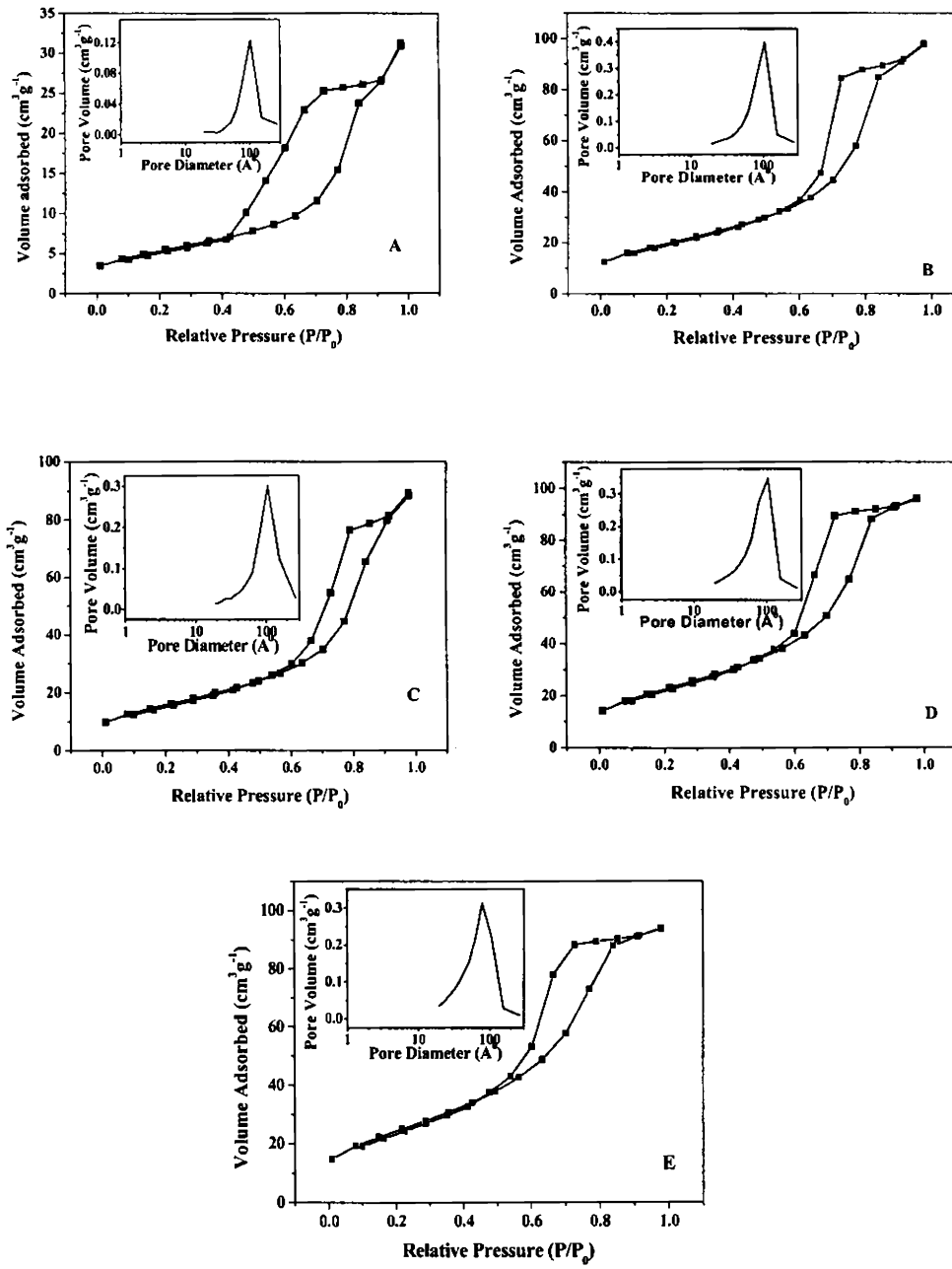

Figure 3.23. Adsorption isotherm and pore size distribution curve (inset) of (A) Pure titania (B) 1 mol% Gd_2O_3 doped TiO_2 (C) 2 mol% Gd_2O_3 doped TiO_2 (D) 5 mol% Gd_2O_3 doped TiO_2 (E) 10 mol% Gd_2O_3 doped TiO_2 , calcined at 600 °C

Surface area results of ytterbium doped titania shows higher surface area than the undoped titania at all temperatures measured (Figure 3.24). A sharp increase was observed for 1 mol% ytterbium doping and further the increase was not a prominent one.

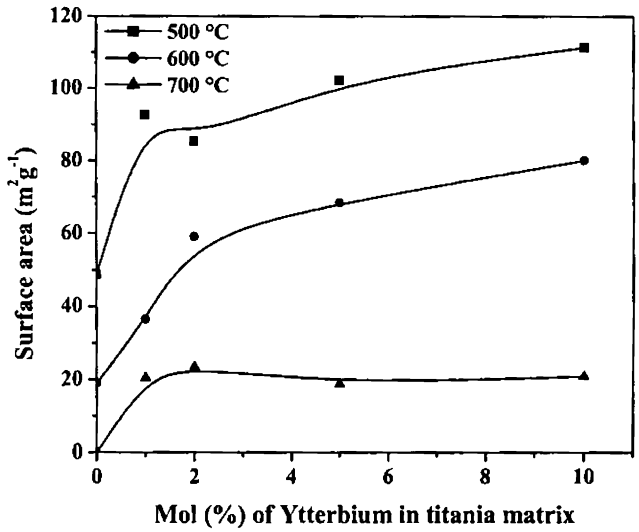

Figure 3.24. Surface area of undoped and ytterbium doped titania calcined at different temperature for 1 h

Surface area and total pore volume of undoped titania calcined at 500°C shows a value of 48.7 m^2g^{-1} and 0.1084cm^3g^{-1} respectively, while the 1, 2, 5 & 10 mol% ytterbium doped composition has 92.6, 85.4, 102.2, 111.3 m^2g^{-1} and 0.1399, 0.1371, 0.1382, 0.1327 cm^3g^{-1} respectively. In the case of 600 °C calcined samples the surface area values of titania and 1, 2, 5, 10 mol% ytterbium doped titania samples are 19.1, 36.6, 59.1, 68.5, 80 m^2g^{-1} and total pore volume 0.0478, 0.0988, 0.1395, 0.1338, 0.1258 cm^3g^{-1} respectively.. After 800 °C calcination 1, 2, 5, 10 mol% ytterbium doped titania samples show surface area values of 20.5, 23.5, 18.9, 20.9 m^2g^{-1} and total pore volume 0.0393, 0.0448, 0.0275, 0.1299 cm^3g^{-1} respectively while undoped titania has a very low surface area (Table 3.3). The results confirmed that the doping of ytterbium in the titania matrix hinders the nucleation

of titania particle and there by prevent the decrease in surface area of the system. It is also observed that the total pore volume also increases in the ytterbium doped titania.

Table 3.3. N_2 adsorption characteristics of undoped and ytterbium doped titania with different calcination temperature

mol.% doping	BET surface area (m^2g^{-1})	Total pore volume (cm^3g^{-1})	Micro pore volume (cm^3g^{-1})	Meso pore volume (cm^3g^{-1})	Pore diameter (nm)
Calcined at 500 °C					
Undoped	48.7	0.1084	0.00392	0.10445	7.9
1 mol.% Yb_2O_3	92.6	0.1399	0.00258	0.13727	6.0
2 mol.% Yb_2O_3	85.4	0.1371	0.00145	0.13564	6.4
5 mol.% Yb_2O_3	102.2	0.1382	0.00216	0.13599	5.4
10 mol.% Yb_2O_3	111.3	0.1327	0.00507	0.12767	4.8
Calcined at 600 °C					
Undoped	19.1	0.0478	0.00015	0.04765	10.0
1 mol.% Yb_2O_3	36.6	0.0988	0.00894	0.08973	10.8
2 mol.% Yb_2O_3	59.1	0.1395	0.00074	0.13876	9.4
5 mol.% Yb_2O_3	68.5	0.1338	0.00035	0.13344	7.8
10 mol.% Yb_2O_3	80.0	0.1258	0.00219	0.12363	6.3
Calcined at 800 °C					
Undoped	Very low				
1 mol.% Yb_2O_3	20.5	0.0393	0.00017	0.03911	7.7
2 mol.% Yb_2O_3	23.5	0.0448	0.00138	0.04337	7.6
5 mol.% Yb_2O_3	18.9	0.0275	0.00088	0.02659	5.8
10 mol.% Yb_2O_3	20.9	0.1299	0.00089	0.12904	24.9

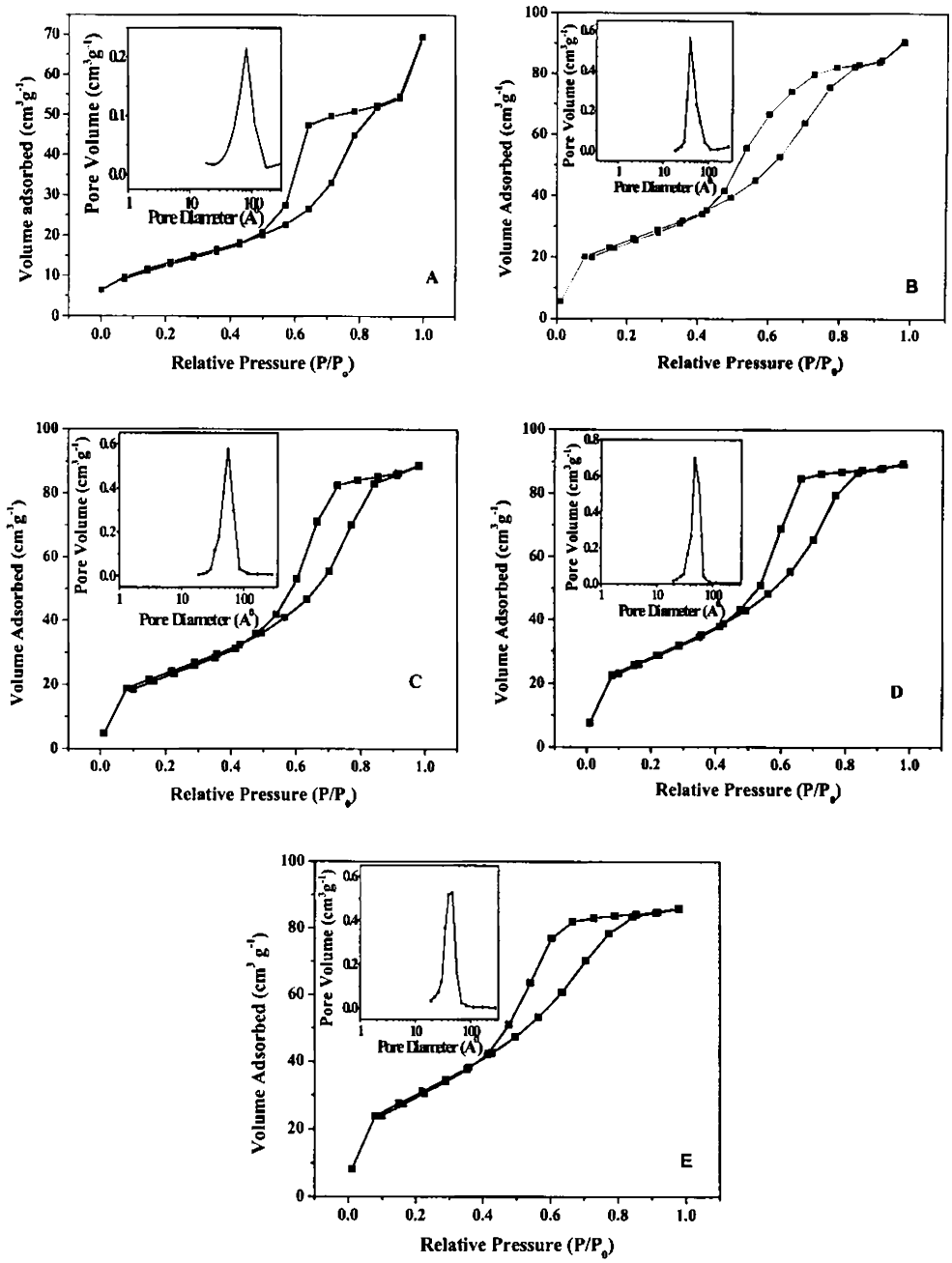

Figure 3.25. Adsorption isotherm and pore size distribution curve (inset) of (A) Pure titania (B) 1 mol% Yb_2O_3 doped TiO_2 (C) 2 mol% Yb_2O_3 doped TiO_2 (D) 5 mol% Yb_2O_3 doped TiO_2 (E) 10 mol% Yb_2O_3 doped TiO_2 , calcined at 500 °C

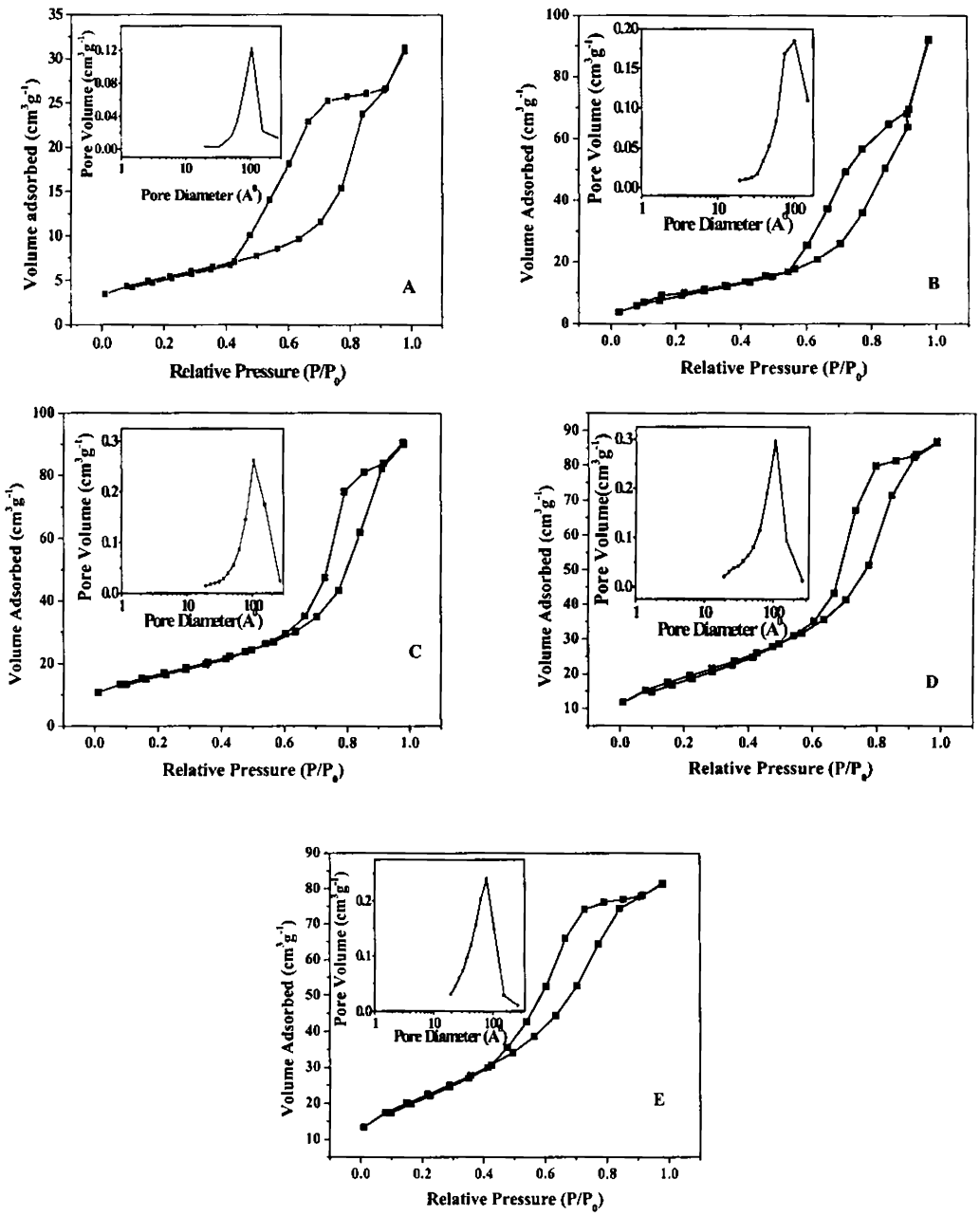

Figure 3.26. Adsorption isotherm and pore size distribution curve (inset) of (A) Pure titania (B) 1 mol% Yb_2O_3 doped TiO_2 (C) 2 mol% Yb_2O_3 doped TiO_2 (D) 5 mol% Yb_2O_3 doped TiO_2 (E) 10 mol% Yb_2O_3 doped TiO_2 , calcined at 600 °C

Ytterbium doped titania is also mesoporous in nature and has the Type IV adsorption isotherm (Figure 3.25 & 3.26). The pore size distribution obtained was narrow and falls in the mesoporous region as provided in the inset of Figure 3.25 & 3.26. The average pore diameter values indicate that all are lower than that of the undoped titania.

The adsorption isotherm of undoped titania has a upward tailing at high relative pressure, an indication of a wide distribution of mesoporosity with some contribution of large pores beyond mesopore scale. In contrast, adsorption isotherm of gadolinium and ytterbium doped titania has a narrow pore size distribution without any contribution of large pores beyond mesopore scale (>50 nm).[43] The hysteresis loop obtained is intermediate between H1 and H2 type, which also indicates that the gadolinium and ytterbium doped mesoporous titania has uniform cylindrical mesopores.[43]

3.4.4 Transmission Electron Micrographs

The TEM images of undoped, 10 mol% tantalum, 10 mol% gadolinium, 2 & 10 mol% ytterbium doped titania samples presented in Figure 3.27 A, B, C, D and E respectively. Undoped titania has a crystallite size of 23 nm and 10 mol% tantalum doped titania has a crystallite size of 6 nm, 10 mol% gadolinium doped has a crystallite size of 4 nm. In the case of 2 and 10 mol% Yb_2O_3 doped titania it is 8 and 7 nm respectively. From this observation it confirms that the doping of tantalum, gadolinium and ytterbium hinders the crystallite growth of titania.

The HRTEM & selected area electron diffraction images (Figure 3.27 A_1, B_1, C_1, D_1 & E_1) indicate that the undoped titania is more crystallised, with well defined electron diffraction pattern.

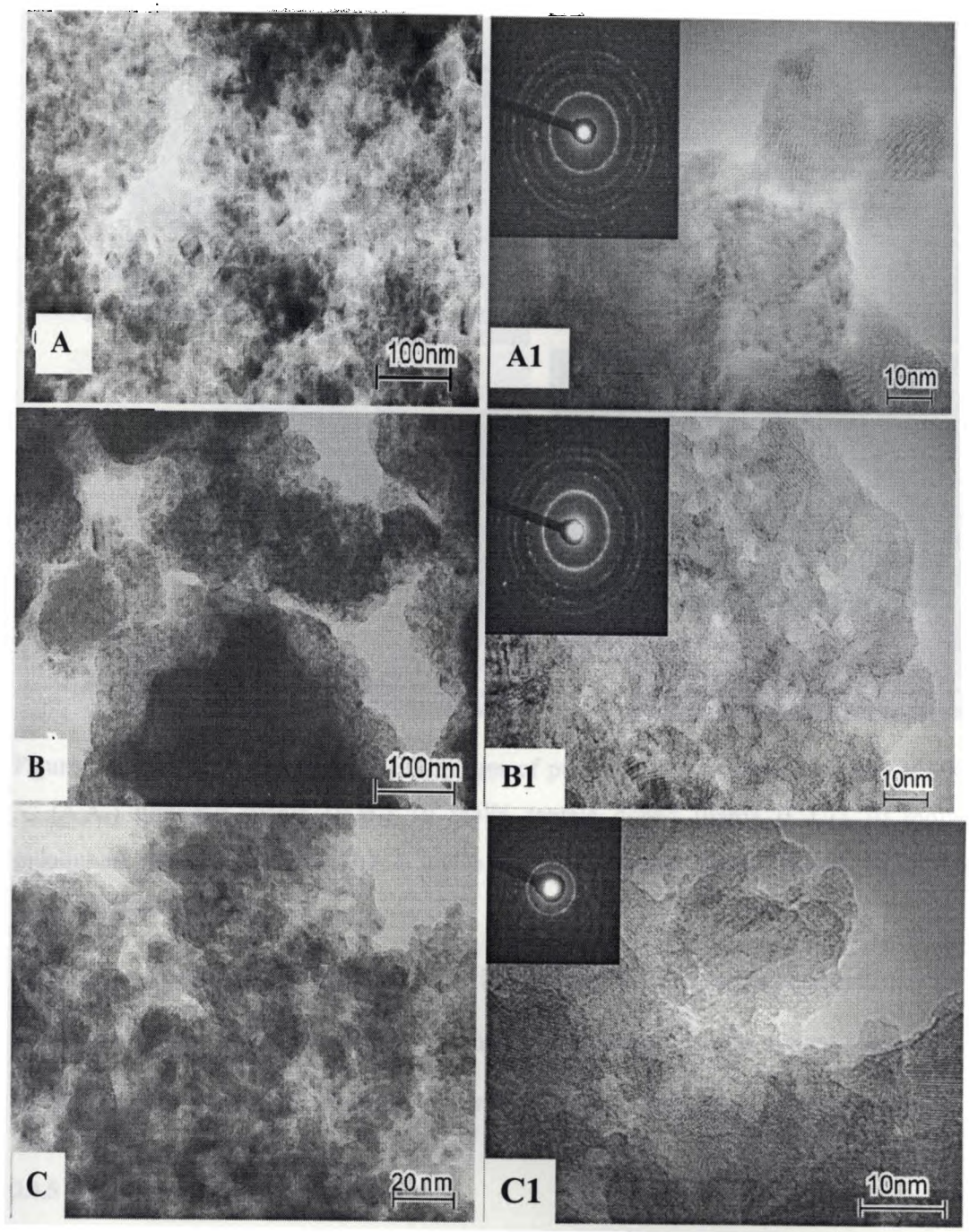
A
100nm
A1
10nm
B
100nm
B1
10nm
C
20 nm
C1
10nm

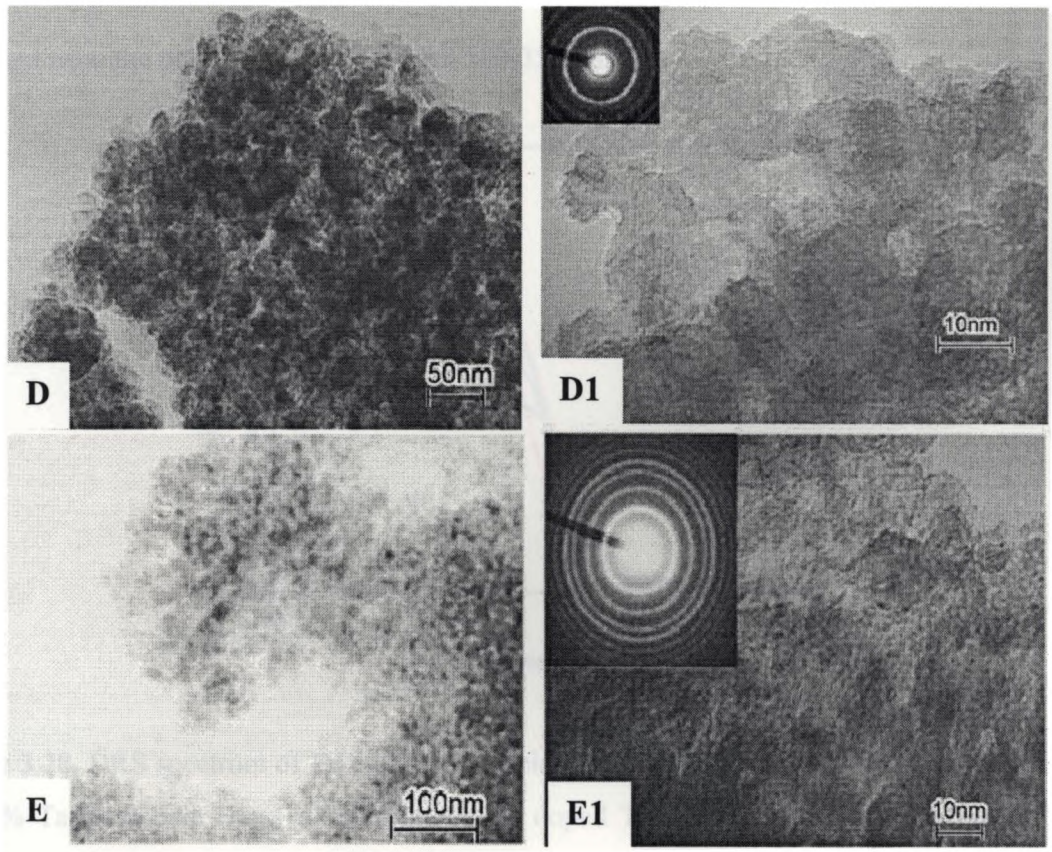

Figure 3.27. TEM, HRTEM & SAED images of pure and doped titania calcined at 600 °C (A,A_1) undoped titania (B,B_1) 10 mol% tantala doped titania (C,C_1) 10 mol% gadolinium doped titania (D,D_1) 2 mol% ytterbium doped titania (E,E_1) 10 mol% ytterbium doped titania

However in doped samples electron diffraction patterns are diffused, which indicates the amorphous nature. It is well correlated with our observation that the dopant hinders the crystallisation of titania, subsequently hinder the anatase to rutile phase transformation.

3.4.5 Diffuse Reflectance Spectrum

The UV- Visible diffuse reflectance spectroscopy was used for observing the optical property of the pure, tantalum, gadolinium and ytterbium doped titania. The

results are given in Figure 3.28, 3.29 & 3.30. Segregated crystallite anatase phase was identified from the observed bands between 300-350 nm.[44]

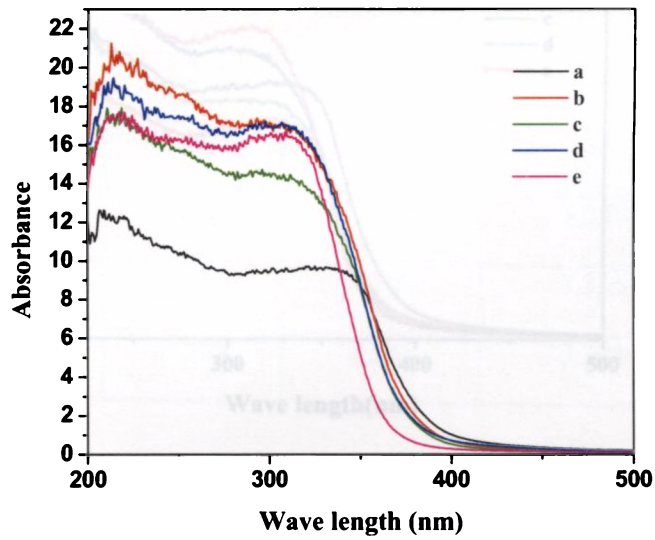

Figure 3.28. DRS spectrum of TiO_2 samples calcined at 500 °C for 1 h (a) Pure TiO_2, (b) 1 mol% Ta_2O_5 doped TiO_2, (c) 2 mol% Ta_2O_5 doped TiO_2, (d) 5 mol% Ta_2O_5 doped TiO_2, (e) 10 mol% Ta_2O_5 doped TiO_2

It was observed that upon increasing the concentration of the dopants the samples start absorption from lower wavelength region. UV-Visible absorption spectra show a blue shift in the absorbance onset value of the doped titania. Further we calculated the bandgap, which is presented in Table 3.4. The blue shift may be due to the quantum size effect of doped titania. Generally the quantum size effect is shown if crystallite size is below 10 nm. [45]

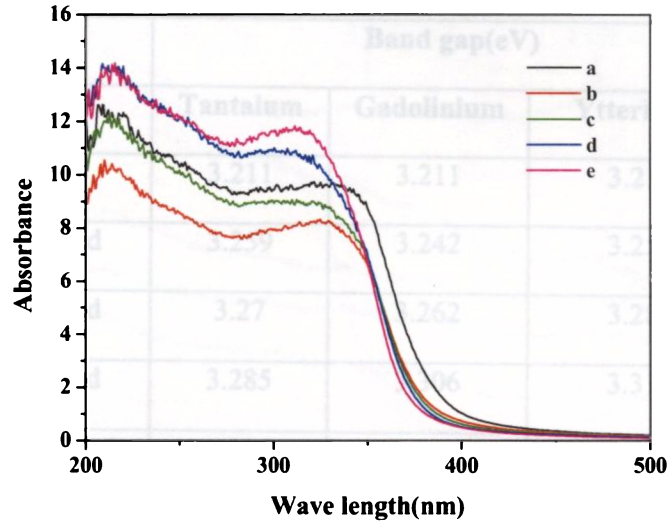

Figure 3.29. DRS spectrum of TiO_2 samples calcined at 500 °C for 1 h (a) Pure TiO_2, (b) 1 mol% Gd_2O_3 doped TiO_2, (c) 2 mol% Gd_2O_3 doped TiO_2, (d) 5 mol% Gd_2O_3 doped TiO_2, (e) 10 mol% Gd_2O_3 doped TiO_2

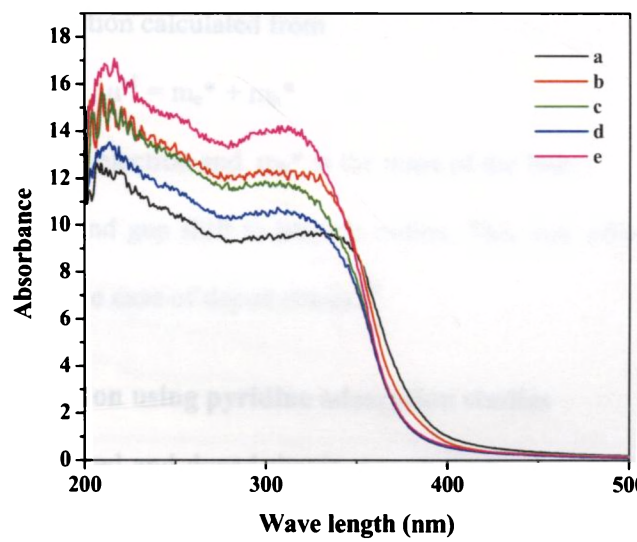

Figure 3.30. DRS spectrum of TiO_2 samples calcined at 500 °C for 1 h (a) Pure TiO_2, (b) 1 mol% Yb_2O_3 doped TiO_2, (c) 2 mol% Yb_2O_3 doped TiO_2, (d) 5 mol% Yb_2O_3 doped TiO_2, (e) 10 mol% Yb_2O_3 doped TiO_2

Table 3.4. Band gap of undoped and doped titania calcined at 500 °C

	Band gap(eV)		
	Tantalum	**Gadolinium**	**Ytterbium**
Undoped	3.211	3.211	3.211
1 mol% doped	3.259	3.242	3.255
2 mol% doped	3.27	3.262	3.289
5 mol% doped	3.285	3.306	3.316
10 mol% doped	3.395	3.331	3.344

The change in band width is related to the particle radius according to the equation 3.3.

$$\Delta Eg = (\hbar^2\Pi^2/2r^2\mu) - 1.8e^2/r\varepsilon \quad (3.3)$$

Where r is the radius of the particle, ε is the dielectric constant of the materials and μ is the reduced mass of the excition calculated from

$$\mu^{-1} = m_e^* + m_h^*$$

where m_e^* is the mass of the electron and m_h^* is the mass of the hole .

This equation relates the band gap shift to particle radius. This size effect is one of the reason for the blue shift in the case of doped titania.[45]

3.4.6 Acidity determination using pyridine adsorption studies

The acidity of undoped and doped titania was studied using pyridine adsorption technique.[46] The FTIR pattern of pyridine adsorbed on undoped and doped titania are presented in Figure 3.31, 3.32 & 3.33. The bands at 1600-1630 cm^{-1} and 1460 cm^{-1} correspond to the presence of Lewis acidic sites in the samples. A band at 1542 cm^{-1} corresponds to the formation of pyridonium ion on protonic sites, ie Brϕnsted acid sites.[47]

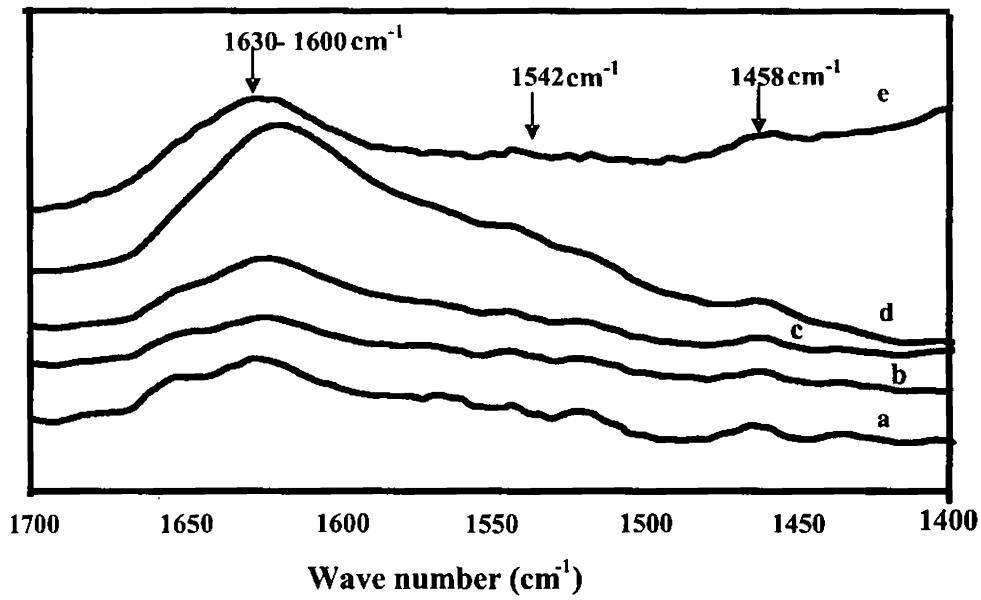

Figure 3.31. Pyridine absorption studies on (a) Pure titania (b) 1 mol% Ta_2O_5 doped TiO_2 (c) 2 mol% Ta_2O_5 doped TiO_2 (d) 5 mol% Ta_2O_5 doped TiO_2 (e) 10 mol% Ta_2O_5 doped TiO_2 , calcined at 600 °C

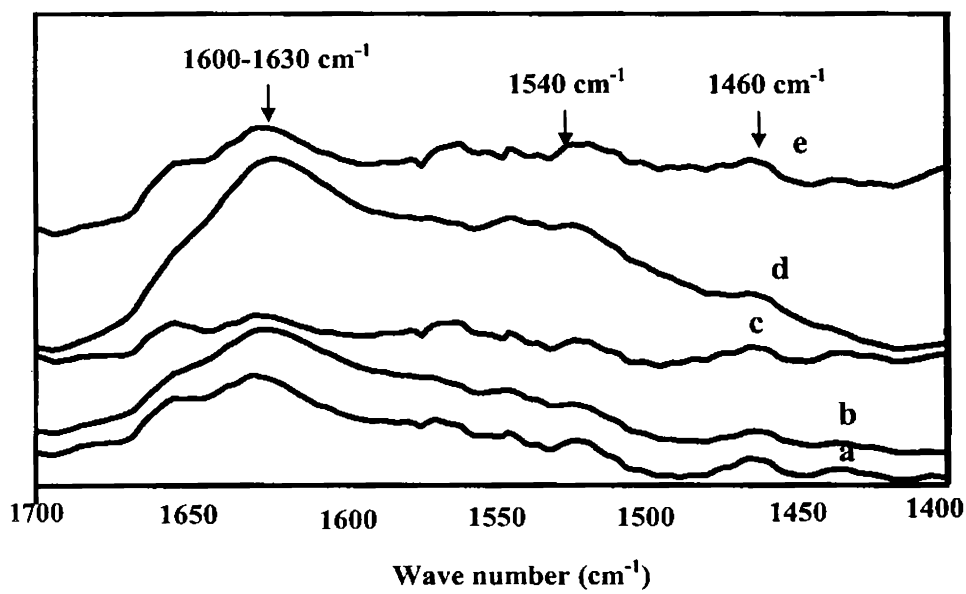

Figure 3.32. Pyridine absorption studies on (a) Pure titania (b) 1 mol% Gd_2O_3 doped TiO_2 (c) 2 mol% Gd_2O_3 doped TiO_2 (d) 5 mol% Gd_2O_3 doped TiO_2 (e) 10 mol% Gd_2O_3 doped TiO_2 , calcined at 600 °C

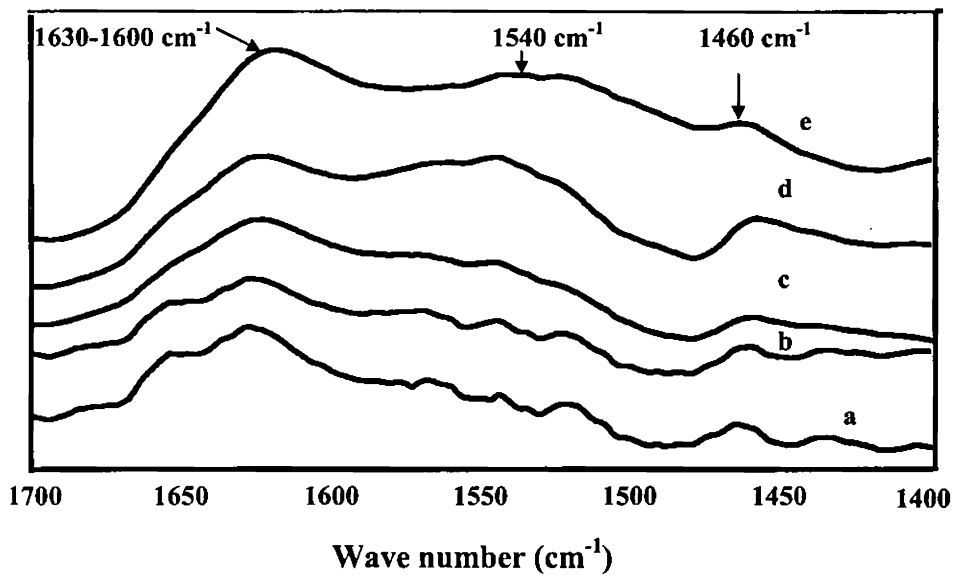

Figure 3.33. Pyridine adsorption studies on (a) Pure titania (b) 1 mol% Yb_2O_3 doped TiO_2 (c) 2 mol% Yb_2O_3 doped TiO_2 (d) 5 mol% Yb_2O_3 doped TiO_2 (e) 10 mol% Yb_2O_3 doped TiO_2 , calcined at 600 °C

Compare to the undoped titania, the intensity of peaks for doped ones is higher pointing out the presence of more acidic sites in doped samples. The increase in acidic sites can be correlated with increase in surface area of the doped samples.

3.4.7 Brϕwnsted Acidity using DMP adsorption technique

Brϕnsted acidity was measured by the thermodesorption studies of 2,6-dimethylpyridine. Satsuma et al.[48] reported that complete elimination of co-ordinately adsorbed 2,6-dimethylpyridine occurs above 300 °C. It has been also reported that complete removal of 2,6- dimethylpyridine occurs above 300 °C, which directly corresponds to the amount of Brϕnsted acid sites.[49] In the present case the fraction of weight loss in the range 300- 600 °C was found out and was taken as the measure of Brϕnsted acidity of the samples. The weight percentage and amount of 2, 6-dimethyl

pyridine desorbed in the pure and tantalum, gadolinium, ytterbium doped titania samples are shown in the Figures 3.34, 3.35 & 3.36.

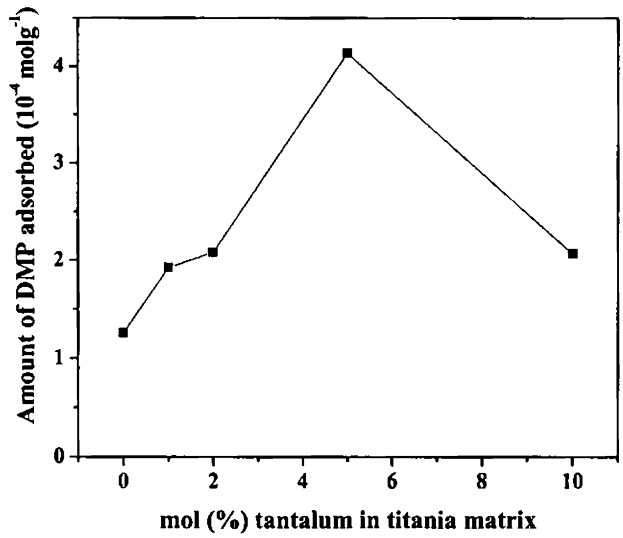

Figure 3.34. Amount of DMP adsorbed versus tantalum concentration in titania matrix

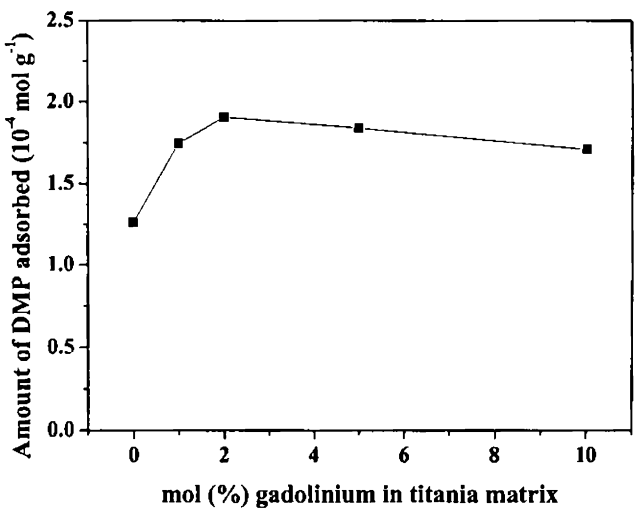

Figure 3.35. Amount of DMP adsorbed versus gadolinium concentration in titania matrix

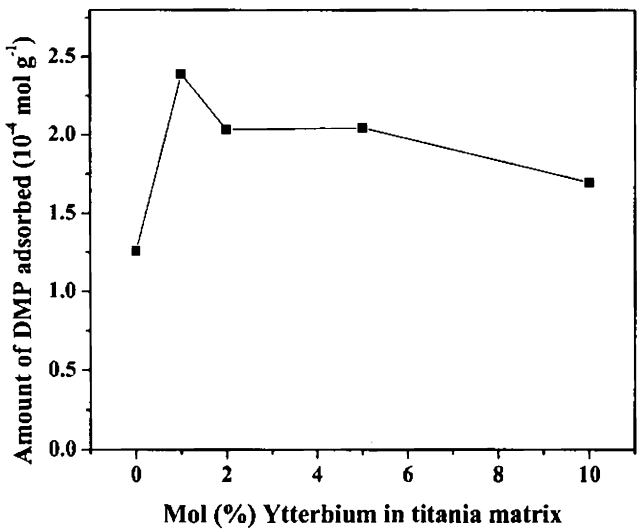

Figure 3.36. Amount of DMP adsorbed versus ytterbium concentration in titania matrix

It was observed that all the tantalum doped systems show more Brϕnsted acidic sites than the pure titania. Upto 5 mol% tantalum doping, there is an increase in Brϕnsted acidity but in 10mol% tantalum doped titania, the Brϕnsted acidity decreases. This may be due to the segregation of tantalum in the titania matrix at higher concentration. In the case of gadolinium doped titania, up to 2 mol% there is increase in the Brϕnsted acidic sites. However there is a slight decrease after 2 mol% gadolinium doped which may be due to the segregation of dopant in the titania matrix. In ytterbium doped titania, maximum Brϕwnsted acidity was obtained for 1 mol% doped sample and after that a slight decrease in acidity is observed. This also may be due to the segregation of dopant in the tiania matrix.

3.4.8 Photoactivity studies

The photocatalytic activity of the titania samples calcined at different temperature tested against methylene blue degradation is provided in Figure 3.37, 3.38 & 3.39. The

increase in tantalum content increases the activity of titania as evident from the graph (Figure 3.37). There is a considerable shift in rate of photoactivity when concentration of tantalum is increased from 1 to 2 mol%. Further increase in photoactivity with increase in tantalum content is not that pronounced. In fact a slight decrease is observed for the 10 mol% tantala doped titania. For comparison of activity a commercially available titania, Hombikat UV 100 was used. 2 mol% tantala doped sample gives titania with much better activity than commercially available Hombikat UV100 titania.

Precursor gel calcined at 500 °C contained only anatase phase for all samples including undoped and tantala doped titania as confirmed from XRD analysis. Hence the ratio of anatase to rutile phase can be ruled out as an influencing factor for the photocatalytic activity for the 500 °C calcined tantala doped titania samples. The difference in surface area alone will not be able to account for the observed photoactivity. The 2 mol% tantala doped titania has a surface area of 92 m^2g^{-1} and has activity two times than that of the 1 mol% tantalum doped titania which has a surface area of 78.8 m^2g^{-1}. At the same time 10 mol% tantala doped titania has a surface area of 63 m^2g^{-1} which is less than that obtained for the 1 mol% tantala doped titania but has photoactivity close to that of 2 mol% tantala doped titania. When calcined at 600 °C for compositions below 2 mol% tantalum doping there is an increase in activity, but for samples with 2 mol% tantala and above there is significant decrease in activity. Even for the 1 and 2 mol% tantala doped titania the surface area decreases but the photoactivity can be seen to increases.

Table3.5. provides the samples tested in the decreasing order of their activity. Crystallite size, surface area and rutile fraction in the sample are all provided for clarity

of discussion. From the data it can be seen that the samples having either crystallite size below 9 nm or which contains a mixture of phases show higher activity. In the absence of rutile phase as in the case of 500 °C samples high activity is observed when crystallite size falls below 9 nm. But when rutile phase is present when the gels are calcined above 500 °C, the activity is influenced by the composition of phases along with surface area. It can be seen that there is an increase in surface area along with the increase in activity and similarly a decrease in rutile percentage.

Table 3.5. Tantala doped titania compositions with decreasing order of their photoactivity

Sample	Calcination Temperature, °C	Crystallite Size, nm	Surface Area, m^2g^{-1}	Percentage Rutile
5% Ta doped TiO_2	500	8.5	87.9	0
2% Ta doped TiO_2	500	8.71	92.2	0
10% Ta doped TiO_2	500	7.15	63.2	0
10% Ta doped TiO_2	600	8.96	49	0
2% Ta doped TiO_2	600	11.66	67.1	17
5% Ta doped TiO_2	600	9.8	61.9	0
1% Ta doped TiO_2	600	15.4	45.1	26
Pure TiO_2	600	19.08	19.1	28.35
1% Ta doped TiO_2	500	11.35	78.8	0
Pure TiO_2	500	12.8	48.7	0

The decrease in crystallite size in the nano regime is associated with a blue shift in absorption edge [45, 50] and this has been found to aid photoactivity by decreasing the rate of recombination of hole electron pairs formed by photon irradiation. Mixture of rutile

and anatase phase has been reported [51] to show better activity than phase pure anatase titania. But from this study it is clear that anatase phase in the nano regime is better than a mixture of anatase and rutile phases. Tantalum doping influences the photoactivity of pure titania through a synergistic contribution from a modified phase composition, surface area and crystallite size.

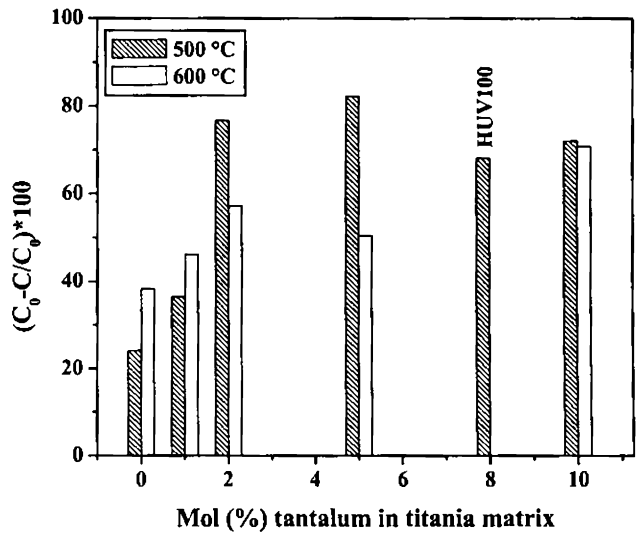

Figure 3.37. Photocatalytic degradation profile of Tantalum doped and undoped titania

The photocatalytic property of gadolimium doped titania calcined at 700 & 800 °C was measured using methylene blue degradation studies (Figure 3.37). The doping increases the photocatalytic property of titania. The increase in gadolinium concentration increases the photoactivity upto 5 mol% but at still higher concentration of 10 mol%, the photoactivity gets decreased to a level less than that of 1 mol% gadolinium doped titania. However, excessive doping makes the space charge layer very narrow so that the penetration depth of light into TiO_2 greatly exceeds the thickness of the space charge layer, resulting in easy recombination of electron-hole pairs and poor photoactivity.[50, 52]

This may be one of the reasons for the lower activity of 10 mol% gadolinium doped titania.

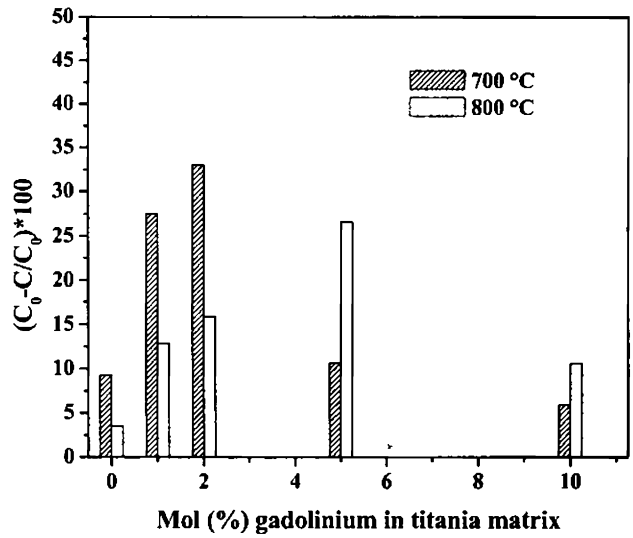

Figure 3.38. Photocatalytic degradation profile of gadolinium doped and undoped titania

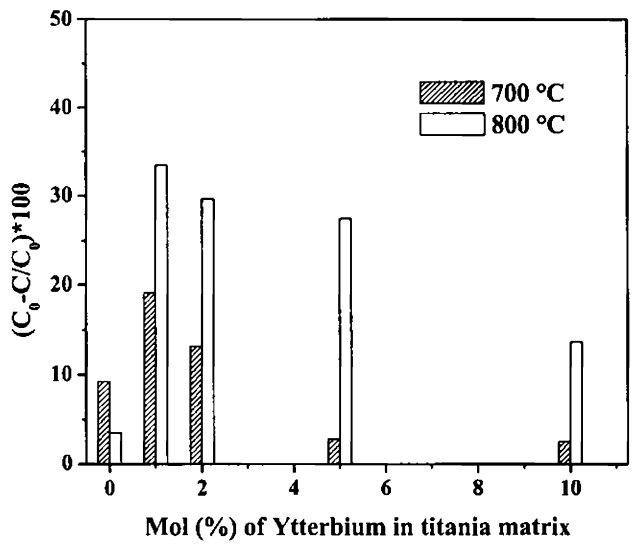

Figure 3.39. Photocatalytic degradation profile of ytterbium doped and undoped titania

This may be one of the reasons for the lower activity of 10 mol% gadolinium doped titania.

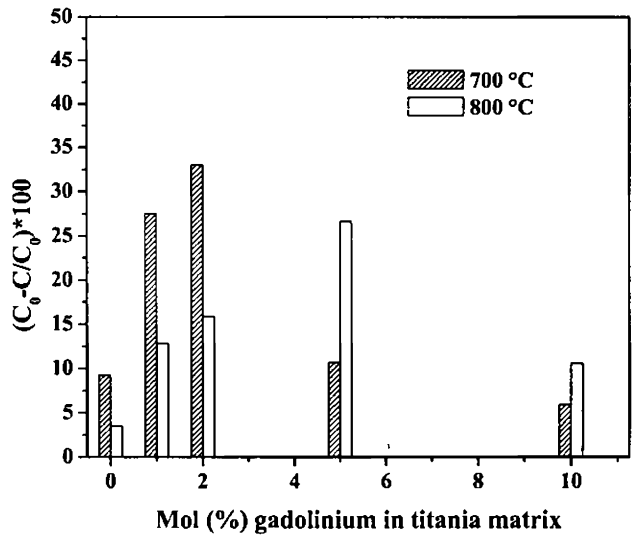

Figure 3.38. Photocatalytic degradation profile of gadolinium doped and undoped titania

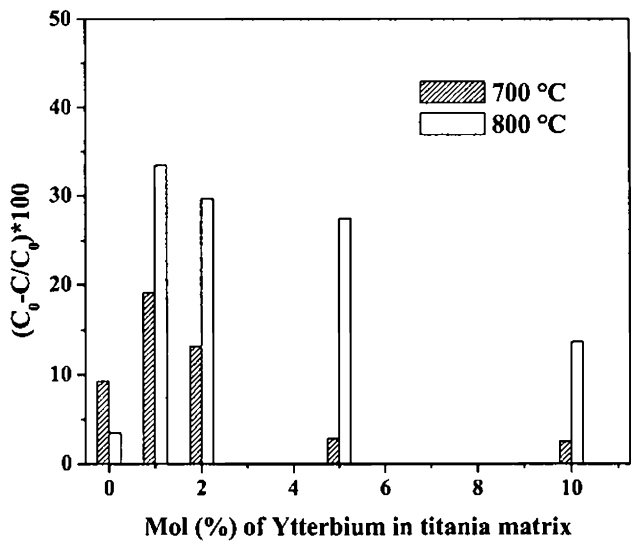

Figure 3.39. Photocatalytic degradation profile of ytterbium doped and undoped titania

In ytterbium doped titania, the maximum photocatalytic efficiency is shown by 1 mol% ytterbium doped titania at 700 and 800 °C. After 1mol% ytterbium the photoactivity decreases gradually. At 700 °C the 5 and 10 mol% show lower activity than the undoped titania. But at 800 °C all the doped compositions show higher activity than the pure titania but the same trend of increase in activity upto 1mol% doping and a decrease after observed. From this observation we can conclude that upto 1mol% ytterbium doping is enough for the photoactivity of titania.

Among the dopants, the Ta^{5+} which has an ionic radius similar to Ti^{4+} and which also did not form any additional phase with titania is most effective in photo catalysis. While the most active tantalum doped composition has an efficiency of 80%, ytterbium and gadolinium compositions show a maximum efficiency of only 35%. Tantalum doped compositions have higher photo activity than the commercially available Hombikat UV 100 titania. The gadolinium and ytterbium doped samples have more photoactivity compared to undoped titania calcined at 700 & 800 °C.

3.5 Conclusions

The anatase to rutile phase transformation was effectively hindered by the presence of tantalum, gadolinium and ytterbium in the titania matrix. In undoped titania, the anatase to rutile transformation starts at 600 °C and completes at 800 °C. An enhanced anatase phase stability was achieved through the doping. In the case of tantalum doped titania the complete anatase to rutile phase transformation occurs at a temperature above 1000 °C while in the case of gadolinium and ytterbium doped titania, it is above 900 °C. The crystallite size also decreased in presence of dopant. TEM images show that undoped titania has a crystallite size of 23 nm at 600 °C, while 10 mol%

tantala, gadolinium and ytterbium doped titania have crystallite size of 6, 4, 7 nm respectively. One significant observation found is that when the crystallite size reaches a critical size between 12-20 nm, anatase to rutile phase transformation occurs. The specific surface area increased 2 to 3 times higher when compared to undoped titania at all the temperatures investigated. This indicates that the dopants effectively hinder the reduction in surface area by controlling the crystallite size and pore stability of the titania. The catalytic activity of the system was measured using pyridine adsorption studies and in all the doped samples the intensity of the adsorbed pyridine and pyridonium ions increase, which means the acidity increases in the doped system compared to the undoped titania. Brϕnsted acidity measurement using the DMP adsorption shows that the Brϕwnsted acidity of tantala doped titania increases upto 5 mol% and then slightly decreases. In gadolinium doped titania, it increases upto 2 mol% and then a slight decrease in acidity was observed. In ytterbium doped system, the maximum Brϕwnsted acitiy is shown by 1mol% ytterbium doped titania and decreases after 1 mol% doping. Tantalum doping is found to increase the photocatalytic activity of titania and doping of tantala above 1 mol% and calcination at 500 °C results in titania photocatalysts with better activity than commercially available Hombikat UV100 titania. In case of gadolinium doped titania, upto 5 mol% doping the photoactivity increases and then decreases. In ytterbium doped titania photoactivity increases upto 1 mol% doping. At higher concentration of ytterbium doping photoactivity decreases.

3.6 References

1. A. Fujishima, K. Hashimoto, T. Watanabe, *TiO_2 Photocatalysis Fundamentals and Applications,* BKC Inc., Tokyo, **1999**.
2. W. J. Stark, K. Wegner, S. E. Partsinis, A. Baiker, *J. Catal.,* 197, **2001,** 182.
3. M. A. Fox, M. T. Dulay, *Chem. Rev.,* 93, **1993,** 341.
4. M. Fujihira, Y. Satch, T. Osa, *Nature,* 293, **1981,** 206.
5. E. Borgarello, N. Serpone, G. Emo, R. Harris, E. Pelizzetti, C. Minero, *Inorg. Chem,* 25, **1986,** 4499.
6. Y. Inel, D. Ertek, *J. Chem. Soc. Faraday Trans.,* 89, **1993,** 129.
7. D. F. Ollis, E. Pelizzetti, N. Serpone, *Environ. Sci. Technol.,* 25, **1991,** 1523.
8. V. F. Stone, Jr. R. J. Davis, *Chem. Mater.,*10, **1998,** 1468.
9. H. S. Yun, K. Miyazuwa, H. S. Zhou, I. Houma, M. Kuwabara, *Adv. Mater.,* 13, **2001,** 1377.
10. S. Karvinen, R-J. Lamminmaki, *Solid State Sci.,* 5, **2003,** 1159.
11. J. A. Navio, M. Macias, M. Gonzalez-Catalass, A. Justo, *J. Mater. Sci.,* 27, **1992,** 3036.
12. J. Moon, H. Takagi, Y. Fujishiro, M. Awano, *J. Mater. Sci.,* 36, **2001,** 949.
13. M. Anpo, M. Takeuchi, *J. Catal.,* 216, **2003,** 505.
14. K. Y. Jung, S. B. Pask, *Appl. Catal. B. Environ.,* 25, **2000,** 249.
15. K. Wilke, H. D. Breuer, *J. Photochem. Photobiol. A-Chem.,* 121, **1999,** 49.
16. A. Rampaul, I. P. Parkin, S. A. O'Neill, J. Desouza, A. Mills, N. Elliott, *Polyhedron,* 22, **2003,** 35.
17. Y. Wang, H. Cheng, Li Zhang, Y. Hao, J. Ma, B. Xu, W. Li, *J. Mol Catal. A-Chem.,* 151, **2000,** 205.
18. Y. Zhang, H. Xu, Y. Xu, H. Zhang, Y. Wang, *J. Photochem. Photobiol. A- Chem.,* 170, **2005**, 279.

19. H. Lin, S. Kumon, H. Kozuka, T. Yoko; *Thin Solid Films*, 315, **1998,** 266.

20. C. Li, J. Wang, X. Wang, H. Chen, W. Su, *Mater. Chem. Phys.*, 74, **2002,** 187.

21. N. Bonini, M.C. Carotta, A.Chiorino, V. Guidi, C.malagu, G. Martinelli, L. Paglialonga, M. Saeerdoti, *Sensor. Actuat. B. Chem.*, 68, **2000,** 274.

22. M. Saeerdoti, M. C. Dalconi, M. C. Carotta, B. Cavicchi, M. Ferroni, S. Colonna, M. L. D. Vona, *J. Solid State Chem.*, 177, **2004,**1781.

23. V. Guidi, M. C. Carotta, M. Ferroni, G. Martinelli, M. Sacerdoti, *J. Phys. Chem. B,* 107, **2003,** 120.

24. C. M. Visinescu, R. Sanjines, F. Levy, V. Marcu, V. I. Parvulescu, *J. Photochem. Photobiol. A-Chem.*,174, **2005,** 106.

25. C. Wang, A. Geng, Y. Guo, S. Jiang, X. Qu, L. Li, *J. Colloid Interfac. Sci.*, 301, **2006**, 236.

26. K. T. Ranjit, I. Willner, S. H. Bossmann, A. M. Braun, *Environ. Sci. Technol.*, 35, **2001,** 1544.

27. J. Nair, P. Nair, F. Mizukami, Y. Oosawa, T. Okubo, *Mater. Res. Bull.*, 34, **1999,** 1275.

28. C. A. LeDuc, J. M. Campbell, J. A. Rosssin, *Ind. Eng. Chem. Res.*, 35, **1996,** 2473.

29. R. Gopalan, Y. S. Lin, *Ind. Eng. Chem. Res.*, 34, **1995,** 1189.

30. C. P. Sibu, S. Rajesh Kumar, P. Mukundan, K. G. K. Warrier, *Chem. Mater.*, 14, **2002,** 2876.

31. T. Peng, D. Zhao, H. Sing, C. Yan, *J. Mol. Catal. A: Chem.*, 238, **2005,** 119.

32. Y. Xie, C. Yuan, *Appl. Surf. Sci.*, 221, **2004,** 17.

33. J. Lin, J. C. Yu, *J. Photochem. Photobiol. A Chem.*, 116, **1998,** 63.

34. S. Hishita, I. Mutoh, K. Koumoto, H. Yanagida, *Ceram. Inter.*, 9, **1983,** 61.

35. Y. Zhang, H. Zhang, Y. Xu, Y. Wang, *J. Solid State Chem.*, 177, **2004,** 3490.

36. R. A. Spurr, H. Myers, *Anal. Chim.*, 29, **1957,** 760.

37. W. Bai, K. L. Choy, N. H. J. Sytelzer, J. Schoonman, *Solid State Ionics*, 116, **1999,** 225.

38. H. Zhang, J. F. Banfield, *J. Mater. Chem.*, 8, **1998,** 2073.

39. A. A. Gribb, J. F. Banfield, *Am. Minerol.*, 82, **1997,** 717.

40. R. D. Shannon, J. A.Pask, *J. Am. Cer. Soc.*, 48, **1965,** 391.

41. F. C. Gennari, D. M. Pasquevich, *J. Mater. Sci.*, 33, **1998,**1571.

42. K. N. P. Kumar, K. Keizer, A. J. Burggraaf, *J. Mater. Chem.*, 3, **1993,** 1141.

43. S. J. Gregg, K. S. W. Sing, Adsorption, Surface area and Porosity, IInd Ed., Academic Press, **1982.**

44. A. M. Prakesh, H. M. Sung-Suh, L. Kevan, *J. Phys. Chem. B.*, 102, **1998,** 857.

45. L. E. Brus, *J. Chem. Phys.*, 79, **1983,** 5566.

46. J. Ryezkowski, *Catal. Today,* 68, **2001,** 263.

47. G. Bosca, *Catal. Today,* 41, **1998,** 191.

48. A. Satsuma,Y. Kamiya, Y. Westi, T.Hattori; *Appl. Catal. A. Gen.*, 194-195, **2000,** 253.

49. K. R. Sunajadevi, S. Sugunan, *Mater. Lett.*, 58, **2004,** 3290.

50. M. A. Henderson, *Surf. Sci.*, 400, **1998,** 203

51. D. S. Muggli, L. Ding, *Appl. Catal B: Environ.*, 32, **2001,** 181.

52. Y. V. Pleskov, *Sov. Electrochem.*, 17, **1981,** 1.

Chapter 4: Development of Functional Coatings on Porous Alumina and Glass Substrate

4.1 Development of Ultra Filtration Membrane on Porous Alumina Substrate

4.1.1 Abstract

Ceramic membranes are of interest because of their higher chemical, thermal and mechanical stability than all other membrane materials. These membranes allow filtration under extreme conditions, like high temperature and extreme pH. In this chapter the fabrication of alumina-titania multilayer ceramic membrane layers on porous alumina support is described. The coating precursor is made from boehmite and titania sols, which is prepared through aqueous sol-gel route. Different compositions of coating solutions are prepared using boehmite and titania sols with hydroxyethyl cellulose (HEC) as binder. The various coating compositions prepared were characterised by viscosity measurements, TGA and DTA. Unsupported membranes were first prepared to check crack free drying and to study the porosity features of the membranes. The compositions corresponding to crack-free and thin membranes were chosen for coating on porous alumina substrates. Thus the one containing 1.5% HEC and 0.4% boehmite was coated as an intermediate layer. The top layer was formed with the composition containing 1%HEC and 0.2% titania. The membranes were characterised by XRD, FTIR and surface area measurements. The morphological features of coated layer were studied using scanning electron microscope. The filtration property of the membrane has been examined by cross-flow filtration method using a colouring agent such as congo red which is a red coloured dye. About 99.3% rejection of congo red was observed.

4.1.2 Introduction

Ceramic membranes are a class of engineering ceramic systems having great potential for application in the field of water desalination, ultrafiltration and separation of gas mixtures. They are also projected as potential candidates for catalytically active and carrier membranes. Ceramic membranes are thin (few nanometers to few micrometres thick) planar structures formed, either as supported or as unsupported configuration by the regular packing of fine ceramic particles (2 to 1 nm) or inorganic polymer clusters. The first ever application of ceramic membranes dates back to the 1940's, after the second World war. They were used for the enrichment of U^{235}.In that process, $U^{235}F_6$ was separated from a mixture of $U^{238}F_6$ and $U^{235}F_6$ using a supported membrane in a tubular configuration. Commonly used materials for making ceramic membranes are Al_2O_3, TiO_2, SiO_2, ZrO_2 or a combinations of these materials. Aluminium, titanium and zirconium are considered as the three most common porous membrane materials. There are also reports on oxide membranes with minor amounts of dopants to improve the thermal and chemical stability.[1] Doping and surface modification can also improve the catalytic performance of the membranes.[2] There are many reports for the preparation of membranes employing solid state-particle-sintering,[3,4] sol-gel,[5, 6] anodic oxidation,[7,8,9] chemical vapour deposition [10,11,12] phase separation and leaching [13]and the reverse micelle method.[14, 15] Out of these methods, solid state-particle-sintering and sol-gel process are considered to be the practical methods. Usually ceramic microfiltration membranes are prepared by solid state-particle-sintering method in which the membranes are fabricated with particles by coating the support and then sintering to form a membrane skin which is chemically attached to the support. Pore size obtained by this

method varies from 0.1 to 1μm and the porosity of the ceramic membranes is in the range of 30-50%. Ceramic ultra filtration membranes are generally prepared by the sol-gel methods. By sol-gel method, the mean membrane pore size mainly assembles between 2 and 20 nm.[16] The sol-gel process involves the hydrolysis and condensation of various metal alkoxide molecules under controlled conditions to form metal-oxygen-metal bridging units.[17, 18] Microporous alumina membranes are used for separation of microbes from drinking water, concentration of fruit juices in food industry and filtration of beverages for their clarification and sterilization. They also find application as substrate for nanofiltration, ultrafiltration and reverse osmosis membranes.[19-23]

4.1.2.1 Structural features of supported ceramic membranes

Supported ceramic membranes consist of a macroporous support which is a few millimeters thick (Figure 4.1.1) with an average pore diameter of 1 to 15μm and with a porous intermediate layer of 10 to 100μm thick. The average pore diameter of the porous intermediate layer is 100-1500 nm. The third top layer, which is the functional membrane layer, usually has a thickness of 0.1 to 10μm with an average pore diameter in the range of 1-100 nm (Table 4.1.1).[24]

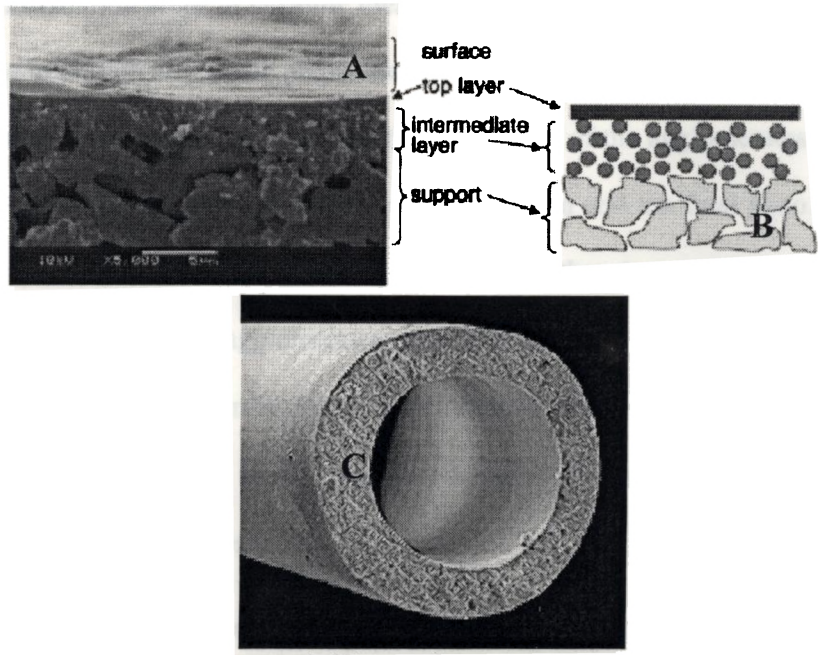

Figure 4.1.1 (A) SEM photo and (B) a schematic representation of an asymmetric composite membrane (C) Cross sectional view of porous membrane support tube

Table 4.1.1 Properties of membrane layers

Layer	Thickness	Average pore diameter
α-Al_2O_3-support	-	1.4μm
α-Al_2O_3 -MF	20-25 μm	0.18μm
Coarse ZrO_2-UF	10 μm	60 nm
Coarse TiO_2-UF	10 μm	50 nm
Fine ZrO_2-UF	100-200 nm	2-3 nm
Fine TiO_2-UF	500 nm	10 nm
ZrO_2-NF	<50 nm	1-2 nm
TiO_2-NF	<50 nm	1-2nm

4.1.2.2 Formation steps of ceramic membranes

The important step in the preparation of sol-gel derived ceramic membranes is the preparation of a stable colloidal sol. The size and nature of the agglomerates in the sol is very important because they affect the ease of formation and the final nano structure of the membranes. The exact role of the agglomerates is that they influence the top-layer growth kinetics. In fact, the agglomerates must be weak and below a certain size in order to give small pores and a narrow pore size distribution.[25] In general, a colloidal sol yields a membrane with pore size in the mesopore range while inorganic polymer solutions yield microporous membranes.

The next step is to apply the sol / solution (dip solution) on a porous support by bringing one side of the support (in the case of flat plate supports) in contact with the dip-solution. An alcogel or a hydrogel layer will be formed on the support and the layer formation mechanism can be film coating or a combination of slip-casting and film coating.[26] The film coating process depends on the viscosity of the dip-solution and the pulling speed of the support from the dip-solution. On the other hand, the slip-casting process depends on the pore characteristics of the support as well as on the viscosity and the surface tension of the dip-solution. After forming an alcogel or a hydrogel layer, the membrane-support system is dried at controlled temperature and relative humidity.

The dipping stage is absent in the preparation of unsupported membranes. They are formed simply by pouring the dip-solution into a glass or a polyethylene petri dish and dried directly to get the xerogel. Drying is one of the most important steps in the preparation of ceramic membranes. During drying, large stresses develop due to the

capillary tension of the pore fluid and these stresses are not relaxed by shrinkage because of the presence of rigid support.

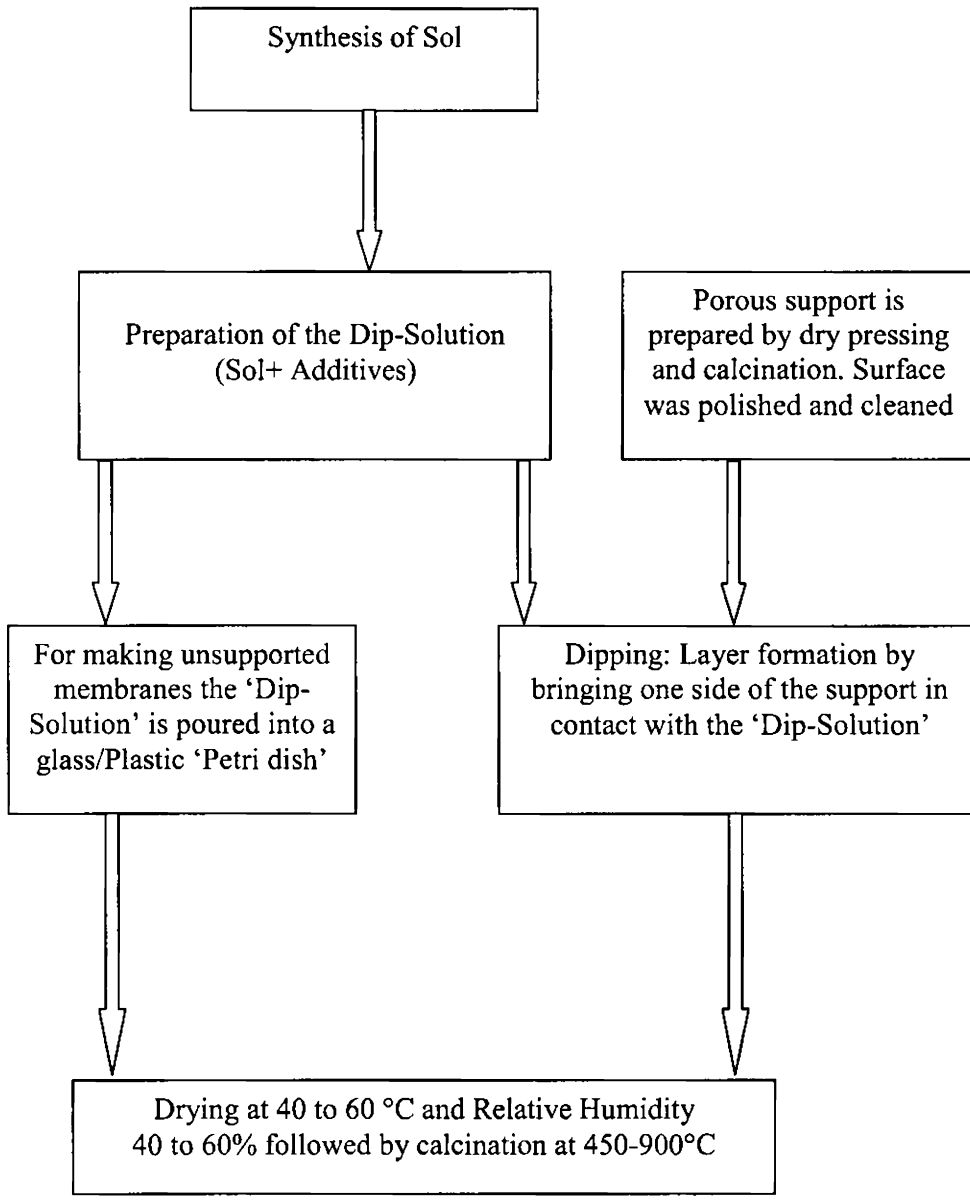

Figure 4.1.2. Flow chart illustrating the formation of ceramic membranes using sol-gel process.

The stress field in the top-layer can become inhomogeneous around hard agglomerates. This makes the membrane top-layer to crack and peel off from the support. Drying

stresses also have a positive role in membrane formation. The stresses cause weak aggregates to break down and may help in further rearrangement and ordering of the primary particles.[27] The final nano structure of the membrane is believed to be established at this stage. There exists a maximum and minimum allowable thickness which should not be surpassed if defect (crack) free membranes have to be obtained. The actual thickness limit depends on the membrane material.[28] The last step is calcination, which gives the mechanical integrity to the membrane-support system. During calcination, physically adsorbed water, hydroxyls, residual organics and nitrates will escape below 450 °C. Flow chart for the preparation of membrane using sol-gel method is presented in Figure 4.1.2.

4.1.2.3 Filtration technology

Filtration technology using membranes has a wide range of applications. So far, organic filters commonly have been used, although these filters have relatively low temperature limitations (typically <200°C) and lack chemical stability. As a new kind of membrane, ceramic filters have a potential capability for replacing organic filters for some applications; because of their superior high temperature (>1000°C) and chemical stability. Ceramic filters are expected to be used in applications such as microfiltration (100 nm < pore size < 10 μm), ultrafiltration (pore size<100 nm), filtration of molten metal, gas separation at high temperature and particle removal from exhaust gas from diesel engines (Figure 4.1.3).[29] Filtration performance of various type of membranes are given in Table 4.1.2.

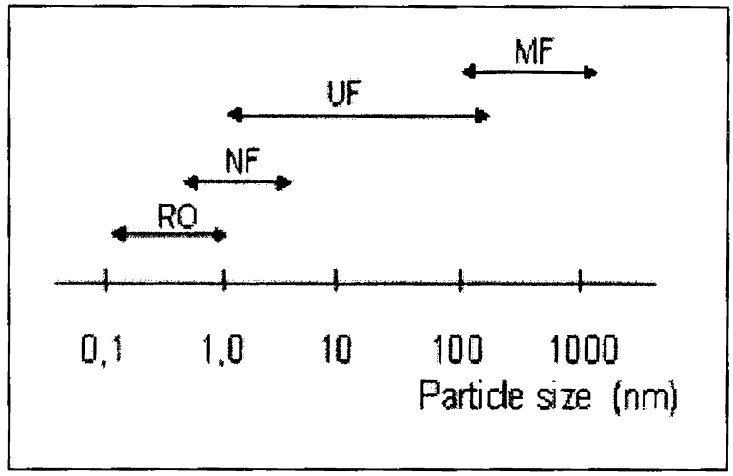

Figure 4.1.3. Diagramatic representation of classification of various types of membranes

Table 4. 1. 2. Filtration performance of various types of membranes

	Microfiltration	**Virus Filtration**	**High-Performance Filtration**	**Ultrafiltration**	**Nanofiltration/ Reverse osmosis**
Components retained by membrane	Intact cells Cell debris	Viruses	Proteins	Proteins	Antibiotics Sugars Salts
Membrane					
Components passed through membrane	Colloidal material Viruses Proteins Salts	Proteins Salts	Proteins Salts	Small peptides Salts	Salts Water
Approximate membrane cutoff range	0.05μm-1μm	100kD-0.05μm	10kD-300kD	1kD-1000kD	<1kD

For membranes used for liquid phase separation, the driving force is mechanical pressure difference, and they are categorized into microfiltration (MF), ultrafiltration (UF), nanofiltration (NF) and reverse osmosis (RO), depending on their pore sizes (Figure

4.1.3). Microfiltration membranes have pore sizes between 100 and 1000 nm and UF and NF are classified at the pore size less than 100 nm. RO membranes have smaller pore size than 1 nm. According to conventional definition and for the convenience of membrane users, molecular weight cut-offs (MWCO) which are based on permeation performance are also often used. NF membranes are categorized to have MWCO between 200 and 1000.[30, 31] Filtration performance of various types of membranes were given in Table 4.1.2.

4.1.2.4 Applications of ceramic membranes

Initially ceramic membranes were used in waste water technology. Meanwhile, successful solutions and possible applications cover all industries.

- Chemical industry

(a) Product separation and cleaning (b)Concentration of polymer suspensions and metal hydroxide solutions (c) Separation of catalysts (d) Recovery of dyes and pigments (e) Desalination of products (f) Cleaning and recycling of organic solvents (g) Metal industry / Surface engineering (h) Recycling and disposal of degreasing and rinsing baths (i) Treatment of oil / water emulsions (j) Recovery of heavy metals (k) Cleaning of waste water from grinding processes (l) Treatment of waste water from glass and glass fibre production

- Biotechnology

(a)Concentration, fractionation, isolation and sterilization of antibiotics, enzymes, proteins, amino acids and vitamins (b) Separation, concentration and dewatering of biomass and algae (c) Disposal of fat emulsions (d) Separation of yeast

- Food and beverages

(a) Clarification of juice and beer (b) Concentration of juice (c)Sterilization of milk and whey (d) Separation and fractionation of milk and whey ingredients (e) Desalination of whey (f) Dewatering of products (g) Purification of drinking water

- Recycling and environment

(a) COD / BOD reduction (b) Oil / water separation (c) Recovery of pharmaceuticals and pesticides (d) Retention of microorganism (e) Retention of heavy metals and radioactive substances (f) Recycling of water from swimming pools (g) Purification of the drain of sewage plants.

4.1.2.5 Benefits of ceramic membranes

(a) Long and reliable lifetime (b) High resistance to temperature and pressure (c) High stability to organic media (d) Rigidity with no creep or deformation (e) Stablity over a wide pH range (f) Corrosion and abrasion resistance (g) Insensitivity to bacterial action (h) Can be repeatedly sterilized by steam or chemicals (i) Ability to be backwashed (j) Consistent pore size (k) Can process highly viscous fluid (l) Possibility of regeneration after fouling (m) Membranes are bonded to substrate by strong ceramic bonds.

4.1.2.6 Disadvantages of ceramic membranes

(a) Brittle and poor geometrical stability (b) Needs to be in the supported configuration (c) High installation and maintenance costs (d) Sealing is very difficult for high temperature application.

Ceramic membranes have a wide variety of applications in chemical industries, food and beverage industries, biotechnology, water purification and recycling etc. The

general mode of adapting ceramic membranes to the different application domains, in particular for liquid filtration, has been to superpose successive porous layers starting from a macroporous support. In order to minimize flow resistance, non interpenetrated layers are superposed with decreasing pore sizes and thicknesses. The resulting multi-layered ceramic structures must be regarded as advanced ceramic materials with unique fluid processing performance. Research is actively done in this area of development of membrane with desired pore structures. Normally all the sol-gel membrane formation starts with alkoxide precursors. To the best of our knowledge there is no report on the preparation of multilayered membrane through an aqueous sol-gel method. The objective of the present work is the development of an aqueous sol-gel method for the preparation of mesoporous membrane layer on the surface of porous alumina substrate for ultra filtration applications.

4.1.3 Experimental

$Al(NO_3)_3.9H_2O$, (sd. Fine Chemicals, India Ltd) 125 g was dissolved in 1 litre water. The solution was heated to 90 °C. Keeping the temperature constant at 90 °C, ammonium hydroxide solution was added drop wise. Addition was continued till the precipitation was complete at pH 8. The precipitate was filtered while solution was hot and washed with distilled water till it becomes free from nitrates. The precipitate was aged for 24h. It was peptised to a stable sol by the addition of 10% HNO_3 at a pH of 3.5. The particle size of the sol was measured using Malvern Zetasizer 3000 HS (U.K) particle size analyzer. Alumina coating solutions of different compositions were prepared using boehmite sol with hydroxylethyl cellulose (HEC) as the binder. The calculated amount of hydroxyethyl cellulose was dissolved in water and added into the boehmite

sol. The resultant solution was homogenized by stirring for half an hour by gentle warming followed by centrifugation. The different wt% of boehmite and hydroxy ethyl cellulose are provided in Table 4.1.3. The viscosities of the above compositions were measured to study the variation of viscosity with shear rate using a Viscorheometer (Rheo Labmc1, Physica, Anton Paar, Germany)

Table 4.1.3. Alumina coating solutions of different compositions were prepared using boehmite sol with hydroxyl ethyl cellulose

Percentage composition of HEC	**Percentage composition of Boehmite**
1	0.1
1	0.2
1	0.3
1	0.4
1	0.5
1.5	0.1
1.5	0.2
1.5	0.3
1.5	0.4
1.5	0.5
2	0.1
2	0.2
2	0.3
2	0.4
2	0.5
2.5	0.1
2.5	0.2
2.5	0.3
2.5	0.4
2.5	0.5

Titanyl oxysulphate ($TiOSO_4$, Aldrich Chemicals, 99.99% purity) was used as precursor for the synthesis of titania sol. In a typical experiment, titanyl oxysulphate was dissolved in 500 ml of distilled water (0.2 M) and hydrolysed by slow addition of ammonium hydroxide (10%, sd. Fine Chemicals, India Ltd) solution under constant stirring at room temperature (32 ^{0}C), until the reaction mixture attained pH 8.5. The precipitate obtained was separated by filtration and was washed free of sulphate ions (confirmed by the $BaCl_2$ test) with distilled water. The precipitate was further dispersed in 1000 ml of hot distilled water and peptised by addition of 10% HNO_3 (Merck, India Ltd) solution. A stable sol was obtained at a pH range of 1.7 to 2.2. Different compositions of coating solutions were prepared by mixing titania sol with hydroxyethyl cellulose dissolved in water (HEC). The compositions were stirred for half an hour and then centrifuged. The compositions prepared were given in Table 4.1.4.

Various compositions of coating solutions prepared from boehmite and titania sols were used for making unsupported membranes. Particle size distribution of the sol was analyzed by Malvern Zetasizer 3000 HS particle size analyzer. 20 ml of the different compositions were poured into separate clean plastic petri dishes and were dried in a humidity chamber at 50 ^{o}C and at 60% relative humidity for 24h followed by drying at 70 ^{o}C. The composition which gave crack free membrane of desired viscosity was chosen for coating purpose. The porous alumina tubes were cleaned well by boiling several times in distilled water and were subsequently dried. Then the tube to be coated was held in the vertical direction with the help of a support stand. A glass tube was attached to the upper end of the porous alumina tube. The lower end of alumina tube was connected to a glass column. The column was lowered beyond the position of the tube and the coating

solution prepared from boehmite sol and hydroxyethyl cellulose of suitable composition and which showed crack-free behaviour when tested as unsupported membrane was introduced into the column.

Table 4.1.4. Titania coating solutions of different compositions prepared using boehmite sol with hydroxylethyl cellulose

Percentage composition of HEC	**Percentage composition of Titania**
1	0.1
1	0.2
1	0.3
1	0.4
1	0.5
1.5	0.1
1.5	0.2
1.5	0.3
1.5	0.4
1.5	0.5
2	0.1
2	0.2
2	0.3

The column containing the coating solution was slowly raised so that the solution rises through the porous alumina tube until it reaches the glass tube attached to the upper portion of the alumina tube. The column was then lowered slowly at a speed of 20 cm per min. so that the level of coating solution also slowly lowered. The coated tubes were dried in a humidity chamber at 50 °C and 60% relative humidity for 24h and then dried at 70 °C. The dried coated tubes were calcined at 800 °C for 5h at a heating rate of 1 °C per

minute followed by atmospheric cooling. Thus an intermediate layer was formed in the alumina tubes.

The top layer was coated in the tubes with the coating solution made from titania sol and hydroxyethyl cellulose. The coating procedure was exactly the same as for coating of intermediate layer. A schematic diagram of coating unit is given in Figure 4.1.4.

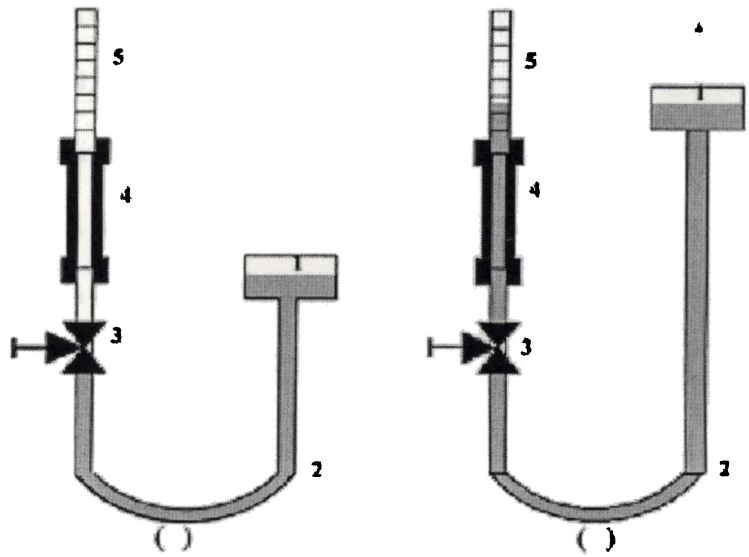

Figure 4.1.4. Schematic diagram of the coating process for the membrane on the inner surface of the tubular support (1) coating solution tank; (2) soft tube; (3) valve; (4) tubular membrane; (5) glass tube

The coated tubes were dried in a humidity chamber at 50 °C and 60% relative humidity for 24h followed by drying at 70 °C. The dried coated tubes were calcined at 500 °C for 3h at a heating rate of 1 °C per min. followed by atmospheric cooling. The TGA and DTA analysis was carried out in the dried coating solutions at a heating rate of 10 °C min^{-1} using a Thermogravimetric analyzer (Shimadzu, TGA 50H, Japan) and Differential thermal analyzer (Shimadzu, DTA 50H, Japan). The surface area measurements and pore analysis were carried out by nitrogen adsorption using Micromeritics Gemini 2375

surface area analyser after degassing each sample at 200 °C for 2 h. XRD patterns of the calcined gels were taken in a Philips X' pert X-ray diffractometer in the diffraction angle 2θ range 10-80° using Cu Kα radiation. The morphology of membrane layer was observed by a Scanning Electron Microscope (SEM JEOL JSM-6700F). Ultrafiltration studies were carried out with Congo red (Mw 696.66 g/mol), a red coloured dye, using indigenously developed flux measurement set up and the photograph of the unit is presented in Figure 4.1.5. The equipment consists of support-holding chamber, a dosing pump, water reservoir, inlet and outlet flow meter, pressure gauge and an open end for collecting the filtrate. Two alumina porous tube supports of dimensions 17 cm length and 8.5 mm diameter can be fixed in the support chamber. The schematic arrangement of the flow stream is presented in Figure 4.1.6.

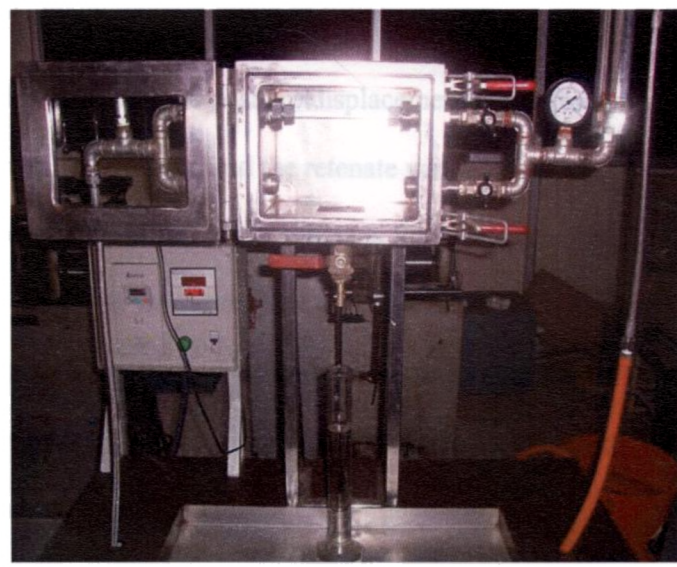

Figure 4.1.5. Photograph of the filtration set up

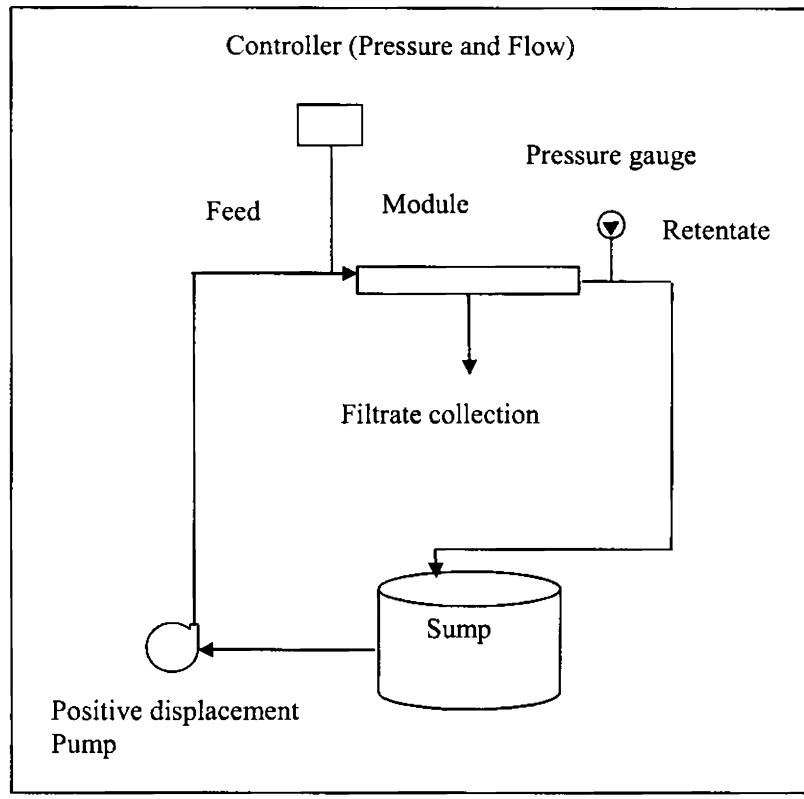

Figure 4.1.6. Schematic representation of filtration setup

The feed is pumped by a positive displacement pump (reciprocating) from a sump through the inlet to the substrate and the retenate was allowed to go back to the sump in a closed loop manner. A controller is provided at inlet line to control the line pressure and flow rate. The filtrate is collected down in a measuring cylinder over definite time interval. The flux is calculated at different time intervals and a plot was made against time vs. flux. By knowing the concentrations of the feed and the filtrate, the percentage of rejection by the membrane is calculated.

4.1.4 Results and discussions

4.1.4.1 Particle size measurements

Figure 4.1.7 (a) and (b) shows the particle size distribution of boehmite and titania sol prepared through an aqueous sol-gel method. Boehmite sol shows unimodal particle size distribution have an average size of 165 nm and titania sol also shows unimodal particle size distribution having an average size of 27 nm. This sol is further used for the preparation of alumina and titania membrane.

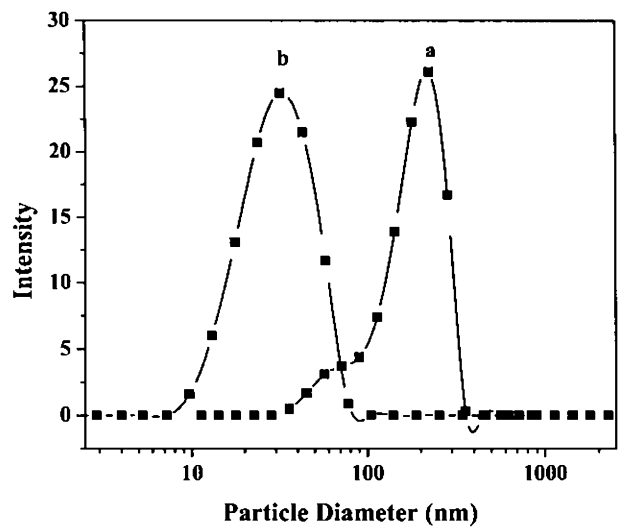

Figure 4.1.7. Particle size distribution curves of (a) boehmite sol and (b) titania sol.

4.1.4.2 Viscosity measurements

The viscosity curves of the different coating compositions prepared using boehmite sol and hydroxyethyl cellulose (HEC) are shown in Figure 4.1.8 a, b, c & d. It is seen that viscosities of all compositions vary with different shear rate. There is a sudden increase in viscosity upto a particular shear rate and after that it shows a gradual decrease. The increase in viscosity corresponds to the gelation of sol particles with

hydroxyethyl cellulose. The decrease in viscosity is due to the collapse of gel structure with a further increase in shear rate.

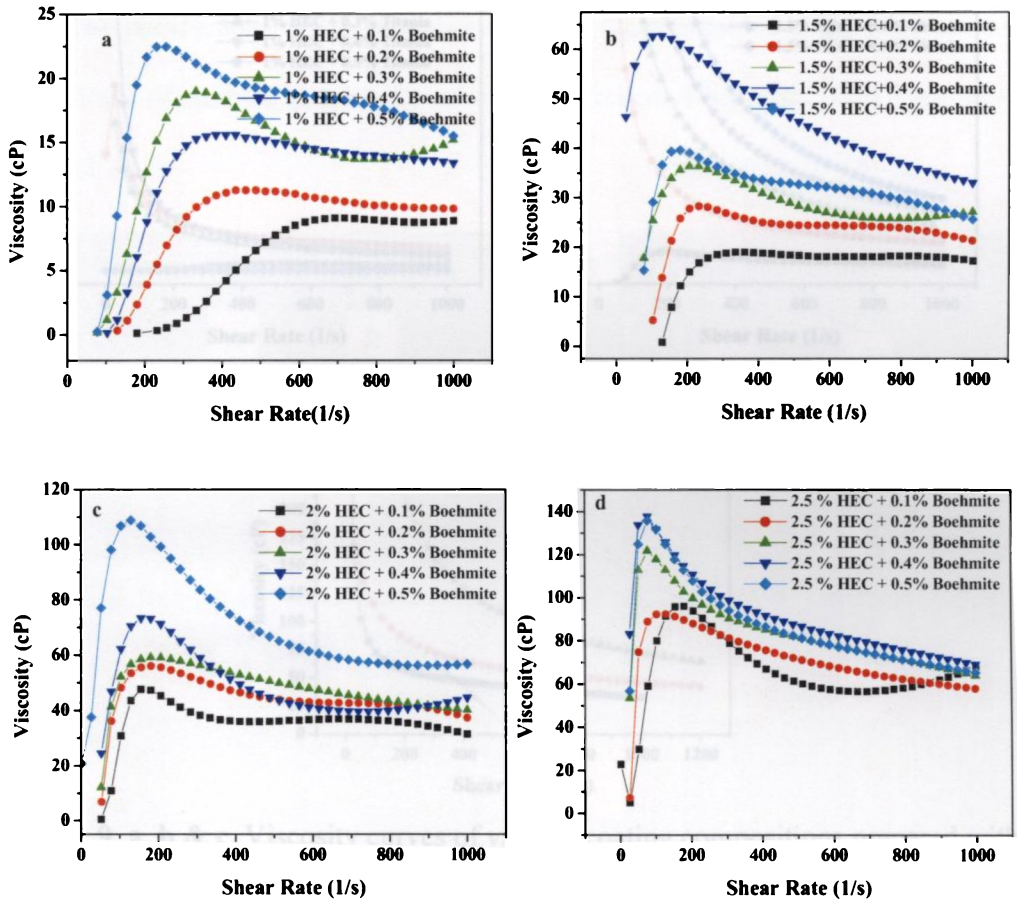

Figure 4.1.8. a, b, c & d. Viscosity curves of various coating compositions prepared with boehmite sol and hydroxyethyl cellulose (HEC).

The viscosity curves of titania and hydroxy ethyl cellulose are given in Figure 4.1.9a, b & c. The viscosities of all compositions except 1% HEC + 0.1% Titania, 1% HEC + 0.5% Titania and 1.5% HEC + 0.1% Titania are initially high due to the fact that the suspension

structure is close to equilibrium. Hence the movement of the particles dominates over the viscous force (first Newtonian region).[32]

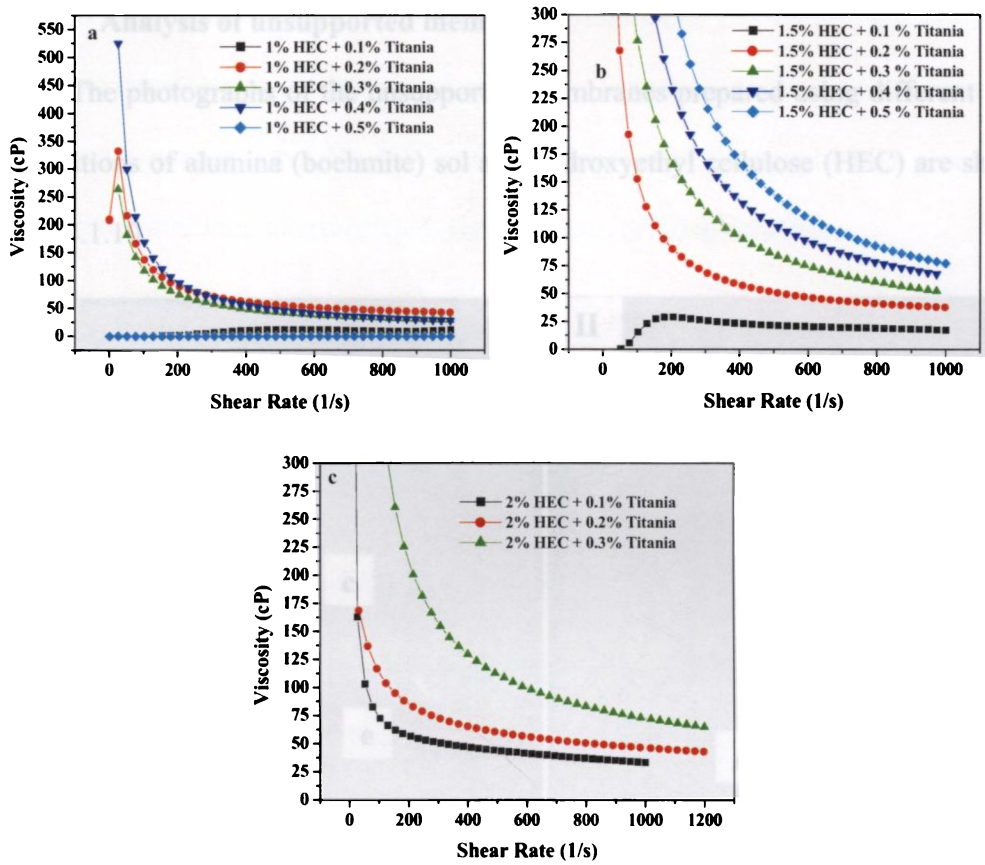

Figure 4.1.9. a, b & c. Viscosity curves of various coating compositions prepared with titania sol and hydroxyethyl cellulose (HEC)

At high shear rates, the viscous forces affect the suspension structure and shear thinning occurs due to progressive breakdown of particulate network or agglomerates (floc). At very high shear rates, viscous forces dominate and normally a plateau in viscosity is observed (second Newtonian region) [32] indicating completely hydrodynamically (arising from the shear field) controlled structure.[33] The remaining three compositions show a small increase in viscosity upto a particular shear rate due to gel formation with

hydroxyethyl cellulose (HEC) and a small decrease in viscosity is observed due to collapse of gel structure with further application of shear rate.

4.1.4.3 Analysis of unsupported membrane

The photographs of the unsupported membranes prepared using different coating compositions of alumina (boehmite) sol and hydroxyethyl cellulose (HEC) are shown in Figure 4.1.10.

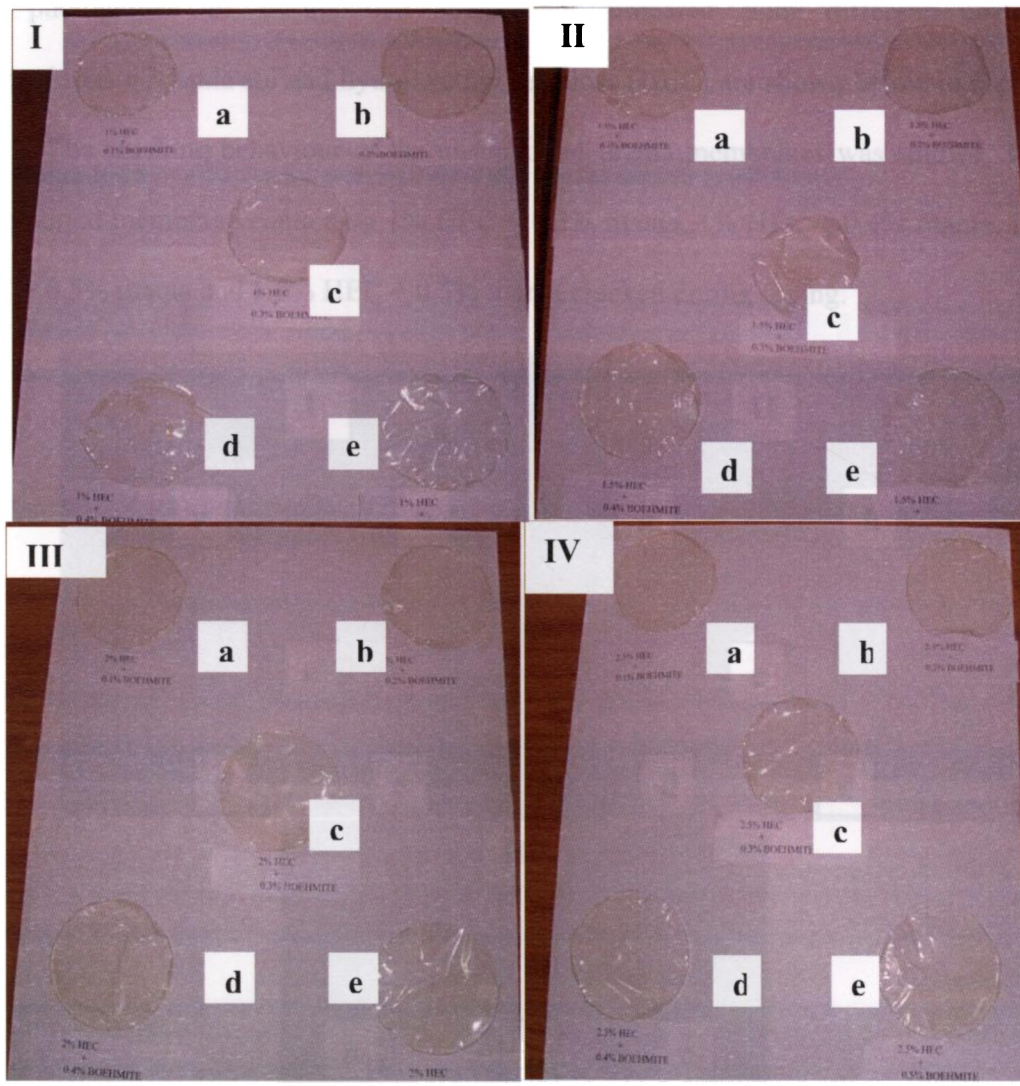

Figure 4.1.10. (I) 1% HEC (II) 1.5%HEC (III) 2%HEC (IV) 2.5% HEC (a) 0.1% Boehmite, b) 0.2% Boehmite, c) 0.3% Boehmite, d) 0.4% Boehmite, e) 0.5% Boehmite.

The cracking behaviour of the unsupported alumina membranes was studied. The unsupported membrane contains 1% HEC + 0.4% boehmite, 1.5% HEC+ 0.3% boehmite and 1%HEC+ 0.5% boehmite cracked during drying. Upon considering the viscosity of the coating composition, thickness and crack free formation of unsupported membrane, we adopted a composition 1.5% HEC + 0.4% boehmite which could easily give a crack free alumina membrane intermediate layer on porous ceramic substrate.

The photographs of unsupported membranes prepared with different coating compositions of titania sol and hydroxyethyl cellulose (HEC) are shown below in Figure 4.1.11. The cracking behaviour of the unsupported titania membranes was studied. The unsupported membrane containing 1% HEC + 0.3% titania, 1% HEC + 0.4% titania, 1% HEC + 0.5% titania and 1.5% HEC + 0.5% titania cracked during drying.

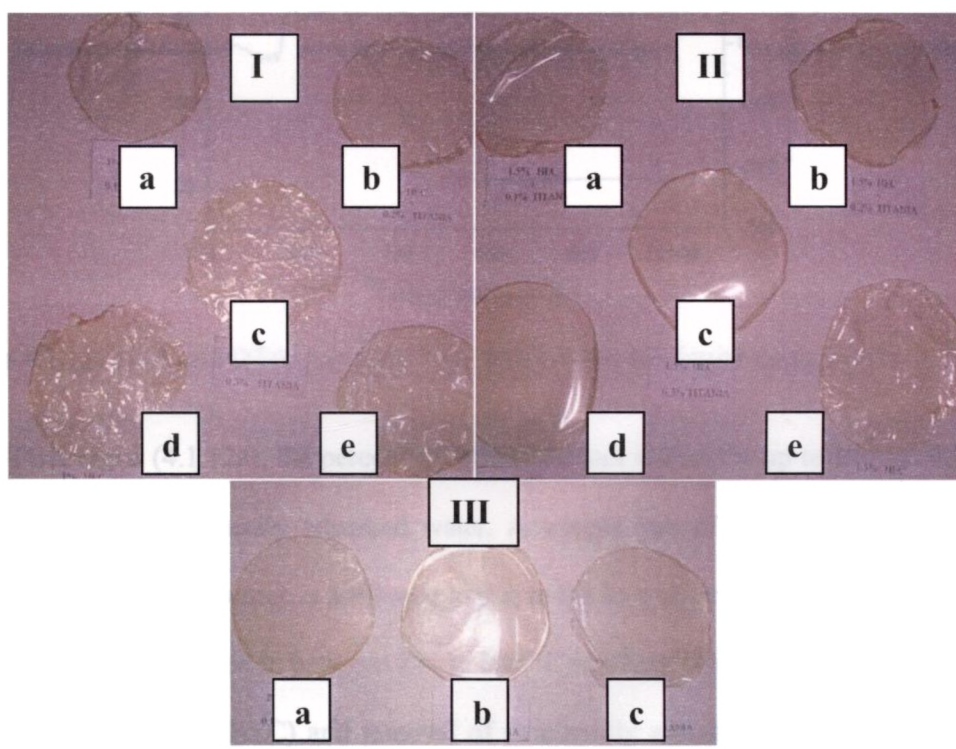

Figure 4.1.11. (I) 1% HEC (II)1.5% HEC (III) 2% HEC a) 0.1% Titania, b) 0.2% Titania, c) 0.3% Titania, d) 0.4% Titania, e) 0.5% Titania.

Upon considering the viscosity of the coating composition, thickness and crack free formation of unsupported titania membrane, we adopted a composition (1% HEC + 0.2% titania) which could easily give a crack free titania membrane top layer on porous ceramic substrate.

4.1.4.4 Thermo gravimetric and Differential thermal analysis

Figure 4.1.12 a & b shows the Thermo Gravimetric and Differential Thermal analysis profiles of the unsupported alumina membrane (1.5% HEC + 0.4%Boehmite) dried at 50 °C and at 60% relative humidity for 24h.

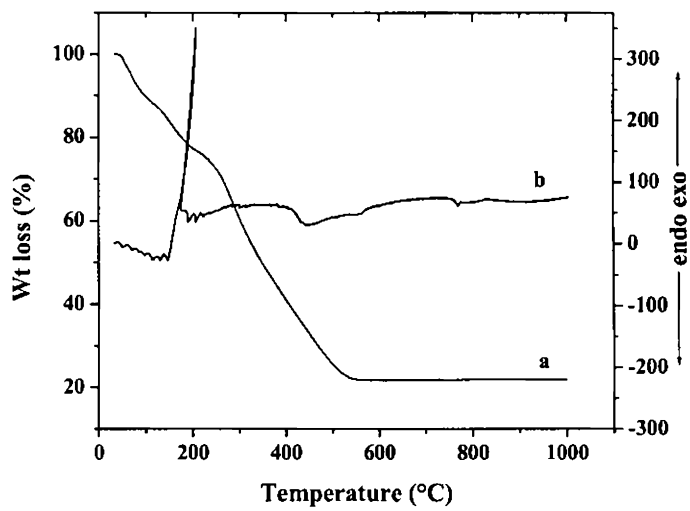

Figure 4.1.12. TGA and DTA curves of 1.5% HEC- 0.4% Boehmite composition.

In the TGA curve (4.1.12a), the percentage of weight loss is 21.87% up to 190 °C due to the elimination of physically adsorbed water. A weight loss of 5.59% is observed in between 191 to 240 °C, which is attributed to due to the loss of nitrate. Similarly a weight loss of 51.57% is observed in between 241 to 540 °C resulting from the decomposition of hydroxyethyl cellulose (HEC) and removal of structurally adsorbed water. Beyond 540 °C, there is no obvious weight loss in the TGA curve.

In the DTA curve (4.1.12b) an endothermic peak at 106 °C corresponds to the elimination of physically adsorbed water. The exothermic peak at 205 °C is due to the loss of nitrate. The exothermic peak at 370 °C corresponds to the decomposition of hydroxyethyl cellulose (HEC).

Figure 4.1.13 shows the TGA and DTA curves of the unsupported titania membrane (1% HEC + 0.2% Titania) dried at 50 °C and at 60% relative humidity for 24 h.

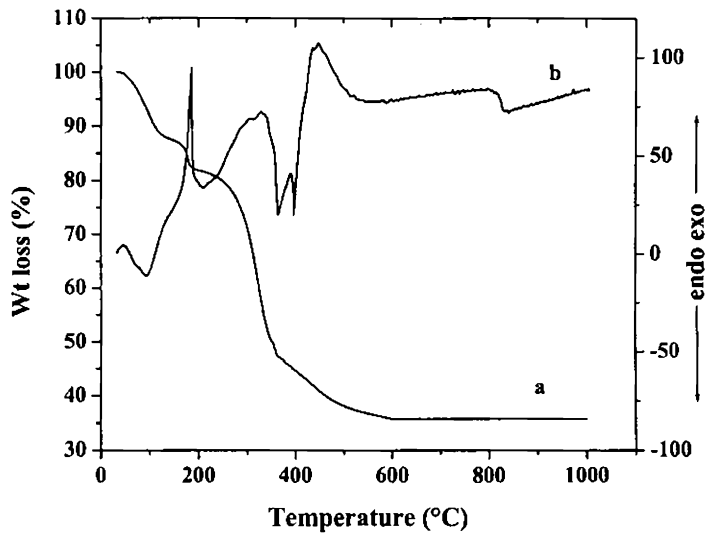

Figure 4.1.13. TGA and DTA curves of 1% HEC-0.2% Titania composition.

In the TGA curve (4.1.13 a), percentage of weight loss is 17% up to 185 °C, which is the results of elimination of physically adsorbed water. The percentage weight loss between 186 to 220 °C is 1.22% which is due to the loss of nitrate. The percentage weight loss from 221 °C to 500 °C is 43% due to consequence of decomposition of hydroxyethyl cellulose (HEC) and removal of chemically coordinated water. There is no major weight loss observed after 500 °C. In the DTA curve (4.1.13b), endothermic peak centered around 100 °C is the result of removal of physically adsorbed water. The

exothermic peak at 190 °C corresponds to the loss of nitrate. The exothermic peak at 320 °C results from the decomposition of hydroxyethyl cellulose (HEC).

4.1.4.5 X-ray diffraction analysis

Powder X-ray diffraction pattern of unsupported alumina membrane (1.5% HEC + 0.4% Boehmite) calcined at 800 °C for 5 h is shown in Figure 4.1.14(a). The peaks correspond to the γ- alumina formed on calcination. The XRD pattern is not sharp due to the spinel structure of γ- alumina formed.[34]

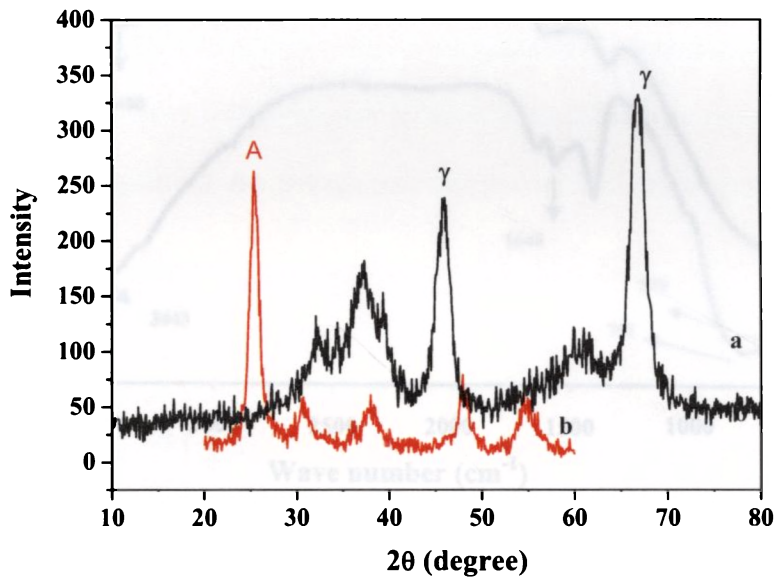

Figure 4.1.14. XRD pattern of (a) unsupported alumina membrane calcined at 800 °C for 5 h (b) unsupported titania membrane calcined at 500 °C for 3 h (A) anatase (γ) alumina .

The XRD pattern of unsupported titania membrane (1% HEC + 0.2% Titania) calcined at 500 °C for 3h is shown in Figure 4.1.14 (b). The broad peak at 2θ value 25.3° is the characteristic (101) plane peak of nanocrystalline anatase titania. From these observations, we can conclude that a γ- alumina intermediate layer and a nanocrystalline

titania top layer were formed in the porous alumina support during the fabrication of membrane layer.

4.1.4.6 Fourier Transform Infrared Spectroscopy (FTIR)

The FTIR spectra of unsupported alumina membrane (1.5% HEC + 0.4% Boehmite) calcined at 800 °C for 5h (Figure 4.1.15.a) and unsupported titania membrane (1% HEC + 0.2% Titania) calcined at 500 °C for 3h (Figure 4.1..15b) is shown in Figure 4.1.15.

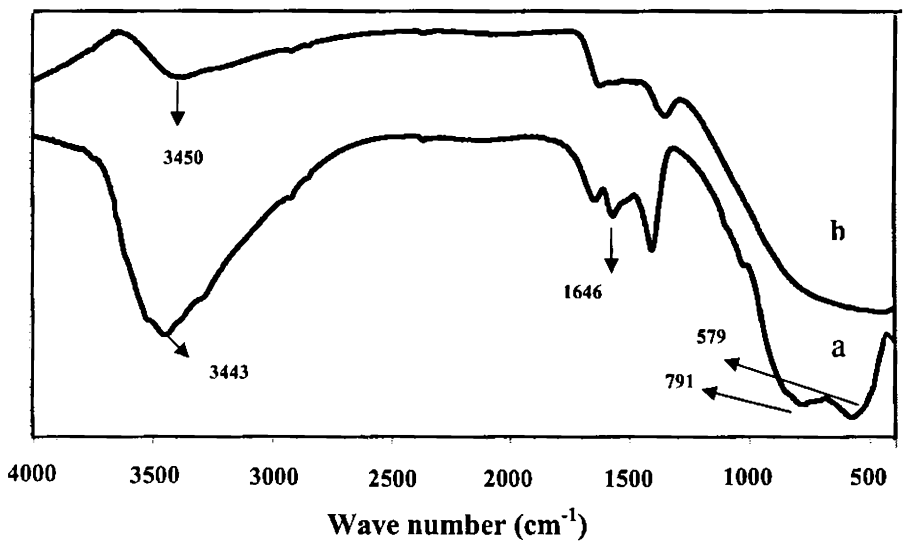

Figure 4.1.15. FTIR Spectrum of (a) unsupported alumina membrane calcined at 800 °C for 5 h and (b) unsupported titania membrane calcined at 500 °C for 3 h.

In the FTIR spectrum of unsupported alumina membrane calcined at 800 °C (Figure 4.1.15 a) the band at 3443 cm^{-1} corresponds to the stretching vibration of O-H bond that results from co-ordinated water on the alumina surface. The bands at 1646 cm^{-1} is due to the bending vibration of O-H bond, which is related to absorbed water. The strong broad band between 500 and 750 cm^{-1} and centered at 579 $cm^{-1}$is due to the vibrations of AlO_6 (v AlO_6). The strong broad band between 900 and 750 cm^{-1} and centered at 791 $cm^{-1}$is

assigned to the $vAlO_4$ vibrations.[35] From this observation, it is concluded that both octahedral and tetrahedral alumina species are present in the system.

The FTIR spectrum of titania 4.1.15 (b) shows bands at 3450 cm^{-1} and 1626 cm^{-1} which corresponds to the stretching and bending vibrations of hydroxyl group. The band below 1000 cm^{-1} is due to the stretching vibrations of Ti-O-Ti network.[36]

4.1.4.7 BET Surface area analysis

The adsorption isotherm and pore size distribution curve of unsupported alumina membrane calcined at 800 °C for 5h are shown in Figure 4.1.16 (a) and (b) respectively. The adsorption isotherm is of type IV which is characteristic of mesoporous material. The pore size distribution curve is bimodal, one is below 6 nm (60 angstrom) and other one is below 40 nm (400 angstrom). An average pore diameter of 10.5 nm is obtained.

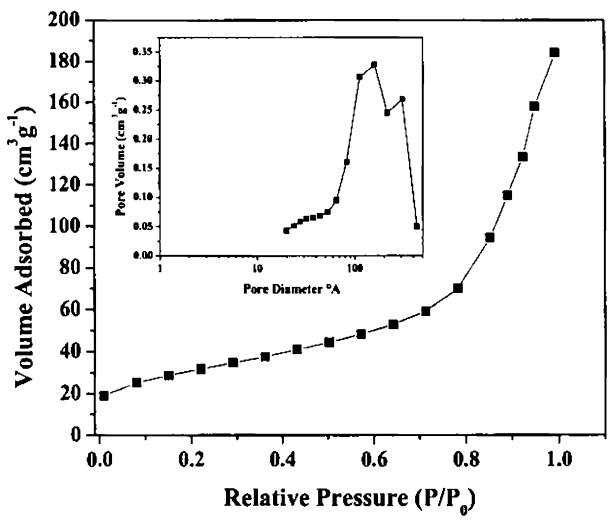

Figure 4.1.16. (a) Adsorption isotherm and (b) Pore size distribution curve (inset) of unsupported alumina membrane calcined at 800 °C for 5 h.

The adsorption isotherm and pore size distribution curve of unsupported titania membrane calcined at 500 °C for 3h are shown in Figure 4.1.17 (a) and (b) respectively. The adsorption isotherm is of type IV which is characteristic of mesoporous material. The pore size distribution curve is bimodal, one is below 4 nm (40 angstrom) and other one is below 30 nm (300 angstrom). An average pore diameter of 13 nm is obtained.

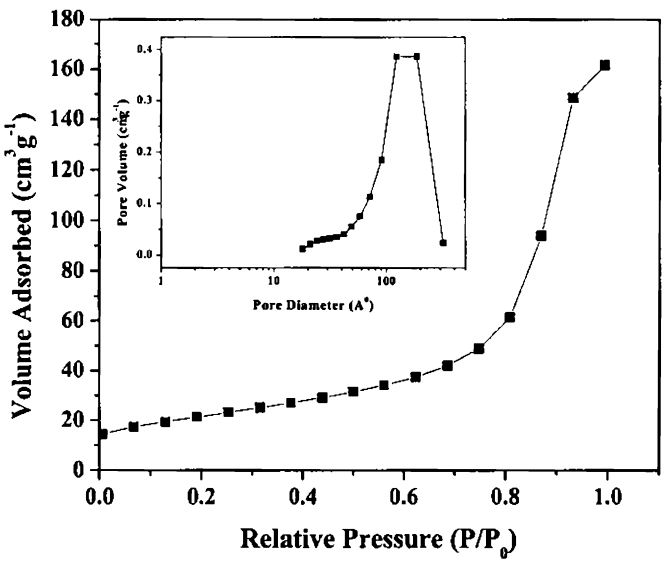

Figure 4.1.17. (a) Adsorption isotherm and (b) Pore size distribution curve (inset) of unsupported titania membrane calcined at 500 °C for 3 h.

Table 4.1.5. Surface area results of unsupported alumina membrane calcined at 800 °C for 5 h & unsupported titania membrane calcined at 500 °C for 3 h.

	BET Surface Area (m^2g^{-1})	**Total Pore Volume (cm^3g^{-1})**	**Average Pore Diameter (nm)**
Unsupported alumina membrane calcined at 800 °C for 5h	108.3	0.2848	10.5
Unsupported titania membrane calcined at 500 °C for 3h	76.7	0.2498	13.0

The surface area results are given in Table 4.1.5. From these observations it is concluded that a mesoporous alumina and titania multi layer membrane are successfully formed on the porous alumina support.

4.1.4.8 Scanning Electron Microscopy (SEM)

The morphological features of uncoated and coated substrates can be studied by Scanning Electron Microscopy (SEM). The SEM pictures of uncoated and alumina coated alumina substrates are shown in Figures 4.1.18 (a) and (b). The fracture of the alumina coated substrate is provided in Figure 4.1.18(c).

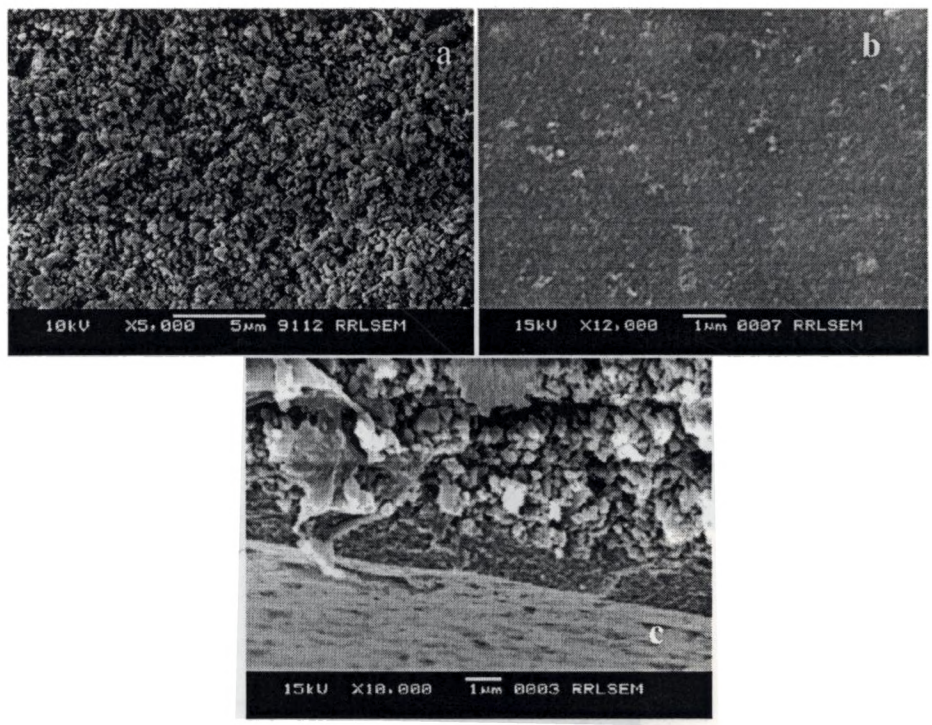

Figure 4.1.18. SEM images of (a) porous alumina surface (uncoated) (b) alumina coated surface (c) fracture of the coated porous alumina substrate.

The integrity of the membrane layer and its incorporation with the porous Al_2O_3 substrate are crucial factors in the fabrication of defect-free membrane since even few cracks, pin-

holes or breakage of weak joints can cause failure of the separation efficiency. Examining the SEM images (plain view) of membrane layer shown in Fig. 4.1.18b we observe that this method is successful to fabricate membrane layer with good integrity and without significant cracks or pin-holes.

From the SEM images, it is observed that a uniform coating layer was formed on the surface of porous alumina substrate. From the fracture micrograph a coating layer of thickness approximately ~1-2 μm is formed on porous alumina substrate. The second layer of titania composition having a particle size of 27 nm was formed over the alumina layer and the total thickness of the layer became ~4-5 μm. This was further used for the ultra filtration application. The scanning electron micrographs of the alumina-titania multilayer coating is given in Figure 4.1.19 a, b & c

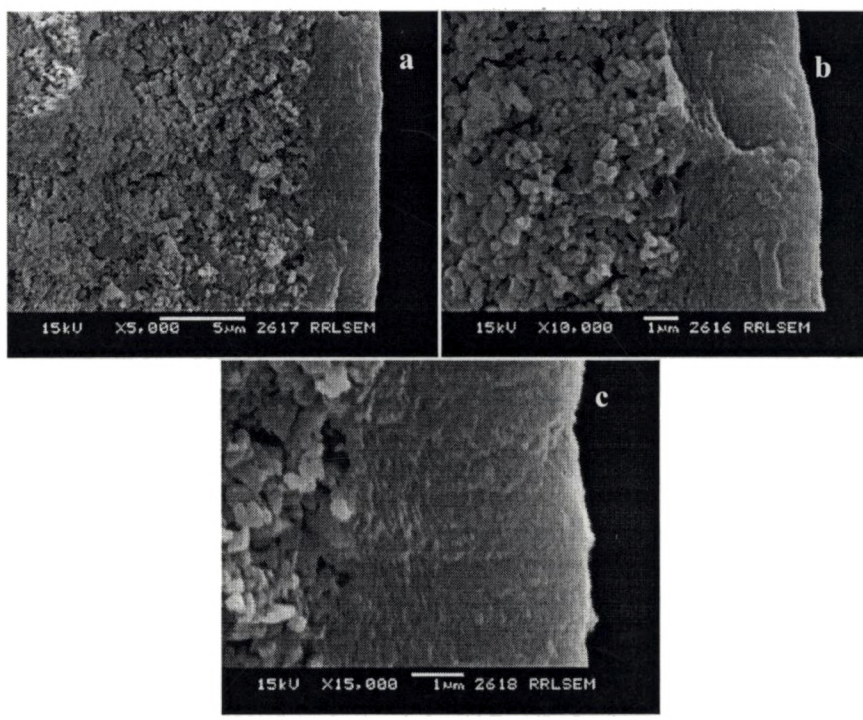

Figure 4.1.19. SEM images of (a) (b) & (c) fracture of the Alumina –titania multi layer coated porous alumina substrate.

4.1.4.9 Filtration studies

The multi-layered membrane fabricated with alumina as intermediate layer and titania as top layer was used for cross-flow filtration studies. Congo red (696.66 g/mol), a red coloured dye, was dissolved in water (200 mg / l) and used as the colouring agent in the feed. The molecular structure of the Congo red dye is given in Figure 4.1.20. The filtration was performed for 10h and the flux was measured at 15 minute intervals. An average flux rate of 40 $l/m^2.h.b$ is obtained. The permeation flux versus time curve is given in Figure 4.1.21. This flux rate is comparable to the flux rate observed in other ultra filtration membranes.[37]

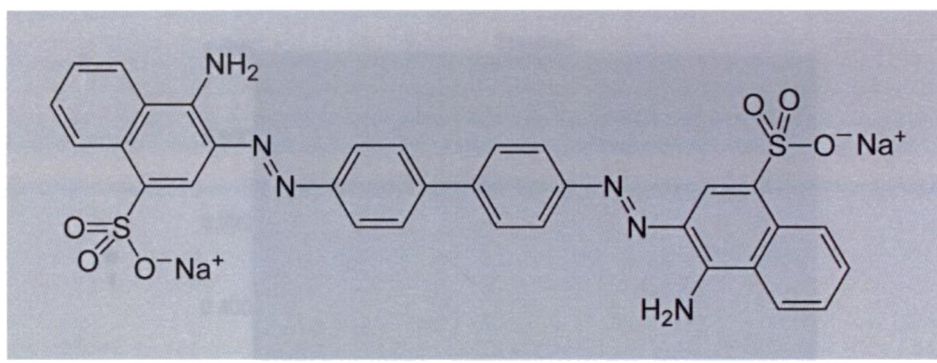

Figure 4.1.20. Molecular structure of Congo red

The filtrate collected after 10h of filtration was analyzed by UV-Visible spectroscopy for determining rejection rate of membrane in the case of Congo red. A standard plot showing concentration Vs. absorbance of the standard samples is shown in Figure 4.1.22. The absorbance of the filtrate was compared with the standard curve. An absorbance value of 0.061 was observed and from the standard plot, concentration of Congo red in the filtrate was found to be 1.2743 mg / l.

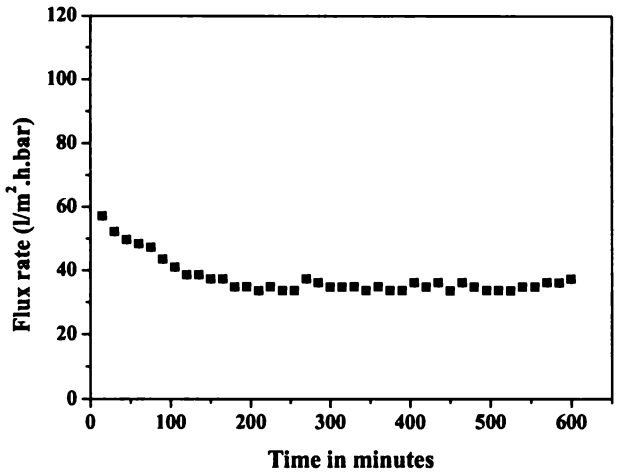

Figure 4.1.21. Permeation flux of alumina-titania multilayer membrane during cross flow filtration with Congo red.

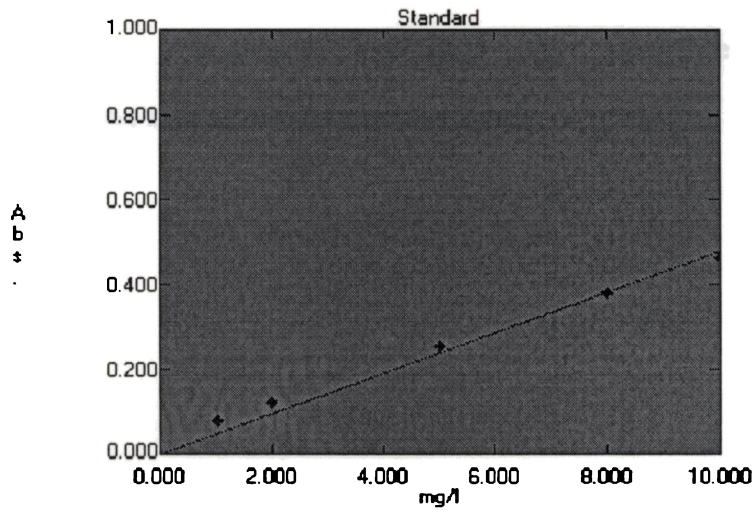

Figure 4.1.22. Standard curve of Concentration (mg/l) vs. Absorbance of congo red dye.

The membrane prepared through the present method showed a very high rejection (~99%) of 'Congo Red' (mol. wt.696.66 g/mol). From these measurements a cut-off value of around 1000 Da can be deduced.[37]

4.1.5 Conclusions

Successful fabrication of alumina-titania multi-layer ceramic membrane on porous alumina substrates was achieved. The coating compositions prepared from boehmite and titania sols with hydroxyethyl cellulose (HEC) as binder were characterised by viscosity measurements, TGA and DTA. Unsupported membranes were prepared and their cracking behaviour was studied. The composition which corresponds to crack-free thin layers was chosen for coating on substrates. The membranes were characterised by XRD, FTIR and Surface area measurements. The morphological features of the membranes were studied using Scanning Electron Microscopy. The filtration property of the membrane was examined by filtration test using congo red as a colouring agent. About 99.3% rejection was observed with congo red. A membrane layer having a molecular cut off value around 1000 Da was developed.

4.2 Development of Photoactive Titania Coating on Glass Surfaces

4.2.1 Abstract

A uniform nanolayer of alumina doped titania coating has been developed on glass surface through an aqueous sol-gel method starting from titanylsulphate and aluminium nitrate as precursor. The thermo gravimetric analysis has been used to study the decomposition characteristic of coating precursor. The UV-Visible absorption spectrum shows that the absorption edge is blue shifted in the presence of alumina in the titania matrix. Scanning Electron Micrographs show that a uniform thin layer was formed on the glass surface. The Type IV behaviour shown by the pure and alumina doped titania powder indicates the mesoporous nature of the titania thin film formed on the glass surface. The 10 mol% alumina doped titania coating powder shows two times higher surface area than pure titania powder. Anatase phase was detected in both pure and 10 mol% alumina coated samples by Raman spectra. The alumina doping increases the photoactivity of titania film and the maximum photoactivity is observed for 2 mol% alumina doped titania film.

4.2.2 Introduction

Titania films have attracted attention due to their applications in anti-bacterial,[38, 39] self-sterilizing,[40, 41] self-cleaning,[42] antisoiling and antifogging coatings. Of the different polymorphic forms of titania, anatase was found to be more photo catalytic active and useful in such type of coatings. For the fabrication of these titania thin layer, sol-gel method was found to be a promising one.[43, 44] The deposition of TiO_2 film by sol–gel method has been reported by few authors.[45-48] Almost all sol-gel process start from alkoxide precursor. But for the bulk production of these coating an alkoxide process is

not found to be economically viable. Kishimoto et al. demonstrated the wettability of titania coating films by sol-gel method using an aqueous solution of $Ti(SO)_4$ containing polyvinyl pyrollidone (PVP) as the coating solution.[49] Ichinose et al.[50, 51] demonstrasted the proparation of peroxo titanic acid (PTA) sol derived from $TiCl_4$ for the preparation of titania film. Lee et al.[52] prepared and characterised peroxo titania sol from $TiCl_3$. Ge et al.[53] prepared the autoclaved sol for the preparation of titania film using titanyl sulphate and H_2O_2. To best of our knowledge no work has been reported for the preparation of alumina doped titania film using simple aqueous sol-gel method. So in the present study an aqueous sol-gel method was developed for the preparation of titania film doped with alumina. Further it was characterized using scanning electron microscopy, atomic force microscopy and photoactivity studies.

4.2.3 Experimental

Titanyl oxysulphate ($TiOSO_4$, Aldrich Chemicals, 99.99% purity) was used as precursor for the synthesis of titania sol. In a typical experiment, titanyl oxysulphate was dissolved in 500 ml of distilled water (0.2 M) and hydrolysed by slow addition of ammonium hydroxide (10%, sd Fine chemicals, India Ltd) solution under constant stirring at room temperature (32 ^{0}C), until the reaction mixture attained pH 8.5. The precipitate obtained was separated by filtration and was washed free of sulphate ions (confirmed by the $BaCl_2$ test) with distilled water. The precipitate was further dispersed in 1000 ml of hot distilled water and was peptised by the addition of 10% HNO_3 (Merck, India Ltd) solution. A stable sol was obtained at a pH range 1.7 to 2.2. To the stable sol 1, 2, 5 and 10 mol % alumina is added as boehmite sol using Al $(NO_3)_3$. $9H_2O$ (sd Fine Chemicals, India Ltd) as a precursor, which was prepared by a procedure reported

earlier.[54] To the undoped and alumina doped titania sol, 2 wt% polyethylene glycol was added. The resultant sol was coated on glass surfaces using a dipcoater machine (KSV dipcoater, Finland). Before the deposition, glass substrates were cleaned in concentrated sulphuric acid, distilled water and then absolute ethanol.TiO_2 thin film was deposited on substrate by a dip-coating process at room temperature with the withdrawing speed of about 2 cm/min. Substrates were immersed into the TiO_2 sol for 1min. Upon withdrawing from the sol, the substrates were dried at 70 °C. The corresponding dried gels were further characterized using Thermogravimetric analyzer (Shimadzu, TGA 50H, Japan). The coated glass slides were calcined at 400 °C for 3h at a heating rate 1°C per min. XRD patterns of the calcined gels were taken in a Philips X' pert X-ray diffractometer in the diffraction angle 2θ range 20-60° using Cu Kα radiation. The crystallite size was calculated using Scherrer equation 4.2.1.

$$\Phi = K\lambda / \beta \cos\theta \qquad (4.2.1)$$

where K is the shape factor taken as 0.9 for the calculations presented, λ the wavelength of the X-ray, β the full width at half maxima, and θ the diffracting angle.The surface morphology of dried TiO_2 thin film was observed by a Scanning electron microscope (SEM JEOL JSM-6700F) and Atomic Force Microscope (Topometrix Inc.) in contact-mode using a silicon tip (Mikro Masch Inc., Estonia) of length: 350 μm, width: 10 μm, height:1 μm, and an end-curvature radius < 10 nm. Spectroscopic analysis of the TiO_2 film was performed using UV-Visible spectrophotometer (Shimadzu UV 2401) in the wave length range of 200–800 nm. The surface area measurements and pore size analysis were carried out by nitrogen adsorption using Micromeritics Gemini 2375 surface area analyser after degassing each sample at 200 °C for 2 h. Raman spectra of the samples was

taken using a FT- Raman spectrometer (Bruker IFS66V). Methylene blue degradation was used for the determination of photocatalytic property of titania film. In presence of titania film, methylene blue solution shows photo catalytic degradation. In a typical experiment, coated glass plates were dipped in an aqueous solution of methylene blue dye (AR Grade, Qualigens Fine Chemicals, India Ltd) for one hour. It was dried in dark, and irradiated with ultraviolet light in a UV chamber with wavelength range from 200 to 400 nm (Rayonet Photo reactor, The Netherlands). The degradation of the dye was monitored after 60 min using UV-Visible spectrometer (Shimadzu, Japan, UV-2401 PC).

4.2.4 Result and Discussion

4.2.4.1 Thermogravimetric analysis

Thermogravimetric analysis shows (Figure 4.2.1) that the coating solutions dried at 70 °C undergo three decomposition steps between the analysed temperature 30 to 1000 °C. Thermo gravimetric analysis curve shows similar decomposition patterns for pure titania coating solution and the 10 mol% alumina doped titania coating solution. But 10 mol% alumina doped titania coating solution shows slight increase in the total weight loss. Pure titania coating solution dried at 70 °C undergoes a total weight loss of 23%, whereas 10 mol% alumina doped titania coating solution results in a total weight loss of 27.5%. The weight loss below 150 °C is due to the removal of loosely bound water in the gel network. The decomposition step between 200 and 400 °C is due to the decomposition of nitrate ions, dehydroxylation of the gel and removal of the polyethylene glycol used in the coating solution. The % of weight loss is 15.4 and 16.6% respectively for titania and 10 mol% alumina doped titania compositions in the temperature range 200 to 400 °C. Weight loss between 400 and 1000 °C is extremely small and, hence, a lack of

clear decomposition step. The higher weight loss in titania–alumina samples may be due to the boehmite species incorporated in the titania gel network. The similarity in the decomposition pattern of alumina doped samples with pure titania may be an indication of the higher degree of homogeneous dispersion achieved between titania and alumina in the doped system through the mixing of the respective colloidal sols.

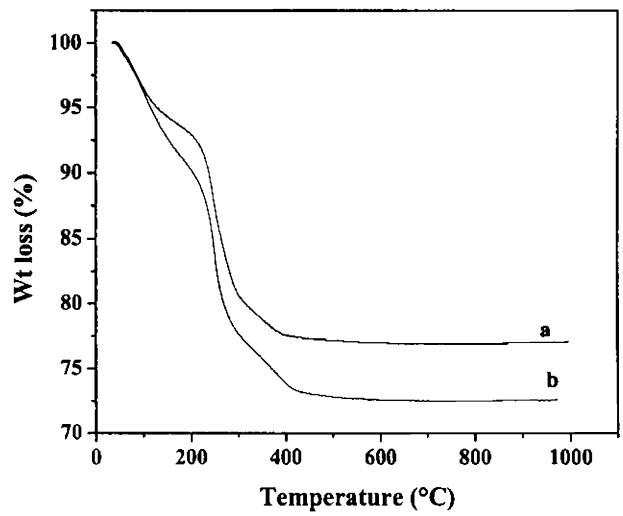

Figure 4.2.1. TGA curve of coating solution (a) titania (b) 10 mol% alumina doped titania.

4.2.4.2 X-ray diffraction analysis

The X-ray diffraction analysis (Figure 4.2.2) indicated that only anatase phase was present in pure and alumina doped titania samples. The crystallite size decreases with increase in the alumina content in the titania matrix (Table 4.2.1). It was 11.3 nm in pure titania and it decreases to 8.1 nm in case of 10 mol% alumina doped titania. The alumina in the titania matrix effectively hinders the crystallite growth of titania.

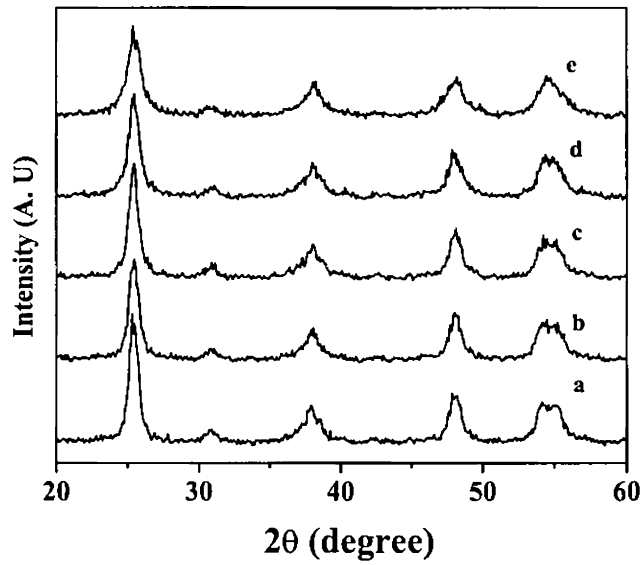

Figure 4.2.2. X-ray diffraction pattern of coating solution calcined at 400 °C for 1h (a) titania (b) 1 mol% alumina doped titania (c) 2 mol% alumina doped titania (c) 5 mol% alumina doped titania (d) 10 mol% alumina doped titania

Table 4.2.1 Crystallite size data of alumina doped titania

Sample	Crystallite size (nm)
TiO_2	11.28
TiO_2 + 1 mol% Al_2O_3	10.78
TiO_2 +2 mol% Al_2O_3	10.11
TiO_2 + 5 mol% Al_2O_3	10.04
TiO2 + 10 mol% Al_2O_3	8.06

4.2.4.3 UV–Visible spectrophotometry

Pure and alumina doped titania thin films deposited on glass substrates calcined at 400 °C are transparent. The corresponding UV–Vis transmittance spectra and Tau plot

for band gap determination are provided in Figure 4.2.3. & 4.2.4. The bandgap against alumina content in the titania matrix for pure and alumina doped titania films calcined at 400 °C are provided in Figure 4.2.5. The titania film has a transmittance between 96 to 87% within the visible region (400 to 800 nm). A significant decrease in the transmittance below 400 nm can be assigned to absorption of light by anatase titania thin film. This leads to the excitation of electrons from the valence band to the conduction band of titania.[55] UV-Visible spectra show that the adsorption edge was shifted to the lower wavelength region when the amount of alumina in the titania thin film increases. These observations indicate that the electronic structure of the overall solid is deeply modified. The UV-visible spectrum of titania coated glass looks like the typical one for anatase.[55,56] It is characterized by an absorption edge whose high wavelength limit is detected with an absorption onset at 385 nm. This edge is associated with the electron transition from the O_{2p} valence band to the Ti_{3d} conduction band and it corresponds to an O^{2-} to Ti^{4+} charge transfer transition. The incorporation of aluminium causes a significant shift of the absorption edge towards lower wavelengths, as previously reported.[57] These observations indicate that the electronic structure of the overall solid is deeply modified. This effect cannot be explained by a simple "dilution" or coverage of the anatase particles by alumina particles or "monolayers" and also cannot be due to a decrease of the particle size of titania, as proposed in the case of silica-titania.[58] In fact, samples with very different particle sizes and surface areas is found to vary much less than in the present case. Moreover, the decrease of the crystal size as measured above is quite limited and is nil between the 2 mol% alumina doped titania and 5mol% alumina doped titania, which

instead shows a very different absorption edge shift. This effect must then be explained by dissolution of Al^{3+} ions into the TiO_2 matrix.

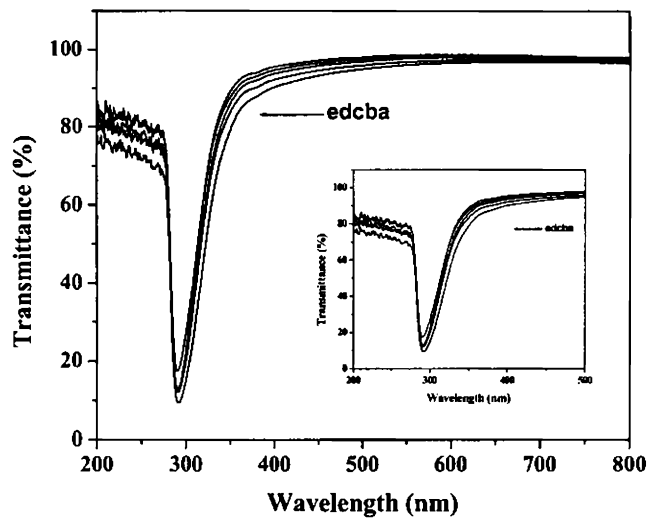

Figure 4.2.3. UV-Visible spectrum of (a) Pure titania (b) 1 mol% Al_2O_3 doped TiO_2 (c) 2 mol% Al_2O_3 doped TiO_2 (d) 5 mol% Al_2O_3 doped TiO_2 (e) 10 mol% Al_2O_3 doped TiO_2

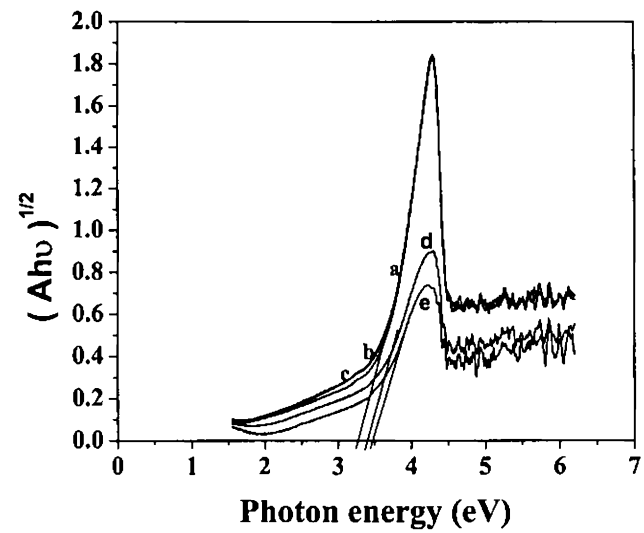

Figure 4.2.4. Tau plot of (a) Pure titania (b) 1 mol% Al_2O_3 doped TiO_2 (c) 2 mol% Al_2O_3 doped TiO_2 (d) 5 mol% Al_2O_3 doped TiO_2 (e) 10 mol% Al_2O_3 doped TiO_2

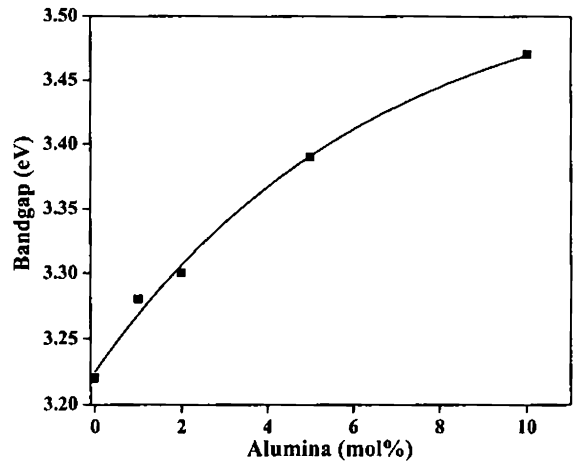

Figure 4.2.5. Band gap versus alumina content in the titania matrix

Accordingly, the Ti_{3d} and the Al_{3p} orbitals mix in the conduction band, and this causes the lower limit of the conduction band to shift up, so that the energy gap increases from near 3.22 eV to near 3.47 eV calculated by Tau plot method. Therefore, the observations from the UV-visible spectra of the samples strongly support the idea that part of the alumina actually dissolves into the anatase bulk giving rise to a solid solution.

4.2.4.4 Scanning Electron Microscopy

Figure 4.2.6. shows Scanning electron micrographs of the pure and alumina doped titania thin films deposited on glass slides calcined at 400 °C. It can be observed that in the pure titania thin film, the particles are grown in to a higher size than the alumina doped titania film. The homogeneously distributed alumina effectively hinder the particle growth of titania. It is already evident from the X-ray diffraction analysis that the crystallite size of all alumina doped composition is lower than the pure titania film.

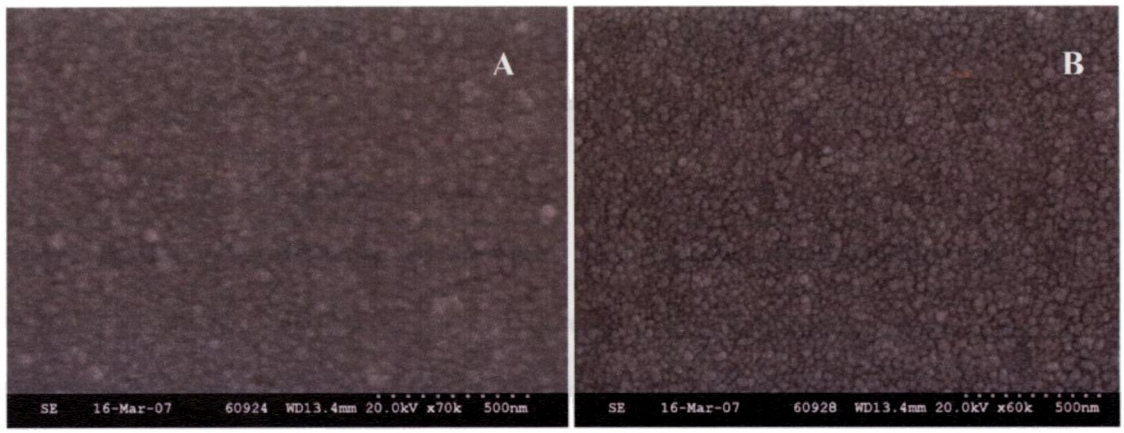

Figure 4.2.6. Scanning Electron Micrographs of (A) undoped titania film (B) 10 mol% alumina doped titania film.

4.2.4.5 Atomic Force Microscopy

The surface structure of coating can be viewed from atomic force microscope (Figure 4.2.7). It shows that, for the pure titanium oxide coating, the particles are grown into large size than the 10mol% alumina doped titania. In the case of coating with addition of alumina, alumina will block the crystallite growth of titania thin film.

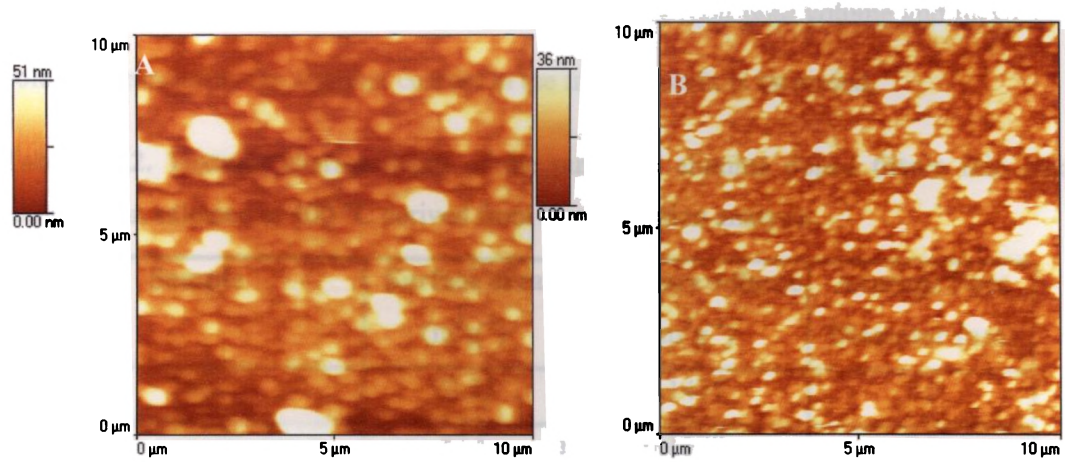

Figure 4.2.7. Atomic Force Micrographs of (A) undoped titania film (B) 10 mol% alumina doped titania thin film

As a result of alumina addition, titanium oxide remains less agglomerated, and the crystallization rate of titanium oxide is reduced, which was already observed from the

crystallite size data obtained from X-ray diffraction. The thickness of the titania layer formed on the glass surface was found out to be ~50nm.

4.2.4.6 BET specific surface area analysis

Textural characteristics of the pure and alumina doped titania thin film composition calcined at 400 °C were derived from N_2 adsorption analysis. Specific surface area (S_{BET}), total pore volume calculated at $p/p_0 = 0.9$, BJH mesopore volume and micro pore volume which were calculated by t-plot method and average pore diameter value are presented in Table 4.2.2. The adsorption isotherms (Figure 4.2.8) of all samples show type IV behaviour with the typical hysteresis loop. This hysteresis loop is characteristic of mesoporous materials [59] and it infers that the mesoporous thin layer is formed on the glass substrate. Surface area results shows that all the doped titania samples have higher surface area than the undoped one after calcinations at 400 °C. In the case of pure titania it is 72 m^2g^{-1} and for 10 mol% alumina doped titania it is 152 m^2g^{-1} which is two times higher than the undoped titania. The total pore volume and mesopore volume increased as the alumina content in the titania matrix is increased.

Table 4.2.2. Textural characteristics of the pure and alumina doped titania thin film composition calcined at 400 °C derived from N_2 adsorption analysis.

Sample	Surface area (m^2g^{-1})	Total pore volume (cm^3g^{-1})	Average Pore Diameter (nm)
TiO_2	72.33	0.1477	7.5
TiO_2 + 1 mol% Al_2O_3	87.5	0.1598	7.3
TiO_2 +2 mol% Al_2O_3	95.8	0.1728	7.2
TiO_2 + 5 mol% Al_2O_3	125.0	0.1978	6.3
TiO_2 + 10 mol% Al_2O_3	152.4	0.2116	5.6

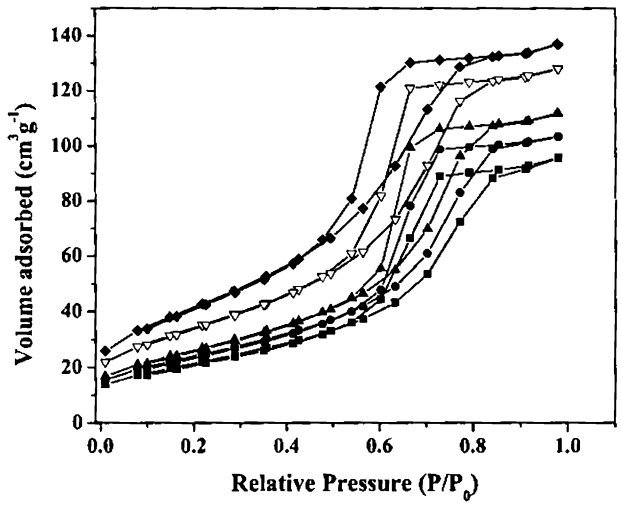

Figure 4.2.8. Adsorption-desorption isotherm of (■) Pure titania (●) 1 mol% Al_2O_3 doped TiO_2 (▲) 2 mol% Al_2O_3 doped TiO_2 (▽) 5 mol% Al_2O_3 doped TiO_2 (♦) 10 mol% Al_2O_3 doped TiO_2

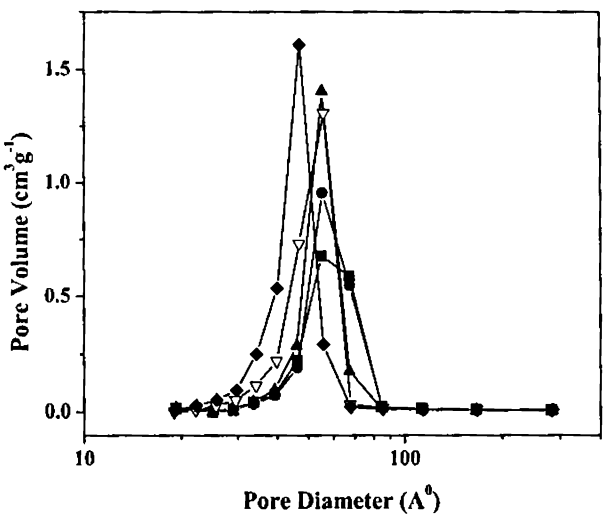

Figure 4.2.9. Pore size distribution curve of (■) Pure titania (●) 1 mol% Al_2O_3 doped TiO_2 (▲) 2 mol% Al_2O_3 doped TiO_2 (▽) 5 mol% Al_2O_3 doped TiO_2 (♦) 10 mol% Al_2O_3 doped TiO_2

The pore size distribution curve (Figure 4.2.9) shows that pores are in mesoporous region and as alumina content increases, the poresize shifted further to lower region, which indicates that the alumina in titania matrix effectively hinders the pore size growth. In adsorption isotherm there was no tailing upward at higher relative pressure and this shows the formation of long-range order mesoporosity without any contribution of large pores beyond mesopore scale (>50 nm).[59]

4.2.4.7 Raman spectroscopy

Figure 4.2.10 shows the Raman spectra of pure and 10 mol% alumia doped titania. The observed peaks at 151, 404, 513 and 634 cm^{-1} can be attributed to the characteristics of the anatase phase. This indicates that the anatase is the predominant phase structure. The maximum at low-frequency of the Raman band, provides an idea of the nanoparticle size, since the particle size can cause large shifts in the location of the raman peaks and their widths, namely, the quantum size confinement effect.[60]

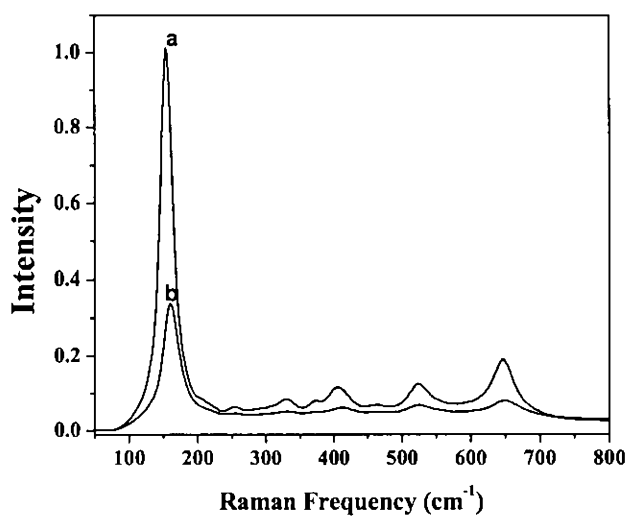

Figure 4.2.10. Raman spectra of (a) undoped titania (b) 10 mol% alumina doped titania

The lowest frequency peak is at 151 cm^{-1} for undoped titania. It can also be evidently seen that the width of this peak increased and resulted in blue shift to 160 cm^{-1} in the case of 10 mol% alumina doped titania. This is due to the lower crystallite size of the sample than the undoped titania.[61]

4.2.4.8 Photo catalytic activity studies

Photoactivity of the titania film was measured using methylene blue degradation studies. The photocatalytic activity of pure titania and titania doped with alumina coatings was studied using the methylene blue degradation technique. Methylene blue shows considerable degradation in presence of titania coating. The degradation was followed through UV spectral measurement. The efficiency of degradation of methylene blue was plotted against alumina content in titania and is given in Figure 4.2.11. It was observed that upto 2 mol% alumina doping, the photoactivity increases and then decreases as the doping concentration of alumina is increased.

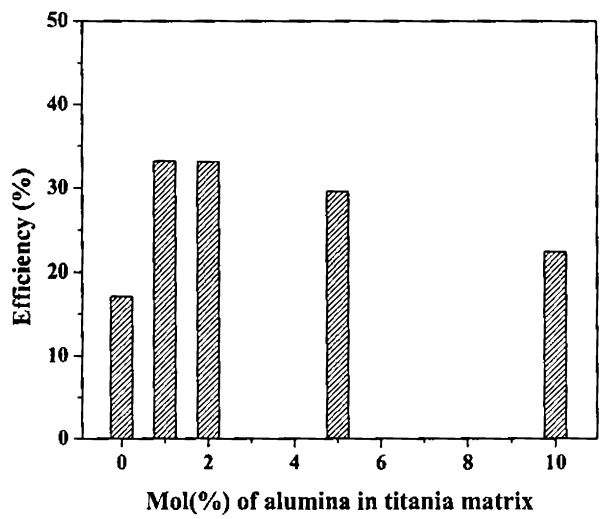

Figure 4.2.11. Methylene blue degradation efficiency against alumina concentration in titania matrix.

The excessive doping makes the space charge layer very narrow so that the penetration depth of light into TiO_2 greatly exceeds the thickness of the space charge layer, resulting in easy recombination of electron-hole pairs and poor photoactivity.[62] This may be one of the reasons for the lower activity of 5 and 10 mol% aluminium doped titania.

4.2.5 Conclusions

An aqueous sol-gel method was developed for the preparation of alumina doped titania thin film. X-ray diffraction analysis indicates that the anatase layer was formed on the glass surface. Titania coatings having transmittance between 85 to 95% were developed on the glass surface using dip coating technique. The alumina addition leads to increase in band gap. Scanning electron micrographs indicates that a uniform thin layer of titania coating was formed on the glass surface. Atomic force micrographs indicate that undoped titania particles were grown into larger size than the 10 mol% alumina doped titania. The thickness of the coating was ~50 nm. Mesoporous nature of the titania layer formed was evident from BET surface area analysis. The pore stability was achieved by alumina doping. Raman spectra were used to confirm the exclusive presence of anatase phase in the coatings. The coated surface was photocatalytic and the alumina doped sample showed higher activity than the undoped one. The present method is hence very useful for the preparation of photocatalytic surfaces from a cheaper precursor, which will enable the bulk production of photocatalytic titania surfaces.

4.6 References

1. Y. T. Wong , N. B. Wong, L. Shi, *J. Mater. Sci.,* 38, **2003,** 973.
2. R. A. Terpstra, B. C. Bonekamp, H. J. Veringa, *Desalination,* 70, **1988**, 395.
3. A. F. M. Leenars, A. J. Burggraff, *J. Colloid Interfac. Sci.,* 105, **1985,** 27.
4. L. C. Klein, D. Gallagher, *J. Membrane Sci.,* 39, **1988,** 213.
5. H. Choi, E. Stathatos, D. D. Dionysiou, *Desalination*, 202, **2007**, 199.
6. T. Van Gestel, H. Kruidhof, D. H. A. Blank, H. J. M. Bouwmeester, *J. Membrane Sci.,* 284, **2006**, 128.
7. T. P. Hoar, N. M. Mott, *J. Phys. Chem. Solids,* 9, **1959,** 97.
8. A. W. Smith, *J. Electrochem. Soc.,*120, **1973**,1068.
9. A. W. Smith, *U.S. Patent 3850762*, **1974**, 762.
10. Y. S. Lin, A. J. Burggraff, *Chem. Eng. Sci.,* 46, **1991,** 3067.
11. Y. S. Lin, A. J. Burggraff, *AICHE. J.*, 38, **1992,** 445.
12. A. J. Burgaff, K. Keizer, B.A. van Hassel, *Solid State Ionics*, 32 & 33, **1991,** 771.
13. H. P. Hsieh, *Inorganic membranes, A. I. Ch. E. Symp. Ser.,* 261, **1988,** 1.
14. T. Yamaki, H. Maeda, K. Kusakabe, S. Morooka, *J. Membrane Sci.,* 85, **1993,** 167.
15. X. S. Ju, P. Huang, N. P. Xu, J. Shi, *J. Membrane Sci.,* 202, **2002,** 67.
16. P. Puhlfurss, A. Voigt, R. Weber , M. Morbe, *J. Membrane Sci.,* 74, **2000,** 123.
17. X. Ding, Y. Fan, N. Xu, *J. Membrane Sci.,* 270, **2006**, 179.
18. L. Q. Wu, P. Huang, N. P. Xu , J. Shi, *J. Membrane Sci.*173, **2000,** 263.
19. C. Yu, L. C. Klein, *J. Am. Ceram. Soc.,* 75, **1992,** 2613.
20. R. Soria, S. Cominotti, *Nanofiltration Ceramic Membranes, Proceedings of International Conference of Membranes and Membrane Processes,* Yokoham, Japan, 18-23,**1996**, p. 6-22.

21. M. Millares, *Method of Fabricating Inorganic Filter Structures, U.S Patent 5656168,* **1997.**

22. R. Castillion, J. P. Laveniere, *Monolithic Ceramic Supports for Filtration Membranes, U. S Patent no.5415775,* **1995.**

23. K. Prabhakaran, S. Priya, N. M. Gokhale, S. C. Sharma, *Ceram. Int.,* 33, **2007,** 515.

24. A. J. Burggraff, K. Keizer, *Inorganic Membranes, ed. R. R. Bhave, V. N. R., New York,* **1991**.

25. Q. Xu, M. A. Anderson, *J. Mater. Res.,* 5, **1991,** 3.

26. A. F. M. Leenaars, K. Keizer, A. J. Burggraaf, *J. Mater. Sci.,* 19, **1984,** 1077.

27. K. N. P. Kumar, *Nanostructured Ceramic Memranes,* Thesis: University Twente, The Netherlands, **1993.**

28. V.T. Zaspalis, *International report no. CT92/282/128,* **1992**, University of Twente, The Netherlands.

29. Y. Kinemuchi, T. Suzuki, W. Jiang, K. Yatsui, *J. Am. Ceram. Soc.,* 84, **2001,** 2144.

30. A. J. Burggraaf, L. Cot, A. J. Burggraaf, L. Cot (Eds.), *Fundamentals of Inorganic Membrane Science and Technology,* Elsvier, Amsterdam, **1996,** p. 17.

31. T. Tsuru, D. Hironaka, T. M. Asaeda, *Sep. Purif. Technol.,* 25, **2001,** 307.

32. B. Bournonville, A. Nzihou, *Powder Tech.,* 128, **2002,** 148.

33. C. G. deKruif, The rheology of colloidal dispersion in relation to the microstructure. In Hydrodynamics of Dispersed Media, ed. J. P. Hulin, A. M. Cazabat, E. Guyon, F. Carmona, Elsevier, Holland, **1990,** pp. 79.

34. R. Z. Zhou, R.L. Snyder, *Acta. Cyst. B,* 47, **1991,** 617.

35. P. Padmaja, G. M. Anilkumar, P. Mukundan, G. Aruldhas, K. G. K. Warrier, *Inter. J. Inorg. Mater.,* 3, **2001,** 693.

36. C. P. Sibu, S. R. Kumar, P. Mukundan, K. G. K. Warrier, *Chem. Mater.*, 14, **2002**, 2876.

37. S. Benfer, U. Popp, H. Richter, C. Siewert, G. Tomandl, *Sep. Purif. Technol.*, 22-23, **2001**, 231.

38. C. Hu, Y. Lan, J. Qu, X. Hu, A. Wang, *J. Phys. Chem. B*, 110, **2006**, 4066.

39. K. V. S. Rao, B. Zhuo, J. M. Cox, K. Chiang, M. Brungs, R. Amal, *J. Biomed. Nanotech.*, 2, **2006**, 1.

40. Y. Kikuchi, K. Sunada, T. Iyoda, K. Hashimoto, A. Fujishima, *J. Photochem. Photobio. A: Chem.*, 106, **1997**, 51.

41. K. Sunada, Y. Kikuchi, K. Hashimoto, A. Fujishima, *Environ. Sci. Technol.*, 32, **1998**, 726.

42. I. P. Parkin, R. G. Palgrave, *J. Mater. Chem.*, 15, **2005**, 1689.

43. R. S. Sonawane, S. G. Hegde, M.K. Dongare, *Mater. Chem. Phys.*, 77, **2002**, 744.

44. J. Yang, S. Mei, J. F. M. Ferreira, *J. Eur. Ceram. Soc.*, 24, **2004**, 335.

45. X. W. Bao, S. S. Yan, C. Feng, J. L. Zhang, *Mater. Lett.*, 59, **2005**, 412.

46. J. C. Yu, X. C. Wang, X. Z. Fu, *Chem. Mater.*, 16, **2004**, 1523.

47. L. Ge, M. X. Xu, E. Lei, Y. M. Tian, H. B. Fang, *Key Eng. Mater.*, 280–283, **2005**, 809.

48. R. S. Sonawane, B. B.Kale, M. K. Dongare, *Mater. Chem. Phys.*, 85, **2004**, 52.

49. T. Kishimoto, Kozuka, H., *J. Mater. Res.*, 2, **2003**, 466.

50. H. Ichinose, A. Terasaki, H. Katsuki, *J. Ceram. Soc. Jpn.*, 104, **1996**, 715.

51. H. Ichinose, A. Kawahara, H. Katsuki, *J. Ceram. Soc. Jpn.*, 104, **1996**, 914.

52. C. K. Lee, D. K. Kim, J. H. Lee, *J. Sol–Gel Sci. Technol.*, 31, **2004**, 67.

53. L. Ge, M. X. Xu, H. B. Fang, Chin, *J. Inorg. Chem.*, 21, **2005**, 394.

54. T. V. Mani, H. K. Varma, K. G. K. Warrier, A. D. Damodaran, *J. Am. Ceram. Soc.*, 74, **1991**, 1807.

55. J. M. Gallardo Amores, V. Sanchez Escribano, M. Daturi, G. Busca, *J. Mater. Chem.*, 6, **1996,** 879.

56. H. Bevan, S. V. Dawes, R. A. Ford, *Spectrochim. Acta Part A:* 13, **1958,** 43.

57. J. Ramirez, L. Ruiz-Ramirez, L. Cedeno, V. Harle, M. Vrinat, M. Breysse, *Appl. Catal. A-Gen.*, 93, **1993,** 163.

58. A. FernBndez, J. Leyrer, A.R. Gonzalez Elipe, G.Munuera, H. K& Zinger. *J. Catal.*, 112, **1989,** 489.

59. S. J. Gregg, K. S. W. Sing, *Adsorption, Surface area and Porosity, IInd Ed., Academic Press,* **1982.**

60. Y. Iida, M. Furukawa, T. Aoki, T. Sakai, *Appl. Spectrosc.*, 52, **1998,** 673

61. V. Swamy, A. Kuznetsov, L. S. Dubrovinsky, R. A. Caruso, D. G. Shchukin, B. C. Muddle, *Phys. Rev. B,* 71, **2005,** 184302.

62. M. A. Henderson, *Surf. Sci.*, 400, **1998,** 203.

Summary

Nanocrystalline titanium dioxide has been widely experimented as catalyst and photo catalyst. The photocatalytic property of titania was effectively used in applications such as water and air purification, water splitting, solar cells and in fabricating self cleaning surfaces. The thesis entitled "**Aqueous sol-gel process for nanocrystalline photocatalytic titania, transparent functional coatings and ceramic membrane**" investigates the plausibility of an aqueous sol-gel process for the preparation of nanocrystalline titania for functional applications.

The present thesis describes a new aqueous sol-gel method for the preparation of nanocrystalline titania using titanyl sulphate as precursor through precipitation-peptisation reactions. The sol stability was monitored using zeta potential measurement and was highly dependant on peptised pH. The lower particle size was obtained in the acidic region. Titania sol having average particle size of 27 nm and a zeta potential value of 35 mV stable for months, could be prepared. The anatase to rutile transformation was found to occur in the region 500-800°C, which is in accordance with earlier reports for nano crystalline titania. The nano crystalline nature was evident from X-ray diffraction patterns and the crystallite size calculated from Scherrer equation was ~20 nm for the titania powders after calcining at 600 °C. Transmission electron micrographs also confirm the result.

The prediction of Shanon and Pask was used to increase the temperature stability of anatase derived from aqueous sol-gel process. Accordingly +3 dopants with size higher than that of Ti occupying lattice sites and +5 dopants with size similar to that of Ti occupying interstitial sites were used which should decrease oxygen deficiency concentration in titania. Oxygen vacancy acts as the nucleation centre for anatase to

rutile phase transformation and also as charge recombination centers. Further process was optimized to investigate other parameters which influence photoactivity such as high specific surface area, small crystallite size and higher anatase to rutile phase transformation temperature. In the present study the influence of +5 dopant tantalum, and +3 dopants, gadolinium and ytterbium on the photocatalytic activity of the titanyl sulphate derived sol-gel titanium oxide is presented. The addition of dopant salts was made to the sol in the process for the preparation of doped titania. Photocatalytic activity of titania was measured by following degradation measurements of methylene blue solution under UV exposure. In the case of tantalum addition, the photoactivity was found to increase and compositions with activity better than commercially available Hombikat UV100 could be prepared. The crystallite size, anatase to rutile phase transformation, specific surface area and photo catalytic property are explained. In this study, we observed that the selected dopants in the titania matrix increase the phase stability of the titania. In the case of tantala doped titania sample the phase stability was obtained above 1000 °C. In gadolinium and ytterbium doped sample also the phase stability is obtained upto 900 °C but in higher concentration of dopant additional phase such as Gd_2TiO_7 and Yb_2TiO_5, these phases increase the rate of anatase to rutile phase transformation at higher temperatures. We have also observed that the anatase to rutile phase transformation happens only when the crystallite size reaches a critical value between ~12-20 nm in tune with reported literatures. Transmission electron micrographs also indicate that the doping with tantalum, gadolinium and ytterbium effectively hinder the crystallite growth. The specific surface area enhanced in the doped system and it shows higher value than the undoped one in the whole range of temperatures studied. The catalytic sites (lewis and brownsted sites) also increased in doped titania.

Gadolinium and ytterbium doped titania show higher photoactivity than the pure titania calcined at 700 and 800 °C.

The aqueous sol-gel derived titania was further used for the preparation of titania films on the surface of porous alumina and glass surfaces. The porous alumina tubular substrate 10 mm diameter had an average pore size of 0.2 μm and was coated with an intermediate layer of alumina using a boehmite sol (average particle size 165 nm) followed by calcinations at 800 °C for 5h. This was followed by coating a titania layer using titania sol (average particle size 27 nm). The coated samples were further characterised using scanning electron microscope, which showed that the alumina intermediate layer has a thickness of ~1- 2 μm. The total thickness of alumina and titania layer was ~4-5 μm. The coated membrane was used for the filtration of organic compound such as congo red. A 99.3% of rejection of dye was observed in the permeate. Further nano titania thin films doped with alumina were formed on glass surface using titania sol derived from titanyl sulphate. Titania coatings having transmittance between 85 to 95 %were developed on the glass surface using dip coating method. The UV visible spectral characteristics indicate a blue shift in the absorption spectrum. Scanning electron microscopic and atomic force microscopic investigations indicate that a thin layer of titania was formed on the glass surface. BET measurement indicates that a mesoporous layer was formed on the glass surface. The alumina addition increases the surface area, total pore volume and mesopore volume of the system. The alumina doped titania thin film shows higher photoactivity than that made using the pure titania.

List of Publications

1. **K. V. Baiju**, P. Shajesh, W. Wunderlich, P. Mukundan, S. Rajesh Kumar, K. G. K. Warrier, Effect of Tantalum Addition on Anatase Phase Stability and Photoactivity of Aqueous Sol gel Derived Mesoporous Titania, *Journal of Molecular Catalysis: A: Chemical,* **(276) 41-46, 2007.**

2. **K. V. Baiju** , P. Periyat , W. Wunderlich, P. Krishna Pillai, P. Mukundan, K. G. K. Warrier, Enhanced photoactivity of Nd^{3+} doped Mesoporous Titania Synthesized Through Aqueous Sol-gel Method, *Journal of Sol-gel Science and Technology,* **(43) 283-290, 2007.**

3. **K. V. Baiju** , P. Periyat, P. Krishna Pillai, P. Mukundan, K. G. K. Warrier ,W. Wunderlich, Enhanced Photoactivity and Anatase Thermal stability of Silica–alumina Mixed oxide Additives on Sol–gel Nanocrystalline Titania, *Material Letters,* **61, 1751-1755, 2007.**

4. **K. V. Baiju**, S. Shukla, K S. Sandhya, J. James, K. G. K. Warrier, Photocatalytic Activity of Sol-gel Derived Nanocrystalline Titania, *Journal of Physical Chemistry C.* **111(21) 7612- 7622, 2007.**

5. **K. V. Baiju,** S. Shukla K. S. Sandhya, J. James K. G. K. Warrier, Role of Surface-Purity in Photocatalytic Activity of Nanocrystalline Anatase–Titania Processed via Polymer-Modified sol–gel, *Journal of Sol-gel Science and Technology,* **DOI 10.1007/s10971-007-1653-4.**

6. P. Periyat, **K. V. Baiju**, P. Mukundan, P. Krishna Pillai, K. G. K. Warrier, Aqueous colloidal sol-gel route to synthesize nanosized ceria-doped titania having high surface area and increased anatase phase stability, *Journal of Sol-gel Science and Technology,* **(43) 299-304, 2007.**

7. **K. V. Baiju**, C. P. Sibu, K. Rajesh , P. Krishna Pillai, P. Mukundan, K. G. K. Warrier, W. Wunderlich, An aqueous sol-gel route to synthesize nanosized lanthana-doped titania having an increased anatase phase stability for photo catalytic application, *Material Chemistry and Physics,* **90 (1) 123-127, 2005.**

8. K. G. K. Warrier, C. P. Sibu, **K. V. Baiju**, Nanocrystalline Titanium Oxide–Its Potential Functional Applications *Indian Ceramic Society Transaction,* **62 (2) 75-87, 2003. (Review article)**

9. **K. V. Baiju**, P. Shajesh, W. Wunderlich, P. Mukundan, P. KrishnaPillai, K. G. K. Warrier, Mesoporous gadolinium doped photo active titania through an aqueous sol-gel method, *(communicated to Journal of Molecular Catalysis A: Chemical).*

10. **K. V. Baiju**, P. Shajesh, P. Mukundan, C. P.sibu, O. Siedel, K. G. K. Warrier, Mesoporous titania thin film doped with alumina using an aqueous sol-gel method, *(to be communicatedto Thin Solid Films).*

Presentations and Posters at Symposia

1. **K. V. Baiju**, S. Shukla, K. S. Sandhya, J. James, K. G. K. Warrier, Photocatalytic Activity of Nanocrystalline Titania Processed via Conventional and Modified Sol-gel, International Conference on Advanced Materials and Composites (ICAMC) 2007, Trivandrum, India, October, 24-26, 2007.
2. **K. V. Baiju**, S. Shukla, K. S. Sandhya, J. James, K. G. K. Warrier, "Significance of Crystallinity, Surface Area, and Nanocrystallite Size in Photocatalytic Behavior of Nanocrystalline Titania",International Conference on Materials for the Millenium, MatCon 2007, Kochi, India, March, 1-3, 2007.
3. **K. V. Baiju**, S. Shukla, K.S. Sandhya, J. James, K. G. K. Warrier, "Sol-Gel Derived Nanocrystalline Titania Powders as Photocatalysts", National Conference on Emerging Trends in Engineering Materials, NCETEM-2007, Patiala, India, February 1-3, 2007.
4. **K. V. Baiju**, S. Shukla, K.S. Sandhya, J. James, K. G. K. Warrier, "Nanocrystalline Titania Powders via Sol-Gel Process for Photocatalytic Application", CeraTech 2007, 70th Annual Session of the Indian Ceramic Society, Andhra University, Visakhapatnam, India, January 8-10, 2007.
5. **K. V. Baiju**, P. Mukundan, P. Krishna Pillai, K. G. K. Warrier, "Photoactivity and anatase thermal stability of silica–alumina mixed oxide additives on sol–gel nanocrystalline titania", CeraTech 2007, 70th Annual Session of the Indian Ceramic Society, Andhra University, Visakhapatnam, India, January 8-10, 2007.
6. K. G. K. Warrier, **K. V.Baiju**, K. Rajesh, " Challenges in the preparation of Nano size particles and Fabrication to Application materials and Devices" Presented in International conference on Powder Metallurgy PM-05, Mumbai, India, February, 3-6, 2005.
7. Pradeepan Periyat, **K. V. Baiju**, C. P. Sibu, P. Perumal, P. Krishna Pillai, P. Mukundan, K. G. K. Warrier; "Nanocrystalline photocatalytic titanium oxide for catalysts, self-cleaning and antialgal coatings",Presented a poster in International Conference on Metals and Materials, Trivandrum, India, November,19, 2004.
8. **K. V. Baiju**, P. Mukundan, P. Krishna Pillai, K. G. K. Warrier, "Development of nanotitania membranes for catalytic application", National Seminar on Membrane Science & Technology: Challenges And Opportunities, Regional Research Laboratory , Jorhat, Assam, India, February,12-13, 2004.
9. C. P. Sibu, **K. V. Baiju**, P. Krishna Pillai, P. Mukundan, K. G. K. Warrier; "Sol-Gel process for nanocrystalline titania and it's applications", Presented a poster in International Ceramic Congress, Chennai, India, January 8-11, 2004.
10. **K. V. Baiju**, C. P. Sibu, P. Mukundan, P. Krishna Pillai, K. G. K. Warrier, "Synthesis of sol-gel derived nanocrystalline titania for possible application as

catalysts", National seminar on frontiers in clay research, Regional Research Laboratory, Trivandrum, India, March, 20-21, 2003.

11. **K. V. Baiju**, C. P. Sibu, P. Krishna Pillai, P. Mukundan, K. G. K. Warrier, "Synthesis of structurally modified nano titanium oxide from Titanyl sulphate for application in ceramic membranes", National Seminar on Science and Technology of Advanced Engineering Materials (STAEM-2003), Trivandrum, India, February, 20-21, 2003.
12. K. Rajesh, **K. V. Baiju**, P. Mukundan, P. Krishna Pillai, K. G. K. Warrier, "Aqueous sol-gel nano processing for rare earth phosphate ceramics", Presented in International Conference on Ceramic Processing Science (8th ICCPS meeting), Hamburg, Germany, September 2-5, 2002.
13. C. P. Sibu, **K. V. Baiju**, S. Sivakumar, K. G. K. Warrier, "Development of self-cleaning surfaces through active nanosize titania coatings", National Seminar on Challenges of Titanium Industry in India, , Trivandrum, Kerala, India, April, 19-20 , 2002.